AD_____

Award Number: W81XWH-06-1-0329

TITLE: Detection and Evaluation of Early Breast Cancer via Magnetic Resonance Imaging: Studies of Mouse Models and Clinical Implementation

PRINCIPAL INVESTIGATOR: Sanaz Arkani-Hamed

CONTRACTING ORGANIZATION: University of Chicago
Chicago, IL 60637

REPORT DATE: March 2007

TYPE OF REPORT: Annual Summary

PREPARED FOR: U.S. Army Medical Research and Materiel Command
Fort Detrick, Maryland 21702-5012

REPORT DOCUMENTATION PAGE

Form Approved
OMB No. 0704-0188

1. REPORT DATE	2. REPORT TYPE	3. DATES COVERED
01-03-2007	Annual Summary	6 Feb 2006 – 5 Feb 2007

4. TITLE AND SUBTITLE

Detection and Evaluation of Early Breast Cancer via Magnetic Resonance Imaging: Studies of Mouse Models and Clinical Implementation

5a. CONTRACT NUMBER

5b. GRANT NUMBER
W81XWH-06-1-0329

5c. PROGRAM ELEMENT NUMBER

6. AUTHOR(S)

Sanaz Arkani-Hamed

Email: sarkani@uchicago.edu

5d. PROJECT NUMBER

5e. TASK NUMBER

5f. WORK UNIT NUMBER

7. PERFORMING ORGANIZATION NAME(S) AND ADDRESS(ES)

University of Chicago
Chicago, IL 60637

8. PERFORMING ORGANIZATION REPORT NUMBER

9. SPONSORING / MONITORING AGENCY NAME(S) AND ADDRESS(ES)
U.S. Army Medical Research and Materiel Command
Fort Detrick, Maryland 21702-5012

10. SPONSOR/MONITOR'S ACRONYM(S)

11. SPONSOR/MONITOR'S REPORT NUMBER(S)

12. DISTRIBUTION / AVAILABILITY STATEMENT
Approved for Public Release; Distribution Unlimited

13. SUPPLEMENTARY NOTES
Original contains colored plates: ALL DTIC reproductions will be in black and white.

14. ABSTRACT

Mice are widely used in the study of breast cancer to increase understanding of cancer development and to evaluate new therapies. Noninvasive imaging methods are a crucial component of the effective use of mouse models of breast cancer. However, prior imaging studies of mammary cancer in mice have focused on large palpable tumors at an advanced stage of invasion, that are rarely orthotopic and are poor models for the human cancers commonly seen clinically. Here, high resolution MR was used to image spontaneous, early and nonpalpable cancers transgenic mouse model of breast cancer. After correlation with histology, MRI was able to clearly detect large ~5mm tumors, small lnonpalpable~0.51.5mm tumors, and even smaller ducts distended with preinvasive ductal carcinoma in situ ~300500 microns in diameter, with very high sensitivity and specificity. This is the first report of in vivo imaging of early, spontaneous mouse mammary cancer. Because of its similarity to human breast cancer, in vivo MRI of early orthotopic murine mammary cancer will be an important tool for real time study of the development and progression of breast cancer in vivo. These techniques can be used to develop new therapies that target early breast cancer and to find new ways of detecting early breast cancer.

15. SUBJECT TERMS
early detection, MRI, mouse models, DCIS

16. SECURITY CLASSIFICATION OF:			17. LIMITATION OF ABSTRACT	18. NUMBER OF PAGES	19a. NAME OF RESPONSIBLE PERSON
a. REPORT	b. ABSTRACT	c. THIS PAGE			USAMRMC
U	U	U	UU	133	19b. TELEPHONE NUMBER *(include area code)*

Table of Contents

INTRODUCTION

Women diagnosed with breast cancer today have significantly better survival outcomes compared with their counterparts of 30 years ago. It is widely accepted that the primary reason has been improved detection of earlier cancer due to screening mammography. Thus, it is clinically important to detect and effectively treat localized breast cancer and MR imaging of breast cancer has recently emerged as a very sensitive tool for the detection of breast cancer. Mouse models of breast cancer are widely used as a 'test bed' for development of improved imaging methods, for studies of cancer development, and to evaluate new therapies. Non-invasive imaging methods are crucial to the effective use of these models, since early cancers are not palpable or visible to the eye. However the imaging technology in this area has not kept pace with the needs of biologists, and non-invasive imaging of early orthotopic cancers is not adequately developed. MR imaging of mouse mammary cancer, including in transgenic mouse models, is no exception to this trend of focusing on large tumors.

The purpose of this work is two pronged: 1) to perform quantitative and qualitative analysis of clinical breast dynamic contrast enhanced magnetic resonance images (DCEMRI), particularly of DCIS lesions, and 2) to image early cancer, including DCIS, in a transgenic mouse model using high resolution MRI.

BODY

During the first year of funding of this award, we have managed to accomplish many of the aims of the approved Statement of Work.

Task 1. To evaluate the development of ductal carcinoma *in situ* (DCIS) in mammary glands of a transgenic mouse model via MRI.

a. *Develop in vivo high resolution imaging of mouse mammary glands.*
b. *Perform detailed correlation of MRI with histology to improve understanding of features on MR images.*
c. *Perform serial MRI studies to follow mice while DCIS develops and continue to follow the transition to invasive cancer.*

Task 2. To perform quantitative and qualitative analysis of clinical breast dynamic contrast enhanced magnetic resonance images (DCEMRI).

a. *Maintain research database.*
b. *Quantitative assessment and mathematical modeling of enhancement patterns in lesions of many pathology subtypes.*
c. *Quantitative assessment of parenchymal enhancement patterns in the normal breast.*
d. *Use recently developed imaging methods and develop novel imaging acquisitions*.

Task 1a and 1b: We have developed the techniques to image early cancer, including DCIS, in the Sv40 TAg transgenic mouse model of breast cancer and performed a sensitivity and specificity study by making correlations with histology [see manuscript in Appendix: ***In vivo* Imaging of Ductal Carcinoma in situ and Other Early Breast Cancers in Mice**]. In our study, we found that high resolution MRI has high sensitivity and specificity for small non-palpable cancers and DCIS lesions.

Task 2a, 2b and 2c: We have also continued to maintain the research database, which now contains over 2800 records with ~800 malignant lesions and ~300 benign lesions. We have performed a semi-quantitative and qualitative study of the kinetic and morphologic findings of 79 pure DCIS lesions in clinical DCEMRI data [see manuscript in Appendix: **MR Imaging of Pure Ductal Carcinoma *in situ*: Kinetics, Morphology and Comparison with Mammographic Presentation and Nuclear Grade**]. We have also used a mathematical model to analyze the kinetic patterns of enhancement in malignant and benign lesions, and have particularly studied the patterns of DCIS lesions vs. both invasive cancers and benign lesions [see manuscript in Appendix: **Differentiation between benign and malignant breast lesions detected by bilateral dynamic contrast enhanced MRI: A sensitivity and specificity study**]. We have also performed a semi-quantitative and qualitative study of the kinetic and morphologic findings of 145 IDC lesions when grouped by molecular marker status—for example, we compared the kinetics of estrogen receptor positive vs. negative lesions and found that ER negative lesions displayed more suspicious kinetics, with strong washout[see abstract in Appendix: **Dynamic MR Imaging of Invasive Ductal Carcinoma: Studying Kinetics by**

Estrogen Receptor, Progesterone Receptor and Her2/Neu Amplification Status]. Finally, we have also performed a study on the enhancement characteristics of normal parenchymal tissue in 180 women [see manuscript in Appendix: **Qualitative and Quantitative Characteristics of Parenchymal Enhancement on Breast MRI**]

KEY RESEARCH ACCOMPLISHMENTS

- We have developed techniques to image early cancer, including DCIS, in transgenic mice *in vivo* [see manuscript in Appendix: ***In vivo* Imaging of Ductal Carcinoma in situ and Other Early Breast Cancers in Mice**]
- We have performed a preliminary sensitivity and specificity study by correlating MR images with histological sections, and found that high resolution MRI has a high sensitivity and specificity to early cancer, including DCIS [see manuscript in Appendix: ***In vivo* Imaging of Ductal Carcinoma in situ and Other Early Breast Cancers in Mice**]
- We have also continued to maintain the research database, which now contains over 2800 records with ~700 malignant lesions and ~200 benign lesions
- We have performed a semi-quantitative and qualitative study of the kinetic and morphologic findings of 79 pure DCIS lesions in clinical DCEMRI data, and have found that these lesions show non-mass-like clumped enhancement, with a wide variety of kinetic characteristics [see manuscript in Appendix**: MR Imaging of Pure Ductal Carcinoma *in situ*: Kinetics, Morphology and Comparison with Mammographic Presentation and Nuclear Grade**]
- We have also used a mathematical model to analyze the kinetic patterns of enhancement in malignant and benign lesions, and have particularly studied the patterns of DCIS lesions vs. both invasive ductal carcinoma (IDC) and benign lesions. We found that DCIS lesions enhance less and washout less than IDC lesions, and seem to overlap considerably with the kinetics of benign lesions [see manuscript in Appendix: **Differentiation between benign and malignant breast lesions detected by bilateral dynamic contrast enhanced MRI: A sensitivity and specificity study**]
- We have also performed a semi-quantitative and qualitative study of the kinetic and morphologic findings of 145 IDC lesions when grouped by molecular marker status—for example, we compared the kinetics of estrogen receptor positive vs. negative lesions and found that ER negative lesions displayed more suspicious kinetics, with strong contrast washout [see abstract in Appendix: **Dynamic MR Imaging of Invasive Ductal Carcinoma: Studying Kinetics by Estrogen Receptor, Progesterone Receptor and Her2/Neu Amplification Status**]
- We have also performed a study on the enhancement characteristics of normal parenchymal tissue in 180 women, and found that 10% of cases show strong enhancement that could obscure lesions. In addition, we found that dense breasts show extensive and stronger parenchymal enhancement compared with less dense breasts. [see manuscript in Appendix: **Qualitative and Quantitative Characteristics of Parenchymal Enhancement on Breast MRI**]

REPORTABLE OUTCOMES

Manuscripts:

1. **MR Imaging of Pure Ductal Carcinoma *in situ*: Kinetics, Morphology and Correlation with Mammographic Presentation and Nuclear Grade**. This article was submitted to *Radiology* in Dec 2006, and has been provisionally accepted for publication (with revisions). This is work from Task 2b.
2. **Differentiation between benign and malignant breast lesions detected by bilateral dynamic contrast enhanced MRI: A sensitivity and specificity study.** This article was submitted for publication in *Magnetic Resonance in Medicine* in February 2007. This is work from Task 2b.
3. ***in vivo* Imaging of Ductal Carcinoma *in situ* and Other Early Breast Cancers in Mice.** This article will be submitted for publication in *Radiology* in March 2007. This is work from Task 1a and 1b.
4. **Qualitative and Quantitative Characteristics of Parenchymal Enhancement on Breast MRI.** This article will be submitted for publication in *American Journal of Roentenology* in March 2007. This is work from Task 2c.

Abstracts and Presentation: Full versions of these abstracts can be found in the Appendix.

1. **MR Imaging of Pure Ductal Carcinoma in Situ: Kinetics, Morphology, and Correlation with Mammographic Presentation and Nuclear Grade.** Oral presentation at the Radiological Society of North America (RSNA) meeting in November 2006. This is work from Task 2b.
2. **Parenchymal enhancement on breast MRI may be a marker for cancer risk: correlation of parenchymal enhancement with breast density.** Poster presentation at the San Antonio Breast Cancer Symposium in Dec 2006. This is work from Task 2c.
3. **Improving the Diagnostic Accuracy of 3D Breast DCEMRI Data Using an Empirical Mathematical Model**. Accepted for poster presentation at the International Society for Magnetic Resonance in Medicine (ISMRM) meeting in May 2007. This is work from Task 2b.
4. **Molecular Markers and DCEMRI of Breast Cancer: Relationship with Kinetics in Invasive Ductal Carcinoma**. Accepted for poster presentation ISMRM in May 2007. This is work from Task 2b.
5. **MRI of Ductal Carcinoma *in situ* and Other Early Mammary Cancers in Transgenic Mice.** Accepted for poster presentation at ISMRM in May 2007. This is work from Task 1a and b.
6. **Dynamic MR Imaging of Invasive Ductal Carcinoma: Studying Kinetics by Estrogen Receptor, Progesterone Receptor and Her2/Neu Amplification Status Molecular Markers.** Accepted for oral presentation at American Roentgen Ray Society (ARRS) meeting in May 2007. This is work from Task 2b.

Informatics: The database I helped to develop and currently maintain (Task 2a) is being used by UC researchers to develop improved methods for analysis of MRI data. In addition, Philips Medical Systems is collaborating with us to use the database for development of CAD software that can be used clinically

Funding Applied for based on work supported by this award:

1. SPORE –project II
2. Two DOD proposals have recently been submitted relating to this funding.
3. We applied for pilot funding from the University of Chicago Cancer Resource Center.
4. We are currently in the process of writing an RO1.

CONCLUSIONS

In our first year of funding we have 1) imaged early cancer, including DCIS, in transgenic mice with high sensitivity and specificity, and 2) performed detailed quantitative and qualitative analysis of the MR features of malignant and benign lesions, in particular of DCIS lesions, as well as normal tissue enhancement patterns. The overall goal of this project is to improve the understanding and detection of early cancer via MRI. On the clinical side, we have compiled a rich source of phenomenological data—that pure DCIS enhance and washout less than invasive cancers, and that normal tissue enhancement can be strong and extensive, for example. On the animal side, we have developed the tools necessary to study early cancers and normal tissue enhancement in mice. With these tools we can move on to studying the development of cancer—for example, study what features of the normal parenchyma predict the development of DCIS, and the transition from DCS to IDC (Task 1c).

So what? There are a number of potential implications of this work:

- We have found that pure DCIS lesions have different kinetic patterns of enhancement compared with invasive cancers. The longer time to peak enhancement and the lower initial enhancement of pure DCIS lesions, should be considered in some computer aided diagnosis (CAD) schemes where thresholds may be set too high and too early, and possibly run the risk of a false negative diagnosis.
- Analysis of conventional 3D DCEMRI data with the empirical mathematical model (EMM) provides at least the diagnostic accuracy of qualitative kinetic parameters described in the BI-RADS® lexicon, and offers a few key advantages. For example, tt can be used to standardize kinetic data between institutions—currently, when radiologists are presented with an outside MRI for evaluation, there is no way to relate the kinetic findings of the outside case to experience at the home institution. For example, if MR images at the outside institution are acquired every 90 seconds, and at the home institution the dynamic protocol acquires images every 60 seconds, the EMM can be used to present the outside kinetic data with 60 second time resolution.
- The American Cancer Society has recommended MRI for screening in certain groups of women at high risk for breast cancer. Our study on characterizing normal tissue enhancement on breast MRI may be useful for radiologists beginning screening programs.
- To our knowledge, ours is the first report of MR imaging of early, spontaneous mouse mammary cancer. In vivo MR imaging of early murine mammary cancer opens up new approaches for research and clinical applications by exploiting the full utility of transgenic mouse models. One possible application is in pre-clinical evaluation of breast cancer therapies. A popular method for conducting such studies is administering therapy to a group of mice with palpable, often non-orthotopic tumors, and measuring the reduction in tumor size—sometimes with imaging. However, these cancers are unlikely to model the response to therapy of the majority of cancers diagnosed in women. Non-invasive imaging offers an important option that allows longitudinal, serial studies for evaluating the effects of therapy on cancers of several stages, including small tumors and DCIS.

REFERENCES: The references are included in each manuscript (see Appendix).

APPENDIX

Manuscripts

In vivo MR Imaging of Ductal Carcinoma *in situ* and Other Early Breast Cancers in Mice

Sanaz Arkani[1] M.Sc., Suzanne Conzen[2] M.D., Thomas Krausz [3] M.D., Marta Zamora[1] B.Sc., Erica Markewicz[1] B.Sc., Sean Foxley[1] M.Sc., Xiaobing Fan[1] Ph.D., Dianna Pang[2] B.Sc., Brad Williams[2] B.Sc., So-young Kim[2] B.Sc., Gillian Newstead[1] M.D. and Gregory Karczmar[1] Ph.D.

To be submitted to Radiology as an Original Research paper
Word Count: 2949

Institution Address:

[1] University of Chicago, Department of Radiology
5841 S. Maryland Ave, MC 2026
Chicago, IL 60637

[2] University of Chicago, Department of Hematology/Oncology
5841 S. Maryland Ave, MC 2115
Chicago, IL 60637

[3] University of Chicago, Department of Pathology
5841 S. Maryland Ave, MC 6101
Chicago, IL 60637

Corresponding Author:

Gregory Karczmar
University of Chicago, Department of Radiology
5841 S. Maryland Ave, MC 2026
Chicago, IL 60637
Phone: (773) 702-0214
Fax: (773) 834-9047
Email: gskarczm@uchicago.edu

In vivo MR Imaging of Ductal Carcinoma *in situ* and Other Early Breast Cancers in Mice

Original Research

Advances in Knowledge:

1. To our knowledge, we are reporting the first *in vivo* images of the early stages of spontaneous and non-palpable mouse mammary cancer—including *in situ* carcinoma—with histopathologic correlation. We have found that high spatial resolution MR imaging has high sensitivity and specificity to early cancer.

2. We found that gradient echoes images with T_1- weighting and fat saturation produced the clearest images of mammary glands and cancer.

3. Dynamic contrast enhanced MR imaging of early mouse mammary cancer demonstrated that, as with women, DCIS lesions and small tumors exhibit contrast uptake.

Implications for Patient Care:

1. There are no direct impacts to patient care from this study. However, the detection of early cancers, including *in situ* cancer, in a mouse model opens new possibilities for clinical applications. Because of its similarity to human breast cancer, *in vivo* MRI of early orthotopic murine mammary cancer will be an important tool for **a)** real-time noninvasive study of the development and progression of breast cancer, **b)** preclinical testing of candidate breast cancer therapies that target early cancers, and **c)** developing improved MR imaging methods for detection of early cancers and pre-cancerous conditions.

Abstract

Purpose: The purpose of our study was to develop methods for high spatial resolution MRI of early murine mammary cancer —including *in situ* cancer —with histopathologic correlation.

Materials and Methods: This institutions Animal Care and Use Committee approved our study of 12 C3(1) SV40 large T antigen mice between 10-18 weeks of age. A pair of inguinal mammary glands in each mouse was imaged using a T_1-weighted gradient echo sequence, with and without fat suppression. High spectral and spatial resolution images and dynamic contrast enhanced images were also acquired. H&E sections of the glands were obtained after excision and fixation in formalin. We used a polyethylene grid with 2.5 mm spacing embedded in partially deuterated agar that produced a pattern on MRI that was used for registration of tissue sections and images. On one representative H&E section, the tumors and ducts distended with DCIS were identified by an experienced pathologist, and their grid locations noted. The corresponding grid positions in the MR images were examined to see if correlative structures were discernable.

Results: FLASH GE images were able to detect 1/1 large (~5mm) tumor, 15/16 small (~1mm) tumors, and 14/17 ducts distended with DCIS greater than 300 microns. There were no false positives—a clear MR finding corresponded to cancer in all glands. The FLASH GE images with fat saturation provided the clearest images of the glands and the cancer.

Conclusions: Our findings demonstrate that MR imaging can detect early cancers in mice with high sensitivity and specificity, and this is an important step towards the more effective use of non-invasive imaging in pre-clinical studies of breast cancer.

Introduction

Women diagnosed with breast cancer today have significantly better survival outcomes compared with their counterparts of 30 years ago (1). This is attributed to improvements in treatment as well as improved detection of earlier cancer due to screening mammography(2, 3). Currently, 64% of newly diagnosed breast cancers in women are at a localized stage, and 15-25% are preinvasive ductal carcinoma *in situ* (DCIS)(4-6). Some have suggested that the continued down-staging of cancer at diagnosis is essential for further decreases in mortality rates (7). Thus, it is clinically important to detect and effectively treat localized breast cancer.

Mouse models of breast cancer are widely used as a 'test bed' for development of improved imaging methods, for studies of cancer development, and to evaluate new therapies. In the past, these studies have usually involved large, palpable, non-orthotopic tumors that are at an advanced stage of invasion, and are not optimal models for human disease (8). Newer, more realistic transgenic mouse models of breast cancer have tremendously advanced the understanding of cancer biology and have lead to improvements in detection and treatment of early cancers(9, 10). Non-invasive imaging methods are crucial to the effective use of these models, since early cancers are not palpable or visible to the eye. However the imaging technology in this area has not kept pace with the needs of biologists—the majority of *in vivo* imaging studies of mammary cancer in mice focus on the characteristics of large, palpable and invasive tumors that are not orthotopic or spontaneous (11-15). MR imaging of mouse mammary cancer, including in transgenic mouse models, is no exception (16-23). Bremer et al injected transgenic mice with fluorescent imaging probes, using fluorescence and MR imaging to image

tumors when they were either visible or palpable(17). Rodrigues et al studied the response to herceptin of 0.4 cm^2 – 2.0 cm^2 tumors (16). Galie et al first imaged mice with ultrasound when the tumors were between 0.8 g and 1.5 g, and MRI was performed 2 days later (18).

Because of the clinical importance of studying early breast cancer, and the tremendous utility of mouse models for developing and testing new imaging methods and new therapies, the purpose of our study was to develop methods for high spatial resolution MRI of early murine mammary cancer —including *in situ* cancer—with histopathologic correlation. In this report, 'early murine mammary cancer' is defined as non-palpable and spontaneous mammary cancer. We have selected a transgenic mouse model in which the mammary cancer progresses through stages of development similar to human ductal carcinoma, including the progression of DCIS to invasive ductal carcinoma (IDC). Mice were imaged at several stages of early cancer development. Since we were targeting non-palpable tumors, we developed a technique to allow spatial correlation between these MR images and histology.

Materials and Methods

Animals

Twelve C3(1) SV40 large T antigen mice were selected for high resolution MR imaging(24). This mouse model targets expression of large T antigen to the mammary gland in females via the C3 promoter. Female mice develop mammary cancer that resembles human ductal carcinoma, including progression through atypical ductal hyperplasia (~8 weeks), DCIS (~12 weeks), and invasive ductal carcinoma (~16 weeks)(25). All mice succumb by 6 months of age to multi-focal mammary carcinoma and in some cases lung metastasis. In an effort to capture various stages of early cancer, mice were imaged at several ages: 1 at 10 weeks, 2 at12 weeks, 1 at 14 weeks, 4 at 16 weeks, 3 at 17 weeks and 1 at 18 weeks. All procedures were carried out in accordance with our institutions Animal Care and Use Committee approval. Animals were anesthetized prior to imaging experiments, and anesthesia was maintained during imaging at 1.5% isoflorane. Respiration and heart rate were monitored.

MRI

Set-up: To facilitate spatial correlations between MR images and histology, a fine polyethylene mesh ~ 3.0 cm x 2.0 cm in size with 2.5 mm spacing, was embedded in partially deuterated agar and wrapped around each mouse. This grid produced a pattern on MRI that was used for registration of tissue sections and images. The agar also reduced susceptibility artifacts due to the air-tissue interface near the mammary gland, and the addition of 60% deuterated water reduced signal from the agar so that the signal from the nearby mammary gland was not overwhelmed. The inguinal mammary glands on one side of each mouse were selected for imaging. The inguinal intramammary lymph node was palpated, and the grid was positioned

with the lymph node roughly in the center. By palpating the intramammary inguinal lymph node, and positioning the mouse accordingly, we were able to insure that the inguinal glands were indeed being imaged. To facilitate alignment of MR images with histology after the grid was removed, colored pens were used to mark the corners of the grid and their corresponding positions on the skin.

MR Imaging: During imaging, animals were anesthetized and the heart rate and breathing was monitored. The animals were kept warm with a heater blowing warm air, and the body temperature monitored. Imaging was performed with a Bruker 4.7 Tesla magnet equipped with a self-shielded gradient set that delivers maximum gradient strength of 10 gauss/cm. A homebuilt half-bird cage coil with a 3 cm x 3 cm open surface area was used that produced high flux density in the mammary gland. Gradient echo images were obtained (FLASH, TR/TE: 675/7 ms, axial orientation, slice thickness 0.5 mm, in-plane resolution 117 microns, FOV=3.0x3.0cm) with and without fat suppression. Spin echo images were also acquired (RARE, TR/TE: 3000/29 ms, RARE acceleration factor = 4, axial orientation, slice thickness 0.5 mm, in-plane resolution 117 microns, FOV=3.0x3.0cm) with and without fat saturation. High spectral and spatial resolution (HiSS) images were obtained using EPSI (echo-planar spectroscopic imaging (26) with a slice thickness of 0.5 mm, in-plane resolution of 117 microns and a spectral resolution of ~ 6 Hz, using a method detailed in prior work (27). Finally, dynamic contrast enhanced MR images (DCEMRI) were also obtained (TR/TE: 30/3.5 ms, slice thickness 1.0 mm, in-plane resolution 117 microns). The FLASH GE images without fat saturation were acquired initially across the entire sensitive volume of the coil (~2cm) to map out the whole grid. The subsequent

image sets were obtained on a subset of axial slices that contained structures of interest (i.e., candidate cancers).

Tissue Sectioning and Staining

After imaging, the mice were immediately sacrificed and the skin, with the mammary glands still attached, was removed from the body and fixed overnight in formalin. This preserved the position of the glands on the skin, allowing grid alignment by matching the colored marks made earlier. Digital photographs were taken of the fixed excised gland on the grid. The inguinal mammary glands (attached to the skin) were submitted to the Pathology Core Facility for paraffin embedding, sectioning and staining. The paraffin embedded glands were sectioned top down, or coronally (4 micron thickness). The tissue sections were evaluated under supervision of a breast pathologist with over 20 years of professional experience to identify the lymph node, tumors and ducts distended with DCIS greater than 300 microns.

Image Analysis and Correlation with Histology

The agar grid allowed us to compare the axial slices of the MR images with both the coronal H&E sections and the digital photograph of the excised inguinal glands. We defined a coordinate system ***(z,x)*** on the grid, and used it to relate grid positions on the H&E sections to those on the MR images. We designate '***z'*** as the direction of the main magnetic field. During imaging, the ***x*** dimension of the grid was wrapped around the mouse. Axial slices correspond to cross sections through the mouse along the ***z*** direction. We assigned ***z*=0, *x*=0** to the top left

corner of the grid. There were two steps in correlating the MR images with histology: (i) reliably identify the inguinal mammary glands and the lymph node, and (ii) determine if cancer could be identified. We performed this analysis by relating grid positions on the MR images with both the grid positions on the H&E sections and digital photographs of the glands.

Mammary glands were difficult to locate precisely. To insure that the inguinal mammary glands were imaged, palpation of the inguinal intra-mammary lymph node was used as a guide, together with *a priori* information about the geometry of the gland. After the imaging experiment, the position of the glands in the MR images was verified by using the digital photograph of the fixed inguinal glands as the standard for determining the location and extent of the inguinal mammary glands. The glands were first identified by a trained observer with 3 years of mammary gland pathology experience on the photographs. The overall extent of the glands in the z and x direction was determined from the photographs. Then, the extent of the mammary gland in the z and x direction was measured in the FLASH GE MR images.

One representative H&E section was selected per mouse, and served as the standard for determining the location of the lymph node and any cancer lesions. We were not able to directly transfer the MRI-detectable grid onto each H&E section. However, we were able to infer the grid coordinate system by using photoshop to lay a digital image of the H&E section on top of the digital photograph of the excised specimen, using the lymph node to register the two. By doing so, we could determine the $(z_{LN},x_{LN})^{H\&E}$, $(z_{tumor},x_{tumor})^{H\&E}$, $(z_{DCISr},x_{DCIS})^{H\&E}$ position of the lymph node, tumors and ducts distended with DCIS greater than 300 microns in size on the H&E sections, respectively. The corresponding grid position and surrounding pixels in the FLASH

GE MR images were examined to see if correlative structures were discernable, and if so, the grid locations noted as $(z_{LN},x_{LN})^{MR}$, $(z_{tumor},x_{tumor})^{MR}$, $(z_{DCIS},x_{DCIS})^{MR}$. The other images (FLASH GE with fat saturation, RARE with and without fat saturation, and HiSS) were also examined.

One axial MR slice was selected for DCEMRI kinetic analysis. On this image, several ROI's were drawn on the following 5 areas, if applicable: *i*) mammary gland area without cancer, *ii*) lymph node, *iii*) large tumor, *iv*)small tumor, and *v*) DCIS lesions. We performed a simple kinetic analysis of the signal intensity vs. time curve by measuring the enhancement percentage at 1 minute(28), $E_1=(S_1-S_0)/S_0$, where S_1 was the signal intensity in the ROI at 1 minute and S_0 was the pre-contrast signal intensity.

Statistical Analysis

There were several sources of error in our experiment that affected how well the H & E sections could be correlated with MR images. These included alignment of the grid on the skin during imaging and excision, as well as the indirect inference of a coordinate system on the H&E sections. We determined the systematic error in this experiment was approximately 2.5 mm, or 1 grid space. Features that co-registered within systematic error were assumed to coincide. This was a safe assumption, since the features that were evaluated were relatively sparse; a tumor located on the MR image was very likely to coincide with a tumor at approximately the same grid position on H&E stained sections.

In addition, we calculated the average $\boldsymbol{E_1}$ in the 5 areas of interest: *i*) mammary gland area without cancer, *ii*) lymph node, *iii*) large tumor, *iv*)small tumor, and *v*) DCIS lesions.

Results

In all twelve mice, the mammary gland extent on the digital photograph and the FLASH GE MR image agreed. Thus, the mammary glands were accurately identified, outlined between the skin and the abdominal wall. In addition, the position of the lymph node on histological sections matched with the FLASH GE MR images in all glands. Thus, the intramammary inguinal lymph node was also accurately identified on MR images.

In the whole population, there were 16 small non-palpable tumors ~0.5-1 mm in size, 1 large (~5mm) tumor and 17 ducts distended with DCIS greater than 300 microns in diameter. FLASH GE images were able to detect 1/1 large (~5mm) tumor, 15/16 small tumors (Figure 1), and 14/17 ducts distended with DCIS (Figure 2). All of these findings were clearly distinguishable from the normal gland. There were no false positives—a clear MR finding corresponded to cancer in all glands. The FLASH GE images with fat saturation provided the clearest images of the glands and the cancer (Figure 3). HiSS also provided excellent anatomic detail combined with complete fat suppression. For example Figure 4 shows distended ducts in-plane corresponding to DCIS along with other irregular features in the parenchyma (indicated by arrows). In comparison, T_2 weighted RARE images with and without fat saturation did not depict the cancer well.

Dynamic contrast enhanced imaging demonstrated that the uninvolved mammary gland area exhibited minimal enhancement. However, contrast uptake was demonstrable in the lymph nodes, DCIS and small and large invasive tumors (Table 1).

Discussion

To our knowledge, we are reporting the first *in vivo* images of the early stages of spontaneous mouse mammary cancer with histopathologic correlation (15, 29). We have developed techniques to image mammary cancer in mice at the stage when they are most often imaged in humans: primary cancers that are non-palpable, orthotopic and spontaneous, including pre-invasive (DCIS) and invasive stages of malignant progression. We have found that MR imaging can detect early cancer with high sensitivity and specificity.

In our study, gradient echoes images with various modest T_1- weighting and fat saturation produced the clearest images of mammary glands and cancer. This is likely due to that fact that the distended ducts and tumors are densely packed with water filled cells. The morphology of DCIS lesions was often ductal or stippled. Small invasive cancers appeared as round masses, and the large invasive tumor showed irregular margins, and internal heterogeneity (Figure 3). High spectral and spatial resolution imaging also showed distended ducts and irregularities in parenchymal texture. The simple DCEMRI analysis performed in our study demonstrated that lymph nodes, DCIS and tumors enhanced, while seemingly uninvolved mammary gland area did not. A quantitative analysis of the enhancement kinetics via pharmacokinetic modeling was beyond the scope of this paper, and will be explored in a future study.

Practical Applications

Our work demonstrating *in vivo* MR imaging of early murine mammary cancer opens up new approaches for research and clinical applications by exploiting the full utility of transgenic mouse models(25).

One possible application is in preclinical evaluation of breast cancer therapies. Xenograft models play a dominant role in preclinical trials (8), although transgenic mouse models like the C3(1) Sv40 TAg (30-32), are also used. A common method for conducting such studies is administering therapy to a group of mice with palpable, often not orthotopic tumors, and measuring the change in tumor size using calipers, or sometimes with imaging (30-33). However, these cancers are unlikely to model the response to therapy of the majority of breast cancers diagnosed in women. Another approach is to sacrifice large numbers of mice for histological evaluation at various times during therapy (30). This allows a population-based evaluation of the effects of therapy – but does not allow study of changes in individual cancers over time. Non-invasive imaging is an important option that allows longitudinal, serial studies for evaluating the effects of therapy on cancers of several stages, including small tumors and DCIS. It may also be possible to identify pre-cancerous conditions on MRI and this will make it possible to efficiently study effects of prophylactic therapies that target conditions that can lead to cancer.

The detection of early cancers described in our study provides the basis for serial studies of cancer development that can provide important new insights into the development of mammary cancers. For example, the changes in morphology and kinetics that precede the development of DCIS, or the transition of DCIS to IDC, can be studied. A wide range of other

MR methods, and other imaging modalities combined with MRI can provide additional valuable information.

Detection of DCIS and early cancer in a mouse model opens new approaches to the development of improved MRI and other imaging methods for reliable detection of early cancers. For example, we have found that DCIS lesions in this mouse model enhance after contrast injection, which has also been demonstrated in women clinically(34-36). Further study into the biological reasons and implications of this enhancement can be explored. It may be possible to identify changes in contrast media uptake in the parenchyma that precede the development of DCIS, which may lead to new MR markers for cancer risk (37). This model could also be used to test the efficacy of more sophisticated MR imaging techniques for targeting early cancer.

There are several limitations to our study.

- Use of the agar grid to correlate the MR images with histology is imperfect, with a systematic error of 2.5 mm, and inherent resolution of 2.5 mm.
- Only one representative H&E section was used for correlation with MRI, and qualitative correlations were made.
- Only the inguinal glands were imaged. To take full advantage of a transgenic model, all 10 mammary glands should be imaged.
- Verification of the high sensitivity and specificity of MRI to early murine cancer reported here will require study of a much larger group of mice.

- We used a transgenic mouse model with a very high rate of breast cancer, and this biases evaluation of imaging methods and response to therapy. A logical extension of the work discussed here will be to test MRI detection of early cancers in other mouse strains that develop more natural mammary cancer, albeit with much lower incidence.

Despite these shortcomings, our findings demonstrate that MR imaging can detect early cancers in mice, and this is an important step towards the more effective use of non-invasive imaging in pre-clinical studies of breast cancer.

Acknowledgements

We would like to thank the Segal Foundation, Florsheim foundation, the Biological Sciences Division at the University of Chicago, the University of Chicago Cancer Center, DOD Award W81XWH-06-1-0329 and NIH grants R21 CA104774-01A2 and 1 R01 EB003108-04 for financial support.

References:

1. Ries. 2004.
2. Cronin KA, Feuer EJ, Clarke LD, Plevritis SK. Impact of adjuvant therapy and mammography on U.S. mortality from 1975 to 2000: comparison of mortality results from the cisnet breast cancer base case analysis. J Natl Cancer Inst Monogr 2006:112-121.
3. Berry DA, Cronin KA, Plevritis SK, et al. Effect of screening and adjuvant therapy on mortality from breast cancer. N Engl J Med 2005; 353:1784-1792.
4. ACS. Breast cancer facts and figures.
5. Sumner WE, 3rd, Koniaris LG, Snell SE, et al. Results of 23,810 Cases of Ductal Carcinoma-in-situ. Ann Surg Oncol 2007.
6. Tsikitis VL, Chung MA. Biology of ductal carcinoma in situ classification based on biologic potential. Am J Clin Oncol 2006; 29:305-310.
7. Duffy SW, Tabar L, Vitak B, et al. The relative contributions of screen-detected in situ and invasive breast carcinomas in reducing mortality from the disease. Eur J Cancer 2003; 39:1755-1760.
8. Ottewell PD, Coleman RE, Holen I. From genetic abnormality to metastases: murine models of breast cancer and their use in the development of anticancer therapies. Breast Cancer Res Treat 2006; 96:101-113.
9. Shen Q, Brown PH. Transgenic mouse models for the prevention of breast cancer. Mutat Res 2005; 576:93-110.
10. Kavanaugh CJ, Desai KV, Calvo A, et al. Pre-clinical applications of transgenic mouse mammary cancer models. Transgenic Res 2002; 11:617-633.
11. Seemann MD, Beck R, Ziegler S. In vivo tumor imaging in mice using a state-of-the-art clinical PET/CT in comparison with a small animal PET and a small animal CT. Technol Cancer Res Treat 2006; 5:537-542.
12. Jenkins DE, Hornig YS, Oei Y, Dusich J, Purchio T. Bioluminescent human breast cancer cell lines that permit rapid and sensitive in vivo detection of mammary tumors and multiple metastases in immune deficient mice. Breast Cancer Res 2005; 7:R444-454.
13. Hsueh WA, Kesner AL, Gangloff A, et al. Predicting Chemotherapy Response to Paclitaxel with 18F-Fluoropaclitaxel and PET. J Nucl Med 2006; 47:1995-1999.
14. Tian X, Aruva MR, Rao PS, et al. Imaging oncogene expression. Ann N Y Acad Sci 2003; 1002:165-188.
15. Abbey CK, Borowsky AD, McGoldrick ET, et al. In vivo positron-emission tomography imaging of progression and transformation in a mouse model of mammary neoplasia. Proc Natl Acad Sci U S A 2004; 101:11438-11443.
16. Rodrigues LM, Stubbs M, Robinson SP, Newell B, Mansi J, Griffiths JR. The C-neu mammary carcinoma in Oncomice; characterization and monitoring response to treatment with herceptin by magnetic resonance methods. Magma 2004; 17:260-270.
17. Bremer C, Ntziachristos V, Weitkamp B, Theilmeier G, Heindel W, Weissleder R. Optical imaging of spontaneous breast tumors using protease sensing 'smart' optical probes. Invest Radiol 2005; 40:321-327.

18. Galie M, D'Onofrio M, Calderan L, et al. In vivo mapping of spontaneous mammary tumors in transgenic mice using MRI and ultrasonography. J Magn Reson Imaging 2004; 19:570-579.
19. Artemov D, Mori N, Ravi R, Bhujwalla ZM. Magnetic resonance molecular imaging of the HER-2/neu receptor. Cancer Res 2003; 63:2723-2727.
20. Rodriguez O, Fricke S, Chien C, et al. Contrast-enhanced in vivo imaging of breast and prostate cancer cells by MRI. Cell Cycle 2006; 5:113-119.
21. Robinson SP, Rijken PF, Howe FA, et al. Tumor vascular architecture and function evaluated by non-invasive susceptibility MRI methods and immunohistochemistry. J Magn Reson Imaging 2003; 17:445-454.
22. Geninatti Crich S, Cabella C, Barge A, et al. In vitro and in vivo magnetic resonance detection of tumor cells by targeting glutamine transporters with Gd-based probes. J Med Chem 2006; 49:4926-4936.
23. Daldrup-Link HE, Meier R, Rudelius M, et al. In vivo tracking of genetically engineered, anti-HER2/neu directed natural killer cells to HER2/neu positive mammary tumors with magnetic resonance imaging. Eur Radiol 2005; 15:4-13.
24. Maroulakou IG, Anver M, Garrett L, Green JE. Prostate and mammary adenocarcinoma in transgenic mice carrying a rat C3(1) simian virus 40 large tumor antigen fusion gene. Proc Natl Acad Sci U S A 1994; 91:11236-11240.
25. Green JE, Shibata MA, Yoshidome K, et al. The C3(1)/SV40 T-antigen transgenic mouse model of mammary cancer: ductal epithelial cell targeting with multistage progression to carcinoma. Oncogene 2000; 19:1020-1027.
26. Mansfield P. Spatial mapping of the chemical shift in NMR. Magn Reson Med 1984; 1:370-386.
27. Du W, Fan X, Foxley S, et al. Comparison of high-resolution echo-planar spectroscopic imaging with conventional MR imaging of prostate tumors in mice. NMR Biomed 2005; 18:285-292.
28. Szabo BK, Aspelin P, Wiberg MK, Bone B. Dynamic MR imaging of the breast. Analysis of kinetic and morphologic diagnostic criteria. Acta Radiol 2003; 44:379-386.
29. Arkani. ISMRM poster.
30. Green JE, Shibata MA, Shibata E, et al. 2-difluoromethylornithine and dehydroepiandrosterone inhibit mammary tumor progression but not mammary or prostate tumor initiation in C3(1)/SV40 T/t-antigen transgenic mice. Cancer Res 2001; 61:7449-7455.
31. Huh JI, Calvo A, Stafford J, et al. Inhibition of VEGF receptors significantly impairs mammary cancer growth in C3(1)/Tag transgenic mice through antiangiogenic and non-antiangiogenic mechanisms. Oncogene 2005; 24:790-800.
32. Wu K, Kim HT, Rodriquez JL, et al. 9-cis-Retinoic acid suppresses mammary tumorigenesis in C3(1)-simian virus 40 T antigen-transgenic mice. Clin Cancer Res 2000; 6:3696-3704.
33. Cohen I, Pappo O, Elkin M, et al. Heparanase promotes growth, angiogenesis and survival of primary breast tumors. Int J Cancer 2006; 118:1609-1617.
34. Esserman LJ, Kumar AS, Herrera AF, et al. Magnetic resonance imaging captures the biology of ductal carcinoma in situ. J Clin Oncol 2006; 24:4603-4610.

35. Gilles R, Zafrani B, Guinebretiere JM, et al. Ductal carcinoma in situ: MR imaging-histopathologic correlation. Radiology 1995; 196:415-419.
36. Arkani. MR imaging of Pure Ductal Carcinoma in situ (submitted).
37. Arkani. Parenchyma Presentation at ARRS.

Table 1: The average enhancement percentage at 1 minute (E_1) in ROI's placed on various areas of the mammary gland.

	E_1
Normal mammary gland	1.7%
Lymph Node	102%
DCIS	57%
Small Tumor	78%
Large Tumor	66%

Figure Captions:

Figure 1: Gland with small tumor: *i)* fixed excised gland attached to skin, *ii)* H&E superimposed on digital photograph, *iii)* FLASH GE MR image at ~ z=2. The mammary gland is outlined in pink in *i)* and *iii)*. Green arrows are used to point to the lymph node, and blue arrows to the small tumor in *ii)* and *iii)*. Based on *i)* and *ii)* the small tumor is located at ~ (z=2, x=8). Looking the axial MR slice corresponding to ~ z=2 in *iii)* the small tumor is at x=9.

Figure 2: Gland with DCIS: *i)* fixed excised gland attached to skin, *ii)* H&E superimposed on digital photograph, *iv)* FLASH GE MR image at ~ z=1. The mammary gland is outlined in pink in *i)* and *iii)*. Green arrows are used to point to the lymph node, and blue arrows to the DCIS in *ii)* and *iii).*Based on *i), ii),* and *iii)* the duct distended with DCIS is located at ~ (z=1, x=5). Looking the axial MR slice corresponding to ~ z=1 in *iii)* the DCIS appears at x=5.

Figure 3: Examples of FLASH GE with fat saturation images for a variety of DCIS lesions. Lymph nodes are marked with a thin arrow.

Figure 4: High spectral and spatial (HiSS) resolution image of the same axial slice as in Figure 2.

Figure 1: Gland with small tumor: *i)* fixed excised gland attached to skin, *ii)* H&E superimposed on digital photograph, *iii)* FLASH GE MR image at ~ ***z***=2. The mammary gland is outlined in pink in *i)* and *iii)*. Green arrows are used to point to the lymph node, and blue arrows to the small tumor in *ii)* and *iii)*. Based on *i)* and *ii)* the small tumor is located at ~ (***z***=2, ***x***=8). Looking the axial MR slice corresponding to ~ ***z***=2 in *iii)* the small tumor is at ***x***=9.

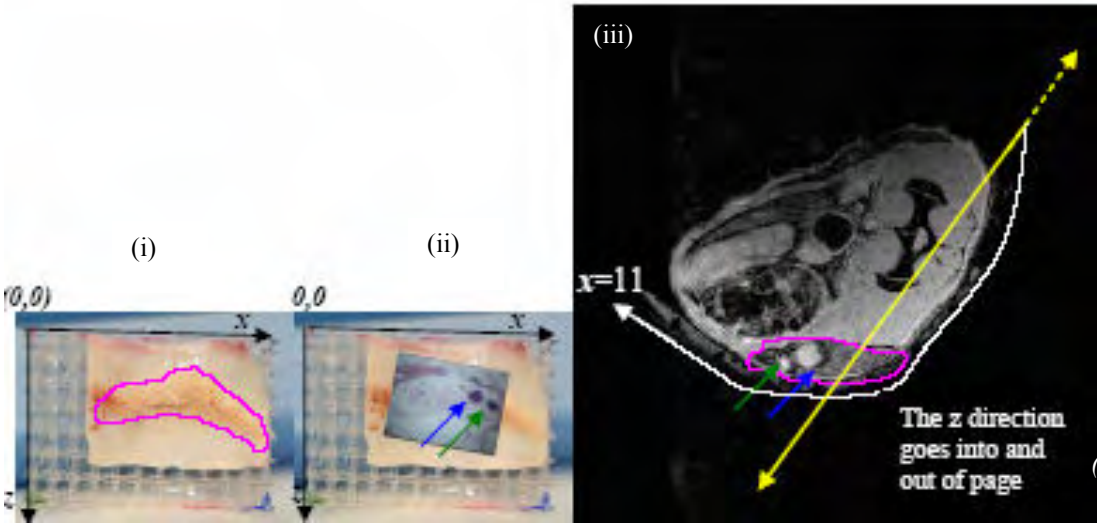

Figure 2: Gland with DCIS: *i)* fixed excised gland attached to skin*, ii)* H&E superimposed on digital photograph, *iv)* FLASH GE MR image at ~ z=1. The mammary gland is outlined in pink in *i)* and *iii)*. Green arrows are used to point to the lymph node, and blue arrows to the DCIS in *ii)* and *iii).*Based on *i), ii),* and *iii)* the duct distended with DCIS is located at ~ (z=1, x=5). Looking the axial MR slice corresponding to ~ z=1 in *iii)* the DCIS appears at x=5.

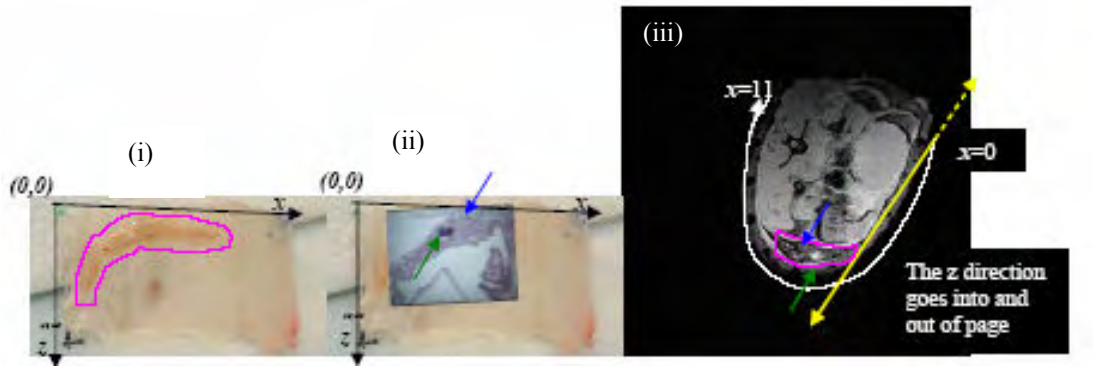

Figure 3: Examples of FLASH GE with fat saturation images for a variety of DCIS lesions. Lymph nodes are marked with a white arrow.

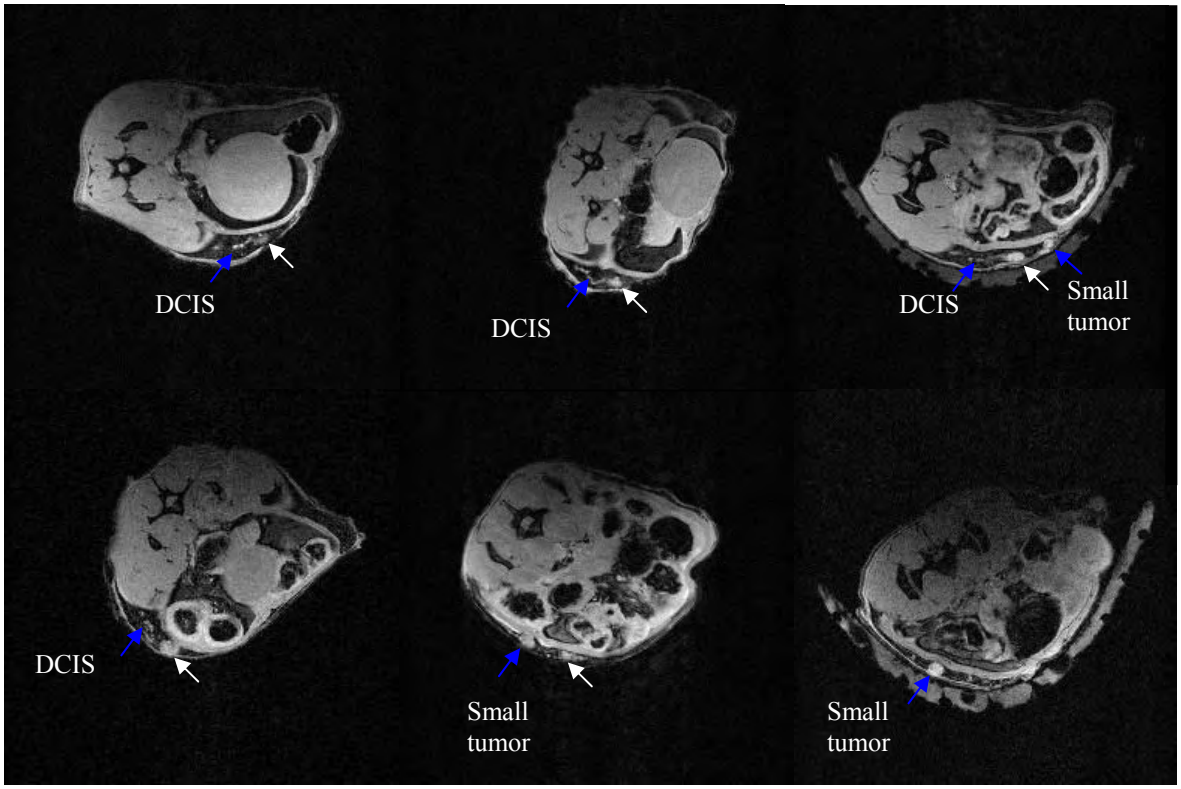

Figure 4: High spectral and spatial (HiSS) resolution image of the same axial slice as in Figure 2.

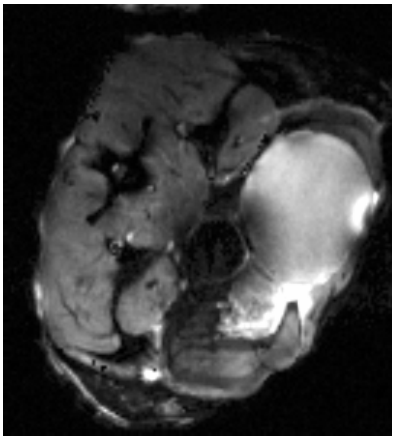

MR Imaging of Pure Ductal Carcinoma *in situ*: Kinetics, Morphology and Comparison with Mammographic Presentation and Nuclear Grade

Original Research

Advances in Knowledge:

1. A qualitative and quantitative evaluation of the morphology and kinetics of 79 pure ductal carcinoma in situ (DCIS) lesions on dynamic contrast enhanced magnetic resonance imaging (DCEMRI) shows that these lesions display a variety of kinetic curve types (persistent, plateau and washout). Compared with published data on invasive cancers, DCIS lesions enhance less, and attain their peak enhancement at a later time.

2. Enhancement kinetics varied significantly with x-ray mammographic appearance rather than nuclear grade. Lesions with fine pleomorphic, fine linear or fine linear branching calcifications, as well as those that appear as masses on x-ray mammography, have stronger washout curves compared to lesions with amorphous or indistinct calcifications.

3. The MRI morphology of pure DCIS lesions was predominantly non-mass, clumped or heterogeneous enhancement in a segmental or linear distribution. MRI lesion morphology did not vary significantly with either nuclear grade or x-ray mammographic presentation.

Implications for Patient Care:

1. Recognition and understanding of the unique morphology and kinetic characteristics of pure DCIS at MR imaging may improve the detection of early breast cancer.

Abstract

Purpose: To retrospectively compare the kinetic and morphologic characteristics of pure ductal carcinoma *in situ* (DCIS) lesions on dynamic contrast enhanced magnetic resonance imaging (DCEMRI) with lesion nuclear grade and x-ray mammographic appearance.

Materials and Methods: The University of Chicago Institutional Review Board approved our Health Insurance Portability and Accountability Act compliant retrospective study with waiver of informed consent. 78 patients with 79 histologically proven pure DCIS lesions were selected. Nuclear grade classification: 17 low, 26 intermediate, 30 high grade lesions and 6 unclassified. X-ray mammograms from 65 lesions were classified as: fine pleomorphic, fine linear or fine linear-branching calcifications (n=31), amorphous or indistinct (n=18), mass (n=10) and occult on x-ray mammography (n=6). Analysis of lesion morphology and kinetic curve shape was made according to the Breast Imaging Reporting and Data System (BI-RADS®) lexicon by one experienced radiologist. Initial enhancement percentage, time to peak enhancement (T_{peak}) and a measure of washout, the signal enhancement ratio (*SER*) were calculated for each lesion.

Results: 25% (20 of 79) and 44% (35 of 79) of pure DCIS lesions exhibited plateau and washout curves, respectively. Lesions with mass-like appearance on x-ray mammography exhibited more suspicious kinetics (T_{peak} =2 min) than lesions with amorphous or indistinct calcifications (T_{peak} =4.5 min). There was no statistically significant difference in enhancement kinetics across nuclear grade. Lesion morphology was predominantly non-mass, clumped or heterogeneous enhancement in a segmental or linear distribution.

Conclusion: Pure DCIS lesions exhibited washout, plateau and persistent curves. Enhancement kinetics varied with x-ray mammographic appearance rather than nuclear grade.

Introduction

Ductal carcinoma *in situ* (DCIS) comprises a heterogeneous group of lesions with variable genetic, biologic and histo-pathologic features. DCIS is generally considered to be a non-obligate precursor of invasive cancer with evidence to suggest that about 30-50% of cases will progress to become invasive(1). DCIS is typically detected on x-ray mammography as calcifications, although it may also appear mass-like in its non-calcified form (2-5). Accurate depiction of the extent of DCIS is essential for successful breast conservation treatment.

Dynamic contrast enhanced magnetic resonance imaging (DCEMRI) of the breast is being used in conjunction with other conventional diagnostic techniques for several clinical purposes. This includes pre-operative evaluation of extent and multifocality of malignancy (6) and post-treatment follow-up(7) . The advantage of DCEMRI is its high sensitivity (6, 8, 9). The contrast media uptake and washout—or kinetics—of invasive lesions typically rise rapidly and washout over time, while benign lesions tend to enhance more slowly and persistently take up contrast over time (10, 11).

There are relatively few prior reports of the appearance of pure DCIS at MR imaging and the kinetic and morphologic appearance of DCIS without evidence of microinvasion has not, as yet, been well characterized (12-14). The reported sensitivity of MRI for DCIS is 77%-96% (12, 15-20). Pure DCIS lesions most often present as non-mass, clumped enhancement in a segmental or linear distribution (13, 16), with mostly plateau or washout curves (12, 13, 16, 17, 21). Pure DCIS lesions therefore are thought to have less suspicious kinetic findings than

invasive cancers(16, 22). Various reports have indicated that low grade pure DCIS lesions show different kinetics than intermediate and high grade lesions (13, 22, 23), whereas others show no difference (15). The number of lesions studied in these prior reports has been relatively small (15-50 patients), and they have mostly focused on morphology and a qualitative kinetic analysis. Thus, the purpose of our study was to retrospectively compare the kinetic and morphologic characteristics of pure DCIS lesions on DCEMRI with lesion nuclear grade and x-ray mammographic appearance.

Materials and Methods

Patients

At this institution, it is a routine protocol to obtain breast MRI for diagnostic imaging, for evaluation of extent of disease, for post-treatment evaluation and for high risk screening. We maintain a clinical database that includes the MR morphologic and kinetic data for all lesions found. The final pathology for the lesions is also entered into the database. MRI and pathology findings for all patients are reviewed at a weekly interdisciplinary breast conference that includes radiologists, pathologists and surgeons. The University of Chicago Institutional Review Board approved our Health Insurance Portability and Accountability Act compliant retrospective study with waiver of informed consent. A review of 1770 records (January 2002-August 2005) yielded 78 women with 79 histologically proven pure DCIS lesions. The average patient age was 56, with a range of 31 to 86 years.

MRI Analysis

Dynamic Protocol: MR imaging was performed on a 1.5T GE Signa scanner (GE Healthcare, Milwaukee, WI) using a dedicated 4 channel breast coil (Invivo, Orlando, FL) with the patient in the prone position. Two protocols had been used. In the first, one pre and five post-contrast images were acquired in the coronal plane using a T_1-weighted 3D spoiled grass sequence (TR/TE= 7.7 msec/4.2 msec, flip angle 30 degrees, slice thickness of 3 mm and in plane resolution of 1.4 mm) with no fat saturation. The first post-contrast acquisition was started 20 seconds after contrast injection and the remaining images were acquired every 68 seconds. In

the second dynamic protocol there were three post-contrast acquisitions. The first two post-contrast acquisitions were obtained as before, followed by acquisition of high spatial resolution sagittal images for 128 seconds, and returning to a final dynamic, 68 second, acquisition. Gadodiamide (Omniscan; Nycomed-Amersham, Princeton, NJ) was injected intravenously at a dose of 0.1 mmol/kg followed by a 20 ml saline flush at the rate of 2.0 ml /sec. The following MR analysis was performed on subtraction images, viewed on a workstation.

Morphologic Analysis: One radiologist (GMN) with 14 years of breast MR experience retrospectively reviewed the images and classified lesion morphology. This analysis was not blinded to patient information or clinical history, but was performed without knowledge of nuclear grade or the x-ray mammographic classification (see below). Morphology was classified by viewing coronal, sagittal and axial reconstructed images. The type, shape, distribution, margins and internal enhancement pattern were assessed according to the Breast Imaging Reporting and Data System (BI-RADS® lexicon). In addition, the maximum extent of the lesion in the sagittal view was measured (Figure 1).

Enhancement Kinetic Analysis: After classifying the morphology, the same radiologist also performed a retrospective kinetic analysis. Using institutional software, the radiologist generated kinetic curves by manually tracing a region of interest (ROI) around the most enhancing part of the lesion as it appears on the first post contrast image in the coronal plane. The average ROI size was 6.3 pixels. A qualitative analysis of the curve shape was made by the radiologist according to the BI-RADS® lexicon by assessing its initial uptake (rapid, medium, slow) and delayed phase characteristics (persistent, plateau, washout). Quantitative kinetic parameters were

also derived from the curves. Percent enhancement (E_1, E_{peak}) and time to peak enhancement (T_{peak}) were measured for each curve as performed by Szabo et al (24). The signal enhancement ratio *SER* was calculated as a measure of washout as done by Esserman et al (25) (see Appendix for further details).

Histologic Classification

The histologic diagnosis of pure DCIS was based on initial review of final lumpectomy or mastectomy specimens, and decided by consensus opinion of two pathologists with 9 and 20 years of experience. There was no evidence for microinvasion and no axillary involvement in this population was found. Histologic classification of nuclear grade was available on 73 of 79 lesions (17 low, 26 intermediate and 30 high grade pure DCIS lesions, with 6 unclassified).

X-Ray Mammographic Classification

X-ray mammograms were available at this institution for 65 lesions and were retrospectively assessed by the same experienced radiologist by viewing diagnostic mammograms on film approximately 4 months after performing the MR morphologic and kinetic analysis. This analysis was not blinded to patient information, and the radiologist was aware of the pure DCIS diagnosis, but not the nuclear grade classification. In 49 of 65 lesions, calcifications were found and the morphology was classified according to the BI-RADS® lexicon as fine pleomorphic, fine linear, fine linear-branching, amorphous or indistinct (Figure 2 and Figure 3). The mammographic findings were divided into four groups: *i.*fine pleomorphic,

fine linear or fine linear-branching calcifications (31 of 65), *ii.*amorphous or indistinct calcifications (18 of 65), *iii*.non-calcified mass (10 of 65), and *iv.*occult (6 of 65).

Statistical Analysis

The 73 lesions with available histologic classification were classified according to nuclear grade (*i.*low, *ii.*intermediate, and *iii.*high) and the 65 lesions with mammographic data available were also classified (*i.*fine pleomorphic, fine linear or fine linear-branching calcifications, *ii.*amorphous or indistinct calcifications, *iii.*non-calcified mass, and *iv.*occult). The number of lesions with each kinetic and morphologic classification was determined for all 79 lesions and for each subpopulation. We compared the proportion of washout, plateau and persistent (or rapid, medium and slow) curves between lesions stratified by either nuclear grade or stratified by x-ray mammographic appearance, and to test for significance we used the pair-wise Pearson's χ^2 – test, with a p value of < 0.05 indicating statistical significance. We performed a similar analysis of the qualitative morphology variables, for example comparing the proportion of mass, non-mass and focus type enhancement between lesions stratified by either nuclear grade or stratified by x-ray mammographic appearance.

For each of the quantitative kinetic parameters (E_1, E_{peak}, SER, and T_{peak}) the mean and standard deviation of these parameters were calculated for all 79 lesions as well as the subpopulations of nuclear grade and mammographic classification. We performed a pair-wise comparison of the means of the kinetic parameters in each of these subpopulations, by using the Independent Samples t-test, with a p value < 0.05 indicating statistical significance.

We also determined the discrepancies in the *SER* vs. BI-RADS® assessment of washout as follows: for *SER* > 1.1 any curves classified as plateau or persistent were counted as inconsistent, and for *SER* between 0.9 and 1.1 any curves classified as persistent were counted as inconsistent (see Appendix for details).

Results

MR Findings

The dominant MR features of pure DCIS lesions were non-mass, clumped, heterogeneous or homogeneous enhancement, in a segmental or linear distribution (Table 1). 68 % (54 of 79) of the pure DCIS lesions showed rapid enhancement. The distribution of the delayed phase was more uniform, with 44% (35 of 79) showing washout type curves (Figure 4).

The average kinetic parameter values were (mean ± standard error on the mean): E_1= 188±15%, E_{peak}=242±16%, T_{peak}=212±13 s, SER=0.93±0.04._Based on this quantitative measure of washout, the kinetic curves of pure DCIS lesions exhibited a plateau relative to the first post-contrast point, on average. Overall, the quantitative and qualitative measures of washout were largely consistent. Of the 24 lesions with SER >1.1, 1 was classified as persistent, and 1 as plateau. Of the 17 lesions with an SER between 0.9 and 1.1, 1 was classified as persistent.

MR Findings Compared with Nuclear Grade

The MRI morphology for low, intermediate and high grade did not differ significantly from each other ($p > 0.24$ for all by χ^2 test). The classification of initial rise and delayed phase as well as the kinetic parameters E_1, $E_{peak,}$ SER and T_{peak} also did not differ significantly across the nuclear grades of pure DCIS ($p> 0.06$ for all by χ^2 or Independent Samples t test).

MR Findings Compared with Mammographic Appearance

The morphology on MRI of the four different mammographic classifications did not differ significantly ($p > 0.14$ for all by χ^2 test). Lesions with amorphous or indistinct calcifications were smaller on MRI, with an average size of 23 mm, than those with fine pleomorphic, fine linear or fine linear-branching calcifications, with an average size of 33 mm (p=0.048). The distributions of initial rise were statistically similar for all groups ($p > 0.42$ for all by χ^2 test). The χ^2 test demonstrated statistically significant differences in the distribution of the delayed phase curve types: 90 % (9 of 10) of lesions with a mass appearance on mammography exhibited washout type curves (Figure 5), compared with 45% (14 of 31) of lesions with fine pleomorphic, fine linear or fine linear-branching calcifications (p=0.041 by χ^2 test), and 22% (4 of 18) of lesions with amorphous or indistinct calcifications (p=0.002 by χ^2 test).

Some quantitative parameters also demonstrated a statistically significant difference (Table 2). The average *SER* value for lesions with amorphous or indistinct calcifications was 0.77, while the corresponding values for lesions with fine pleomorphic, fine linear or fine linear-branching calcifications and those with a mass like appearance on mammography were 0.95 and 1.34, respectively. Thus, based on these *SER* values, the kinetic curves of mass lesions strongly washout relative to the first post-contrast point, while the curves of lesions with fine pleomorphic, fine linear or fine linear-branching calcifications reach a plateau, and the curves of lesions with amorphous or indistinct calcifications continue to rise ($p < 0.05$). The average T_{peak} was 4.5 minutes for the amorphous or indistinct group, just under 3.5 minutes for the group with fine pleomorphic, fine linear or fine linear-branching calcifications, and just under 2 minutes for

the mass group ($p < 0.05$). The T_{peak} of mammographically occult lesions was 2.5 minutes, and significantly shorter than the amorphous or indistinct group (p=0.025). However, the enhancement kinetics of mammographically occult lesions did not differ significantly from other groups ($p > 0.39$ for all), although these lesions demonstrated the smallest enhancement percentages. 4 of the 6 occult lesions were high grade.

Discussion

In our study, we have found that pure DCIS lesions typically present with non-mass like, clumped and heterogeneous enhancement on MRI. In addition, DCIS lesions do not always exhibit typical malignant washout kinetic curves, and can show persistent and plateau curve types. Our findings were concordant with those reported in the literature (13, 16).

We have also established several quantitative kinetic parameters of 79 pure DCIS lesions. In a previous study with a similar acquisition timing, the reported initial enhancement percent E_1 for invasive and benign lesions was 273% and 163%, respectively(24). Here we have found that for pure DCIS lesions the average E_1 was 188% implying that pure DCIS lesions enhance less than invasive cancers and more than benign lesions. The reported T_{peak} for invasive and benign lesions was 173 and 430 seconds respectively, whereas our value here was 212 seconds—again an intermediate value between benign and malignant lesions(24). In Esserman et al, the average *SER* value for invasive lesions was 1.35—a strong washout relative to the first post-contrast point (25). Here we found a lower average value of 0.93—pure DCIS lesions plateau relative to the first post-contrast point.

Kinetic curve shape is related to the perfusion and diffusion of contrast media from blood vessels to the extracellular space—it is the unique physiology and vasculature of invasive, benign and pure DCIS lesions that ultimately explains the difference in kinetic curves noted above (26-28). It has been reported that perfusion rates increase from benign to DCIS to invasive cancers(22) and are associated with microvessel density in DCIS lesions(23). Guidi et

al showed an increase in vessel density around ducts with DCIS, although with variable patterns (29). Heffelfinger found that the expression of angiogenic growth factors (such as VEGF) increases from hyperplasia to DCIS(30, 31).

We found no significant difference in enhancement kinetics among different nuclear grades of pure DCIS. This supports previous findings by Viehweg et al (15). On the other hand, a few groups have demonstrated a difference between low grade pure DCIS and intermediate and high grade lesions. In one report (13), this may be due to the fact that 5 of the 12 low grade lesions considered in that paper did not enhance at all—in our study we only considered DCIS lesions with MRI enhancement. In other studies (22, 23), the numbers considered were perhaps too small for statistical significance (only 3 or 4 intermediate and high grade lesions).

To our knowledge, ours is the first report comparing x-ray mammographic appearance to contrast media uptake and washout in DCIS lesions. There has been recent interest in the possibility that x-ray mammographic presentation of breast lesions may be a prognostic indicator (32-36). Tabar et al recently reported that the survival outcomes of women with masses and linear/linear-branching, or "casting" calcifications, are considerably worse than other types of lesions, suggesting that these calcifications represent a duct forming invasive cancer (34). In our study, we found that lesions with fine pleomorphic, fine linear or linear-branching calcifications, and especially those that present as masses on x-ray mammography, are more suspicious by conventional kinetic standards on MRI, compared to lesions with amorphous or indistinct calcifications. In particular, DCIS lesions that appear as masses on mammography exhibit

typically malignant kinetic characteristics on average, with a short T_{peak} and strong washout (*SER*).

Esserman et al (25) studied the relationship between *SER* values of invasive tumors and tumor vascularity and histologic grade. They found that higher *SER* values were associated with higher vascularity and higher Scarff-Bloom-Richardson grade. In our report, the *SER* values were statistically equivalent for pure DCIS lesions of various grades. On the other hand, we found that *SER* values did vary by mammographic presentation. This suggests that x-ray mammographic appearance of pure DCIS may be related to its underlying physiology and biology in a way that nuclear grading is not.

There are several limitations to DCEMRI studies of the kind we have reported here, including placement and size of the ROI and performing quantitative analysis using signal intensity rather than contrast concentration leading to errors due to the variability of the native T_1 of the tissue. In addition, various institutions use different imaging protocols and pulse sequences, making comparisons of quantitative parameters across institutions problematic. Even at our institution we have used two protocols which may compromise the reliability of the kinetic parameters used. We have attempted to minimize this effect by considering parameters that depend on signal intensities measured at the initial and last time points (which are at similar times for both protocols).

There are further limitations of our study. MR and mammographic analysis was performed by one experienced radiologist and reviewed retrospectively. While the MR analysis

was performed without knowledge of the nuclear grade and mammographic classifications, this still raises the question of reproducibility. Although the radiologist performing these evaluations had 14 years of breast MR experience, it would be desirable to increase the number of readers and to perform a fully controlled, blinded study. In addition, we have not performed a detailed analysis of the pathology findings related to the imaging findings—for example comparing lesion extent on histology vs. imaging, as has been done elsewhere (20, 37, 38). With some preliminary conclusions in hand, we may now be in a better position to pursue a more detailed study, incorporating more lesions, more radiologists and improved pathology analysis.

The distinctive morphology of DCIS and the variable kinetic pattern may prompt some to suggest that MR acquisitions that emphasize spatial over temporal resolution are more sensitive to DCIS. Although spatial resolution is important (39), sufficient temporal resolution is also needed to distinguish the more slowly and moderately enhancing non-mass-like morphology of pure DCIS from enhancing parenchyma. While the diagnostic utility of kinetic descriptors may be compromised by the variable kinetic pattern of DCIS, understanding kinetics is important to improve the detection of these lesions. For example, the longer time to peak enhancement and the lower initial enhancement of pure DCIS lesions, should be considered in some CAD schemes where thresholds may be set too high and too early, and possibly run the risk of a false negative diagnosis. Conversely, setting thresholds too low may lead to more false positives and unnecessary biopsies—our results quantifying the enhancement kinetics may help to balance these tradeoffs.

In summary, we have found that the variable kinetic characteristics of pure DCIS lesions were not associated with nuclear grade. Rather, lesions with a mammographic presentation of pleomorphic, linear or linear-branching calcifications and soft tissue masses—as well as mammographically occult, or MR only, lesions—were more likely to exhibit plateau or washout characteristics than lesions with amorphous or indistinct calcifications, and may possibly represent more aggressive disease. Recognition and understanding of the unique morphology and kinetic characteristics of pure DCIS at MR imaging may improve the detection of early breast cancer.

Appendix

The *percent enhancement* measures the uptake of contrast in the lesion relative to the pre-contrast signal level,

$$E_1 = 100 \times \frac{S_1 - S_0}{S_0}$$

$$E_{peak} = 100 \times \frac{S_{peak} - S_0}{S_0},$$

where E_1 is the initial percent enhancement, E_{peak} is the peak percent enhancement, S_1 is the signal in the ROI at the first post contrast point, S_{peak} is the peak signal intensity and S_0 is the pre-contrast signal intensity in the ROI.

The *time to peak enhancement* (T_{peak}) is the time in seconds between the injection of contrast and the peak of the signal intensity vs. time curve.

The parameter used to quantify washout is the *signal enhancement ratio*, which is a measure of the relative signal decrease from the first post contrast time point to the final post contrast point,

$$SER = 100 \times \frac{S_1 - S_0}{S_{last} - S_0}.$$

Here, *SER* is the signal enhancement ratio and S_{last} is the signal intensity in the ROI at the last post contrast point. We can use the *SER* parameter to quantify the washout in the curve by choosing threshold values. A *SER* value of less than 0.9 means that the final signal intensity

increases relative to the first post-contrast point (persistent increase); a *SER* value between 0.9 and 1.1 indicates the final signal intensity is comparable to the first post-contrast point (plateau); a *SER* greater than 1.1 indicates that the final signal intensity decreases relative to the first post-contrast point (washout).

The *SER* measures washout relative to the first post contrast point, whereas the BI-RADS® assessment of delayed phase can involve any part of the kinetic curve. *SER* values > 1.1 correspond to washout relative to the first post contrast time point. Therefore, any curves with *SER* >1.1 that are classified as 'plateau' or 'persistent' are inconsistent. *SER* values between 0.9 and 1.1 correspond to a plateau relative to the first post contrast time point. Therefore, any curves with $0.9 < SER < 1.1$ that are classified as 'persistent' are inconsistent. Note that these curves could be classified as 'washout'—the curve may peak at the second post contrast point, for example, and washout from then on, but still plateau relative to the first post contrast time point. *SER* values < 0.9 correspond to a persistent increase relative to the first post contrast time point. Note that these curves could be classified as 'plateau' or 'washout' as well, depending on the curve data at other time points.

References

1. Recht A, Rutgers EJ, Fentiman IS, Kurtz JM, Mansel RE, Sloane JP. The fourth EORTC DCIS Consensus meeting (Chateau Marquette, Heemskerk, The Netherlands, 23-24 January 1998)--conference report. Eur J Cancer 1998; 34:1664-1669.
2. DiPiro PJ, Meyer JE, Denison CM, Frenna TH, Harvey SC, Smith DN. Image-guided core breast biopsy of ductal carcinoma in situ presenting as a non-calcified abnormality. Eur J Radiol 1999; 30:231-236.
3. Dershaw DD, Abramson A, Kinne DW. Ductal carcinoma in situ: mammographic findings and clinical implications. Radiology 1989; 170:411-415.
4. Ikeda DM, Andersson I. Ductal carcinoma in situ: atypical mammographic appearances. Radiology 1989; 172:661-666.
5. Stomper PC, Connolly JL, Meyer JE, Harris JR. Clinically occult ductal carcinoma in situ detected with mammography: analysis of 100 cases with radiologic-pathologic correlation. Radiology 1989; 172:235-241.
6. Boetes C, Mus RD, Holland R, et al. Breast tumors: comparative accuracy of MR imaging relative to mammography and US for demonstrating extent. Radiology 1995; 197:743-747.
7. Abraham DC, Jones RC, Jones SE, et al. Evaluation of neoadjuvant chemotherapeutic response of locally advanced breast cancer by magnetic resonance imaging. Cancer 1996; 78:91-100.
8. Bone B, Aspelin P, Bronge L, Isberg B, Perbeck L, Veress B. Sensitivity and specificity of MR mammography with histopathological correlation in 250 breasts. Acta Radiol 1996; 37:208-213.
9. Stomper PC, Herman S, Klippenstein DL, et al. Suspect breast lesions: findings at dynamic gadolinium-enhanced MR imaging correlated with mammographic and pathologic features. Radiology 1995; 197:387-395.
10. Kuhl CK, Schild HH. Dynamic image interpretation of MRI of the breast. J Magn Reson Imaging 2000; 12:965-974.
11. Kuhl CK, Mielcareck P, Klaschik S, et al. Dynamic breast MR imaging: are signal intensity time course data useful for differential diagnosis of enhancing lesions? Radiology 1999; 211:101-110.
12. Menell JH, Morris EA, Dershaw DD, Abramson AF, Brogi E, Liberman L. Determination of the presence and extent of pure ductal carcinoma in situ by mammography and magnetic resonance imaging. Breast J 2005; 11:382-390.
13. Neubauer H, Li M, Kuehne-Heid R, Schneider A, Kaiser WA. High grade and non-high grade ductal carcinoma in situ on dynamic MR mammography: characteristic findings for signal increase and morphological pattern of enhancement. Br J Radiol 2003; 76:3-12.
14. Fischer U, Westerhof JP, Brinck U, Korabiowska M, Schauer A, Grabbe E. [Ductal carcinoma in situ in dynamic MR-mammography at 1.5 T]. Rofo 1996; 164:290-294.
15. Viehweg P, Lampe D, Buchmann J, Heywang-Kobrunner SH. In situ and minimally invasive breast cancer: morphologic and kinetic features on contrast-enhanced MR imaging. Magma 2000; 11:129-137.
16. Van Goethem M, Schelfout K, Kersschot E, et al. Comparison of MRI features of different grades of DCIS and invasive carcinoma of the breast. Jbr-Btr 2005; 88:225-232.

17. Orel SG, Mendonca MH, Reynolds C, Schnall MD, Solin LJ, Sullivan DC. MR imaging of ductal carcinoma in situ. Radiology 1997; 202:413-420.
18. Gilles R, Zafrani B, Guinebretiere JM, et al. Ductal carcinoma in situ: MR imaging-histopathologic correlation. Radiology 1995; 196:415-419.
19. Shiraishi A, Kurosaki Y, Maehara T, Suzuki M, Kurosumi M. Extension of ductal carcinoma in situ: histopathological association with MR imaging and mammography. Magn Reson Med Sci 2003; 2:159-163.
20. Schouten van der Velden AP, Boetes C, Bult P, Wobbes T. The value of magnetic resonance imaging in diagnosis and size assessment of in situ and small invasive breast carcinoma. Am J Surg 2006; 192:172-178.
21. Groves AM, Warren RM, Godward S, Rajan PS. Characterization of pure high-grade DCIS on magnetic resonance imaging using the evolving breast MR lexicon terminology: can it be differentiated from pure invasive disease? Magn Reson Imaging 2005; 23:733-738.
22. Furman-Haran E, Schechtman E, Kelcz F, Kirshenbaum K, Degani H. Magnetic resonance imaging reveals functional diversity of the vasculature in benign and malignant breast lesions. Cancer 2005; 104:708-718.
23. Oshida K, Nagashima T, Ueda T, et al. Pharmacokinetic analysis of ductal carcinoma in situ of the breast using dynamic MR mammography. Eur Radiol 2005; 15:1353-1360.
24. Szabo BK, Aspelin P, Wiberg MK, Bone B. Dynamic MR imaging of the breast. Analysis of kinetic and morphologic diagnostic criteria. Acta Radiol 2003; 44:379-386.
25. Esserman L, Hylton N, George T, Weidner N. Contrast-Enhanced Magnetic Resonance Imaging to Assess Tumor Histopathology and Angiogenesis in Breast Carcinoma. Breast J 1999; 5:13-21.
26. Su MY, Cheung YC, Fruehauf JP, et al. Correlation of dynamic contrast enhancement MRI parameters with microvessel density and VEGF for assessment of angiogenesis in breast cancer. J Magn Reson Imaging 2003; 18:467-477.
27. Tuncbilek N, Unlu E, Karakas HM, Cakir B, Ozyilmaz F. Evaluation of tumor angiogenesis with contrast-enhanced dynamic magnetic resonance mammography. Breast J 2003; 9:403-408.
28. Buadu LD, Murakami J, Murayama S, et al. Breast lesions: correlation of contrast medium enhancement patterns on MR images with histopathologic findings and tumor angiogenesis. Radiology 1996; 200:639-649.
29. Guidi AJ, Fischer L, Harris JR, Schnitt SJ. Microvessel density and distribution in ductal carcinoma in situ of the breast. J Natl Cancer Inst 1994; 86:614-619.
30. Heffelfinger SC, Miller MA, Yassin R, Gear R. Angiogenic growth factors in preinvasive breast disease. Clin Cancer Res 1999; 5:2867-2876.
31. Heffelfinger SC, Yassin R, Miller MA, Lower E. Vascularity of proliferative breast disease and carcinoma in situ correlates with histological features. Clin Cancer Res 1996; 2:1873-1878.
32. James JJ, Evans AJ, Pinder SE, Macmillan RD, Wilson AR, Ellis IO. Is the presence of mammographic comedo calcification really a prognostic factor for small screen-detected invasive breast cancers? Clin Radiol 2003; 58:54-62.

33. Peacock C, Given-Wilson RM, Duffy SW. Mammographic casting-type calcification associated with small screen-detected invasive breast cancers: is this a reliable prognostic indicator? Clin Radiol 2004; 59:165-170; discussion 163-164.
34. Tabar L, Tony Chen HH, Amy Yen MF, et al. Mammographic tumor features can predict long-term outcomes reliably in women with 1-14-mm invasive breast carcinoma. Cancer 2004; 101:1745-1759.
35. Thurfjell E, Thurfjell MG, Lindgren A. Mammographic finding as predictor of survival in 1-9 mm invasive breast cancers. worse prognosis for cases presenting as calcifications alone. Breast Cancer Res Treat 2001; 67:177-180.
36. Zunzunegui RG, Chung MA, Oruwari J, Golding D, Marchant DJ, Cady B. Casting-type calcifications with invasion and high-grade ductal carcinoma in situ: a more aggressive disease? Arch Surg 2003; 138:537-540.
37. Esserman LJ, Kumar AS, Herrera AF, et al. Magnetic resonance imaging captures the biology of ductal carcinoma in situ. J Clin Oncol 2006; 24:4603-4610.
38. Kumar AS, Chen DF, Au A, et al. Biologic significance of false-positive magnetic resonance imaging enhancement in the setting of ductal carcinoma in situ. Am J Surg 2006; 192:520-524.
39. Harms SE. The use of breast magnetic resonance imaging in ductal carcinoma in situ. Breast J 2005; 11:379-381.

Table 1: Morphology distribution according to the BI-RADS® lexicon for pure DCIS lesions.

Morphology Classification			Pure DCIS lesions (n=79)	
			No.	% of Total
	Type	Mass	14	17.7%
		Non-Mass	64	81.0%
		Focus	1	1.3%
Mass Only	**Shape**	Round	2	2.5%
		Oval	1	1.3%
		Lobular	0	0%
		Irregular	11	13.9%
	Margin	Smooth	3	3.8%
		Irregular	11	13.9%
		Spiculated	0	0%
	Internal enhancement pattern	Homogeneous	7	8.9%
		Heterogeneous	7	8.9%
		Rim	0	0%
		Dark Internal Septations	0	0%
		Enhancing Internal Septations	0	0%
		Central	0	0%
Non-Mass Only	**Distribution modifiers**	Focal	13	16.5%
		Linear	19	24.1%
		Ductal	0	0%
		Segmental	26	32.9%
		Regional	5	6.3%
		Multiple regions	0	0%
		Diffuse	1	1.3%
	Internal enhancement pattern	Homogeneous	13	16.5%
		Heterogeneous	13	16.5%
		Stippled, Punctate	6	7.6%
		Clumped	32	40.5%
		Reticular, dendritic	0	0%
	Size	Average Sagittal size (mm)	29	±18
		Sagittal size < 20 mm	30	38.0%
		Sagittal size 20 -40 mm	28	35.4%
		Sagittal size > 40 mm	21	26.6%

Table 2: Kinetic parameters of pure DCIS lesions stratified by mammographic appearance (mean ± standard error on the mean).

	Fine Pleomorphic, Fine Linear, Fine Linear-Branching (n=31)	**Amorphous or Indistinct (n=18)**	**Occult (n=6)**	**Mass (n=10)**	***p* values Amorphous vs. Pleomorphic/ Linear**	***p* values Amorphous vs. Mass**	***p* values Pleomorphic/Linear vs. Mass**
E_1	204±28%	170±30%	152±40%	215±34%	----	----	----
E_{peak}	251±29%	242±32%	182±36%	247±39%	----	----	----
SER	0.95±0.06	0.77±0.07	0.89±0.14	1.34±0.19	0.05	0.002	0.01
T_{peak}	200±20 s	265± 25s	148±39 s	109±30 s	0.05	0.0008	0.03

Captions for Illustrations

Figure 1a: Sagittal T_1 weighted 3D SPGR (TR/TE= 7.7 msec/4.2 msec, flip angle 30 degrees, slice thickness of 3 mm and in plane resolution of 1.4 mm) subtraction image of a pure DCIS lesion.

Figure 1b: The corresponding kinetic curve generated by in house software.

Figure 2: Digital mammogram of the right breast ML view with spot magnification, demonstrating faint indistinct calcifications near clip.

Figure 3: Digital mammogram of the left breast ML view with spot magnification demonstrating linear branching calcifications.

Figure 4: The distribution of the qualitative BI-RADS assessment of initial rise (top) and delayed phase (bottom) for all pure DCIS lesions (n=79).

Figure 5: The distribution of the qualitative BI-RADS assessment of delayed phased for lesions based on x-ray mammographic presentation: i. amorphous or indistinct calcifications (n=18), ii. fine pleomorphic, fine linear, fine linear-branching calcifications (n=31), iii. mass (n=10), and iv. occult (n=6).

Figure 1a: Sagittal T_1 weighted 3D SPGR (TR/TE= 7.7 msec/4.2 msec, flip angle 30 degrees, slice thickness of 3 mm and in plane resolution of 1.4 mm) subtraction image of a pure DCIS lesion.
Figure 1b: The corresponding kinetic curve generated by in house software.

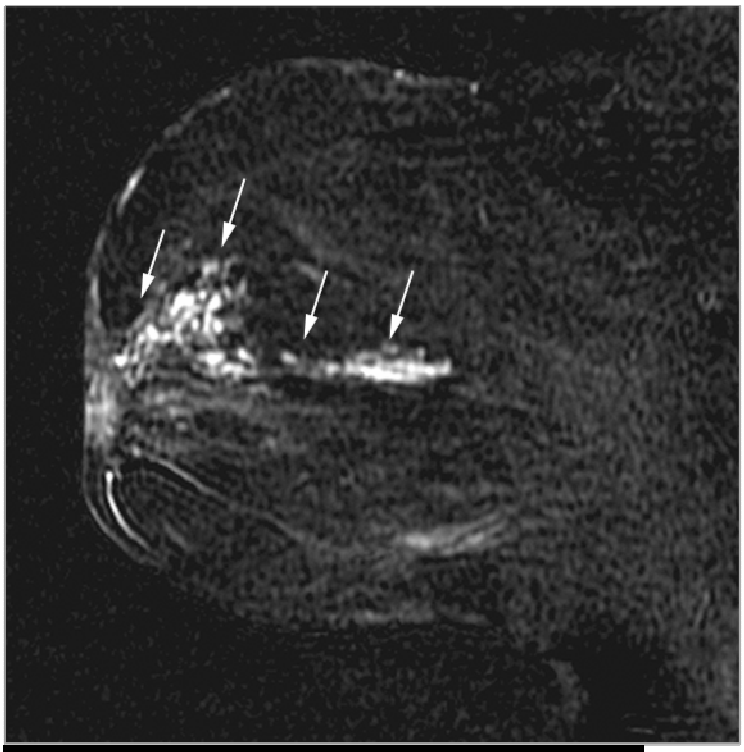

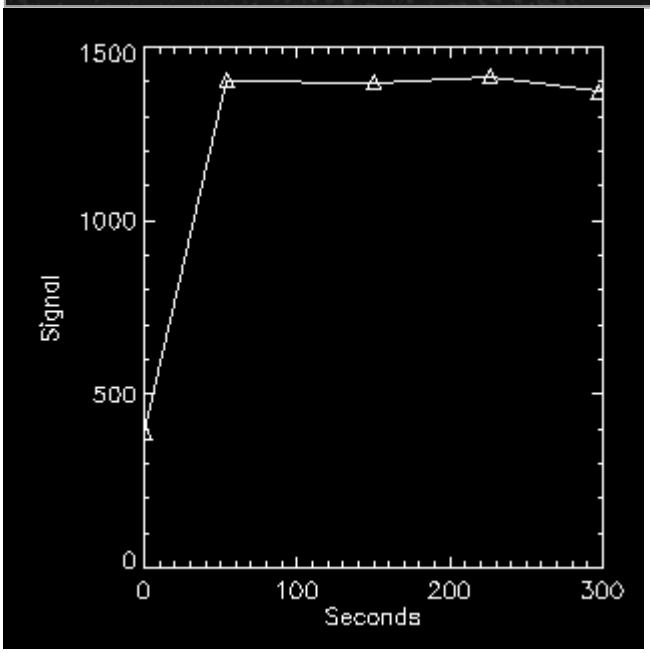

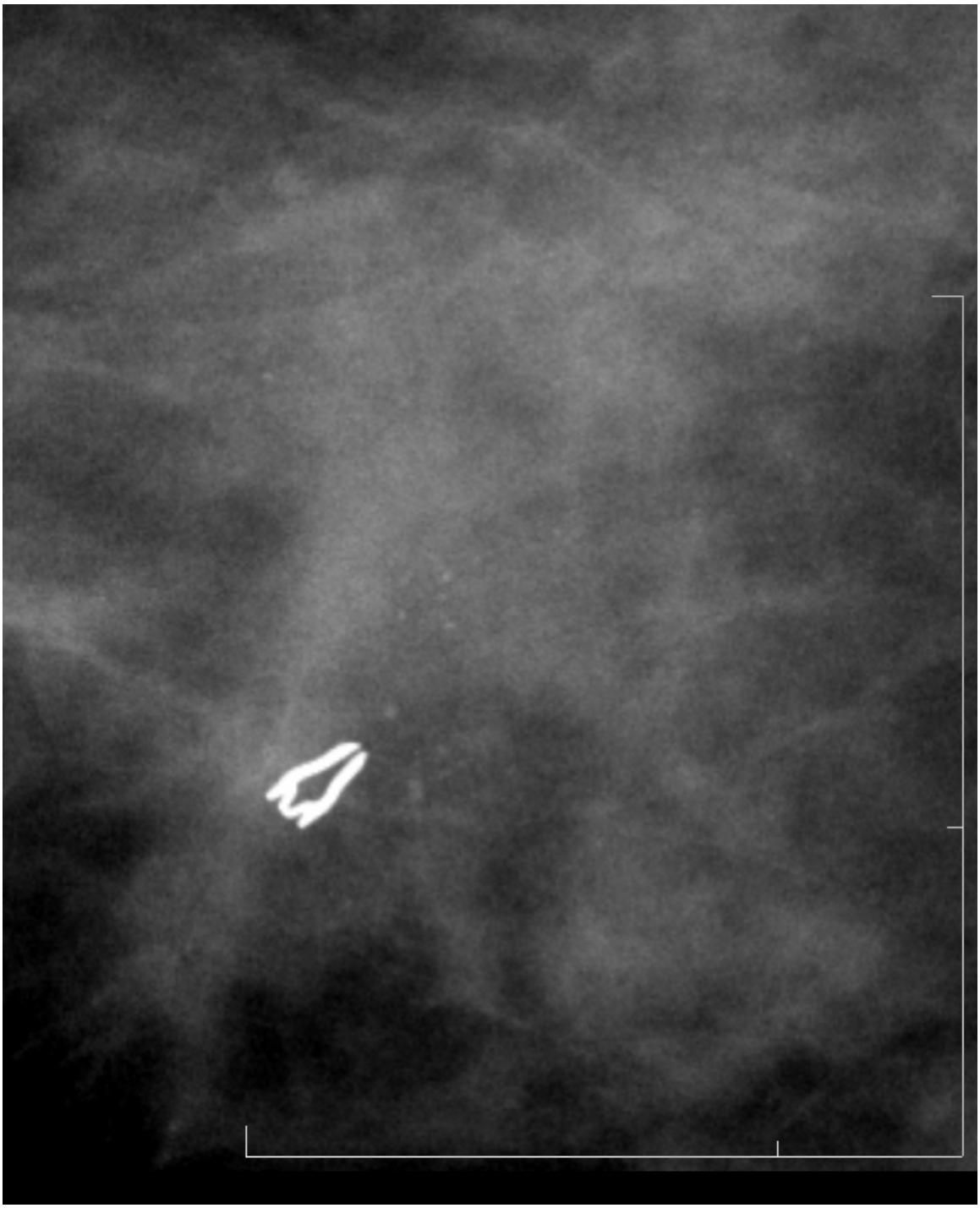

Figure 2: Digital mammogram of the right breast ML view with spot magnification, demonstrating faint indistinct calcifications near clip.

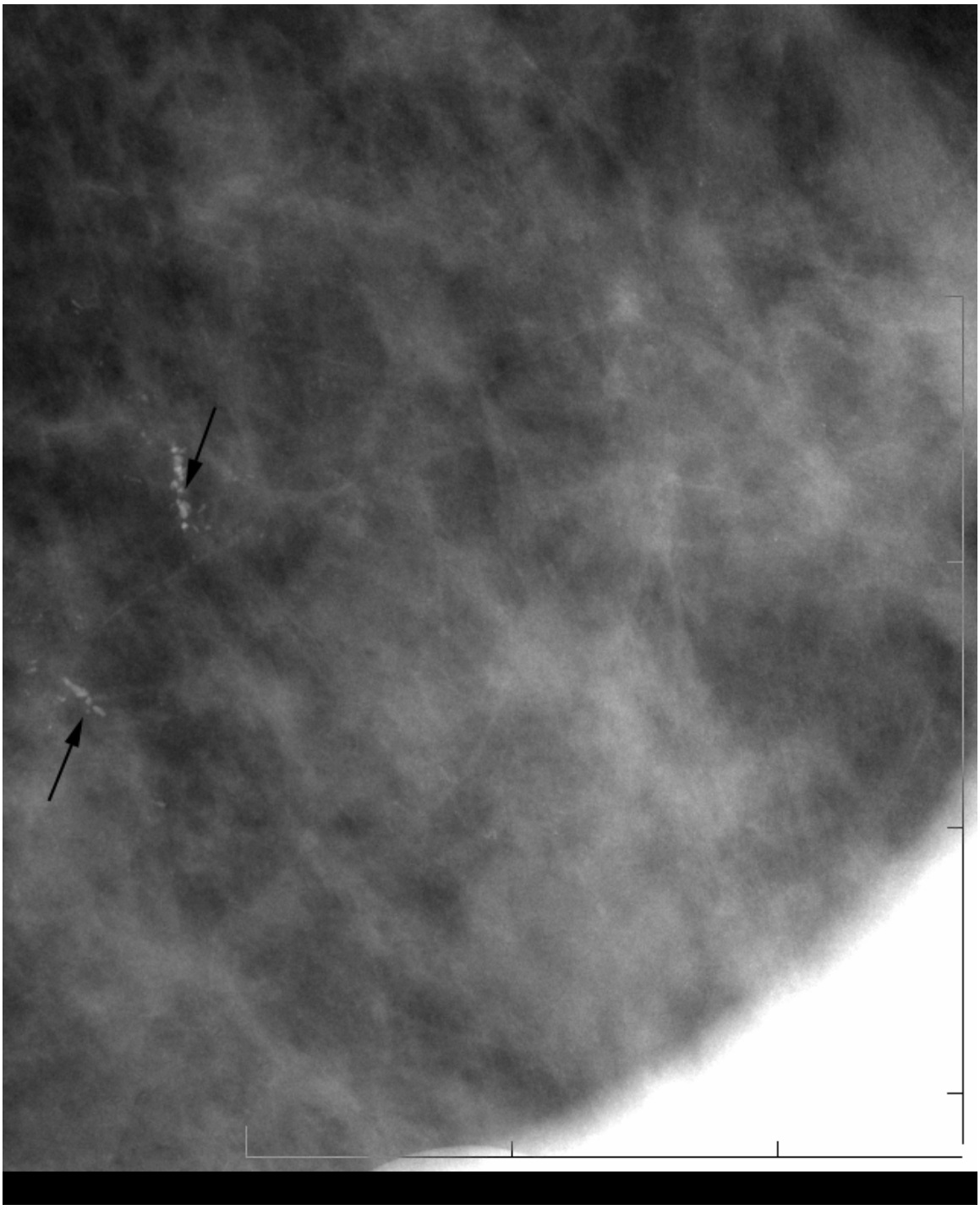

Figure 3: Digital mammogram of the left breast ML view with spot magnification demonstrating linear branching calcifications.

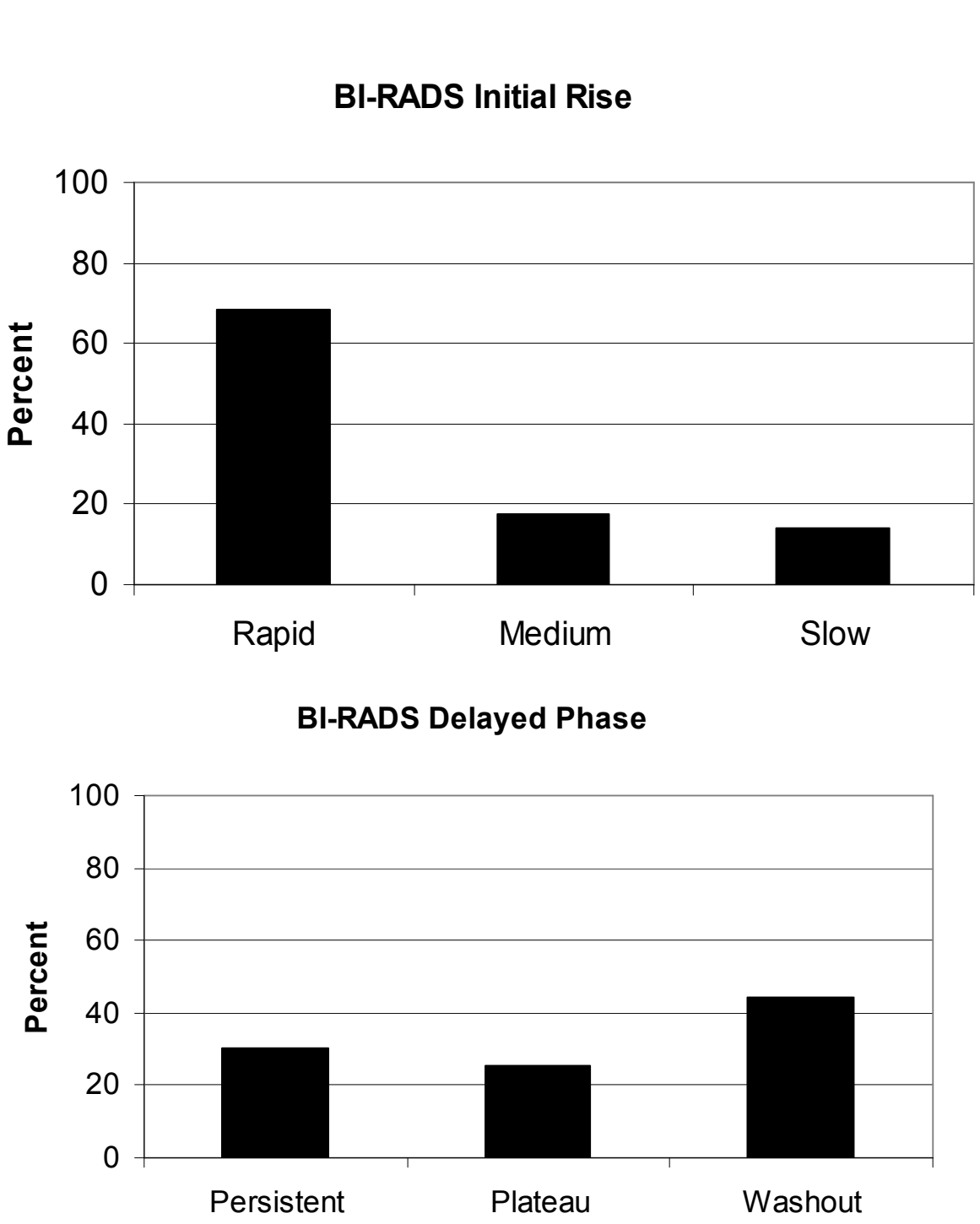

Figure 4: The distribution of the qualitative BI-RADS assessment of initial rise (top) and delayed phase (bottom) for all pure DCIS lesions (n=79).

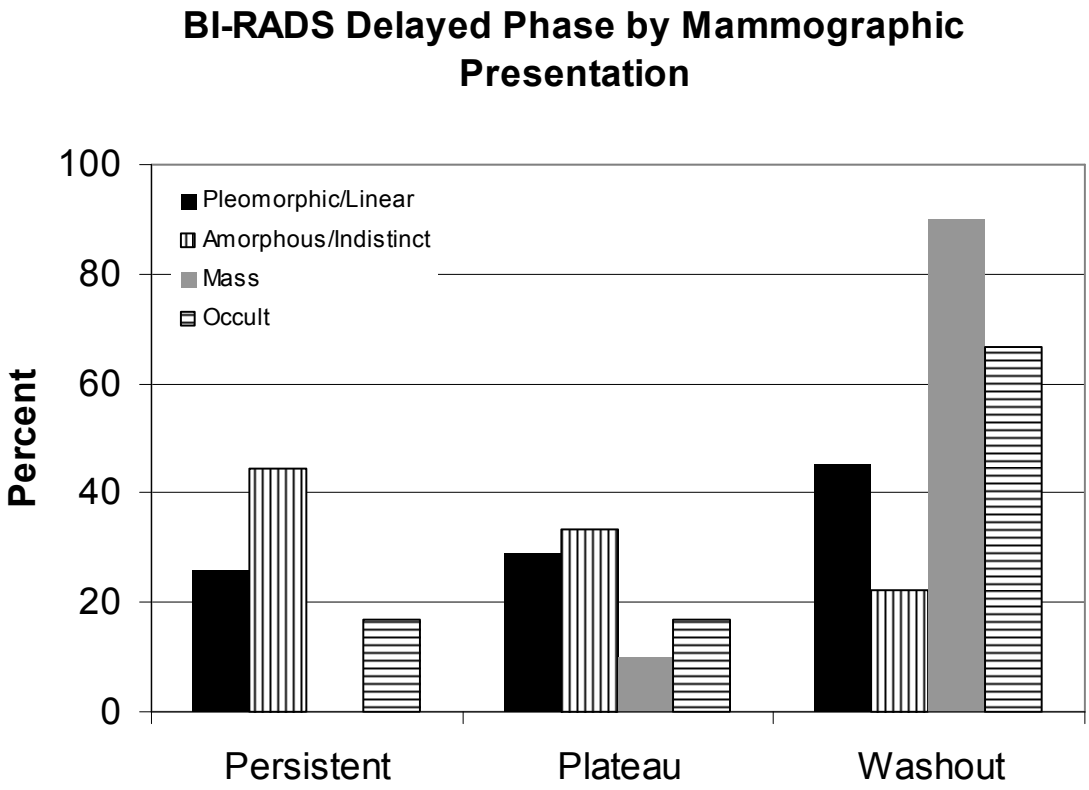

Figure 5: The distribution of the qualitative BI-RADS assessment of delayed phased for lesions based on x-ray mammographic presentation: i. amorphous or indistinct calcifications (n=18), ii. fine pleomorphic, fine linear, fine linear-branching calcifications (n=31), iii. mass (n=10), and iv. occult (n=6).

Differentiation between benign and malignant breast lesions detected by bilateral dynamic contrast enhanced MRI: A sensitivity and specificity study

Sanaz Arkani, Xiaobing Fan, Gregory S. Karczmar, Hiroyuki Abe, Robert A. Schmidt, and Gillian M. Newstead*

Department of Radiology, University of Chicago, Chicago, IL 60637

Submitted as a full paper to Magnetic Resonance in Medicine
Word count: 3736
Short running head: Differentiation Benign Malignant Breast Lesions DCEMRI

*Corresponding Author:

Gillian Newstead, M.D.
Professor
Department of Radiology
University of Chicago
5841 S. Maryland Ave, MC 2026
Chicago, IL 60637

Phone: (773) 702-2781
Fax: (773) 834-9047
Email: gnewstead@radiology.bsd.uchicago.edu

ABSTRACT

The purpose of this study was to apply an empirical mathematical model (EMM) to kinetic data acquired under a clinical protocol to determine if the sensitivity and specificity can be improved compared with qualitative BI-RADS® descriptors of kinetics. 3D DCEMRI data from 100 patients with 34 benign and 79 malignant lesions were selected for review under an IRB approved protocol. The sensitivity and specificity of the delayed phase classification was 91% and 18%, respectively. The EMM was able to accurately fit these curves. There was a statistically significant difference between benign and malignant lesions for several model parameters: the initial uptake rate, initial slope, signal enhancement ratio, and curvature at the peak enhancement (at least $p < 0.04$). These results demonstrated that EMM analysis provided at least the diagnostic accuracy of the kinetic classifiers described in the BI-RADS® lexicon, and offered a few key advantages. It can be used to standardize data from institutions with different dynamic protocols, and can provide a more objective classification with continuous variables so that thresholds can be set to achieve desired sensitivity and specificity. This suggests that the EMM may be useful for analysis of routine clinical data.

Key words: Malignant, Breast, DCEMRI, Sensitivity.

INTRODUCTION

Improvements in breast cancer detection are largely responsible for increasing survival among breast cancer patients (1). Dynamic contrast enhanced magnetic resonance imaging (DCEMRI) is being used in breast imaging for several purposes, including determining extent of malignant disease and post treatment evaluation (2,3). DCEMRI has a high sensitivity to breast cancer, with a lower specificity (4-6). When analyzing DCEMRI, the radiologist assesses both the lesion morphology and kinetics of contrast enhancement. Some studies have suggested that the morphologic information from DCEMRI is more diagnostically useful than the kinetic information (7,8), implying that there may be room for improvement in extracting more diagnostically relevant information from kinetic data.

Ideally, DCEMRI protocols would acquire data with high spatial and high temporal resolution, to fully exploit both the morphologic and kinetic information. Unfortunately, with currently available equipment and techniques, there is always trade off between spatial and temporal resolution in DCEMRI (7). As a result, the signal intensity vs. time—or kinetic—curves typically have only 4-7 data points (9,10) for 3D DCEMRI, which presents a challenge for differentiating benign from malignant lesions. To simplify analysis of the kinetic curves, radiologists qualitatively asses the initial rise and delayed phase according to the BI-RADS® lexicon. Several reports have demonstrated that DCEMRI data from malignant lesions tend to exhibit 'washout' curves, while benign lesions tend to show persistent signal increase with time after contrast injection (11,12). Some groups have performed semi-quantitative analysis of these curves—for example, calculating the time to peak enhancement—to better distinguish between the benign and malignant lesions (10). However, semi-quantitative parameters have limited use since they are susceptible to errors due to noise, and with varying timing of acquisitions across institutions, comparison of these parameters between institutions is problematic.

There have been several studies of pharmacokinetic compartment modeling on breast 3D DCEMRI data, to relate kinetic curves to the underlying physiology of the lesions (13-17). However, for low time resolution 3D DCEMRI data, the accuracy of physiological parameters

obtained from compartmental models is questionable. In addition these models require an arterial input function (AIF), which is difficult to estimate accurately. As an alternative to these approaches, mathematical equations can be used to fit the kinetic curves. For example, Heiberg et al. (18) used a fifth order polynomial to fit the kinetic curves (5-7 points), but the coefficients of polynomial did not show a significant difference between benign and malignant breast lesions. Recently, a 5-parameter empirical mathematical model (EMM) was developed to describe contrast uptake and washout behavior (19), and this model successfully distinguishes between benign and malignant lesions. Unfortunately, the EMM was performed with special protocols that allow acquisition of data with high temporal resolution, but are not clinically feasible (14,19). The limited temporal resolution in conventional 3D bilateral DCEMRI implies that complicated mathematical models cannot be directly applied to kinetic curves to obtain a unique solution.

In this study, a modified EMM with only three parameters was used to analyze 3D bilateral DCEMRI breast data that was acquired according to clinical protocols, with sparse time resolution of 68 seconds. Primary model parameters were determined by fitting the curves to the modified EMM. Secondary diagnostic parameters, such as initial area under curve ('$\mathbf{AUC_{30}}$')(20,21), initial slope of enhancement ('$\mathbf{Slope_{ini}}$')(10,20,22), the time to peak enhancement ('$\mathbf{T_{peak}}$')(10), signal enhancement ratio ('**SER'**)(23), and enhancement curvature at peak ('$\boldsymbol{\kappa_{peak}}$') (24) were derived mathematically from the primary parameters after fitting the kinetic curves. The sensitivity and specificity to malignant lesions using these parameters was also evaluated by using receiver operating characteristic (ROC) analysis, and was compared to the kinetic curve classification according to the BI-RADS® lexicon.

METHODS

Patients

Diagnostic MR imaging is performed at this institution routinely for several clinical purposes: diagnostic imaging, evaluating extent of known disease, post-treatment and surgical evaluation and as a screening tool in high risk women. Bilateral 3D DCEMRI data from 100 female patients was acquired consecutively between May 2002 and June 2003 and reviewed for study under an Institutional Review Board approved protocol, with informed consent waived and under full HIPAA compliance. The age range of the subjects was 24 to 81 years (mean age = 56.2 ± 13.3 years). Based on the consensus opinion of two experienced pathologists, there were 34 benign and 79 malignant lesions used in this study.

MR Imaging

MR imaging was performed on a 1.5T GE Signa scanner (GE Healthcare, Milwaukee, WI) using a dedicated 4 channel breast coil (Invivo, Orlando, FL) with the patient in the prone position. One pre and five post-contrast images were acquired in the coronal plane using a 3D T_1-weighted spoiled grass sequence (TR/TE = 7.7/4.2 msec, flip angle = 30˚, slice thickness = 3 mm, and in plane resolution = 1.4 mm), without fat saturation. The first post-contrast acquisition was started 20 seconds after contrast injection and the remaining images were acquired every 68 seconds. Gadodiamide (Omniscan; Nycomed-Amersham, Princeton, NJ) was injected intravenously at a dose of 0.1 mmol/kg followed by a 20 ml saline flush at the rate of 2.0 ml /sec.

All kinetic analysis was performed by experienced radiologists by using coronal and reconstructed axial and sagittal views to assess the lesion. To generate the kinetic curve, the radiologist traced a small region of interest (ROI) around what was perceived to be the most enhancing part of the lesion on the first post-contrast image. The average ROI size was 7.1 pixels. The plot of signal intensity vs. time for this ROI was assessed by the radiologist according to the BI-RADS® lexicon for initial rise (rapid, medium, slow) and delayed phase (persistent, plateau, washout).

Modified Empirical Mathematical Model

The kinetic curve obtained above was analyzed quantitatively using the modified empirical mathematical model (EMM)(24) First, the average DCEMRI signal intensity as a function of time ($S(t)$) in the selected ROI was calculated. Then the signal changes before (S_0) and after contrast injection (S_n, n = 1, …, 5) were calculated as: $\Delta S = (S_n - S_0)/S_0$. The following modified EMM was used to describe the lesion contrast uptake and washout and to fit the data:

$$\Delta S(t) = A \cdot \left(1 - e^{-\alpha t}\right) \cdot e^{-\beta t}, \qquad [1]$$

where A is the upper limit of the signal intensity, α (min^{-1}) is the rate of signal increase, β (min^{-1}) is the rate of the signal decrease during washout. The goodness of fit parameter R^2 was calculated for each lesion. The reason the EMM uses signal intensity rather than contrast concentration is that we would like to analyze the data in a way that is similar to conventional clinical practice, and would also like to minimize noise amplification.

Derived Diagnostic Parameters

Semi-quantitative diagnostic parameters used commonly in the literature were easily derived from the modified EMM parameters. After some simple mathematical manipulations, we obtained the following derivations for diagnostic parameters:

(a) **Initial area under curve ('AUC_τ'):** The 'AUC_τ' can be calculated by integration of the kinetic curve, i.e.:

$$\mathrm{AUC}_\tau = A \cdot \left[\left(1 - e^{-\beta\tau}\right) \Big/ \beta + \left(e^{-(\alpha+\beta)\tau} - 1\right) \Big/ (\alpha+\beta) \right], \qquad [2]$$

where τ is the time over which signal intensity was integrated. In this study we used τ = 30 seconds.

(b) **Initial slope of enhancement ('$Slope_{ini}$'):** The initial slope of kinetic curve can be calculated by taking derivative of Eq. [1] at initial time $t << 1$:

$$Slope_{\text{ini}} \approx A\alpha\,. \qquad [3]$$

(c) **Time to peak of enhancement ('T_{peak}'):** The time at which the kinetic curve reached peak can be solved by setting the derivative of Eq. [1] equal to zero:

$$T_{\text{peak}} = \frac{1}{\alpha}\log\left(1+\frac{\alpha}{\beta}\right). \qquad [4]$$

Please notice that when $\beta \leq 0$, the curves did not reach the peak within the duration of the experiment. In these cases, we used the last point as the peak intensity.

(d) **Signal enhancement ratio ('SER')**: The signal intensity changes at the first time point (ΔS_1) relative to the last time point (ΔS_L) was used to calculate the '**SER'** using the following formula:

$$SER = \frac{\Delta S_1}{\Delta S_L} = \frac{1-e^{-\alpha t_1}}{1-e^{-\alpha t_L}} \cdot e^{(t_L - t_1)\beta}\,, \qquad [5]$$

where t_1 = 60 s and t_L = 300 s used in this study. A '**SER'** value greater than 1.1 indicates the signal intensity decreases with respect to its value at 60 seconds; '**SER**' less than 0.9 indicates that signal intensity continues to rise; and '**SER**' between 0.9 and 1.1 represents a plateau relative to intensity at 60 seconds.

(e) **Enhancement curvature at peak ('κ_{peak}'):** The curvature at the peak of enhancement was calculated from the definition of curvature formula at time of 'T_{peak}':

$$\kappa_{peak} \approx -A\alpha\beta\,. \qquad [6]$$

Data analysis and Statistical evaluation

For the qualitative evaluation according to the BI-RADS® lexicon, distributions of initial rise and delayed phase were determined for benign and malignant lesions. To compare these distributions the chi-squared (χ^2) test was used, with a p value < 0.05 indicating statistical significance.

The 3D bilateral DCEMRI data were processed using software written in IDL (Research Systems, Inc., Boulder, CO). The average values of diagnostic parameters over all benign and malignant lesions were calculated. In addition, the benign and malignant lesions were further divided into pathologic subtypes. For malignant lesions these subtypes were: invasive ductal carcinoma (IDC), ductal carcinoma in situ (DCIS), invasive lobular carcinoma (ILC) and other. For benign lesions these subtypes were: fibrocystic change (FCC), fibroadenoma, papilloma and other. Two-tailed unequal variance Student's t-tests were performed to evaluate which parameters showed significant differences between the benign and malignant breast lesions, with a p value < 0.05 indicating statistical significance.

In order to determine whether modified EMM parameters varied within pathologic subtypes of benign and malignant lesions (for example, if the parameter 'α' varied significantly among DCIS, ILC and IDC lesions) ANOVA calculations were used, with a p value < 0.05 indicating statistical significance. The ANOVA analysis was performed on the three classified subtypes of malignant lesions (DCIS, ILC and IDC) and the three classified subtypes of benign lesions (fibroadenoma, papilloma and FCC). Receiver operating characteristic (ROC) analysis was performed to compare the diagnostic capability of the parameters derived from the modified EMM with the diagnostic performance of the qualitative BI-RADS® categories of initial rise and delayed phase. ROCKIT software (ROCKIT 0.9B Beta Version, Charles E. Metz, University of Chicago(25)) was used to generate the ROC curves and perform statistical comparisons between them via the bivariate and area test.

RESULTS

BI-RADS® Classification

The distribution of initial uptake and delayed phase for all lesions as well as the breakdown of benign and malignant lesions into pathology subtypes is shown in Table 1. Malignant and benign lesions did not have statistically significantly different distributions of initial rise, but differed in delayed phase distribution with 65% and 38% showing 'washout' curves, respectively (p = 0.03). Similarly, DCIS and IDC lesions were significantly different in delayed phase, with 50% and 78% showing 'washout', respectively (p = 0.04). Considering 'washout' and 'plateau' to be indicative of malignancy (10,12) the sensitivity and specificity were 91% (95% confidence interval (CI) 83-96%) and 18% (95% CI 7-35%), respectively. For initial phase criteria, considering 'rapid' to be indicative of malignancy, the sensitivity and specificity were 89% (95% CI 79-95) and 26% (95% CI 13-44%), respectively. In most prior studies of the kinetics of benign and malignant lesions, only IDC lesions were considered (10,12). When considering only the IDC lesions, the sensitivity of 'washout' and 'plateau' as described in the BI-RADS® lexicon improved to 97% (95% CI 85-100%), and the sensitivity of 'rapid' improved to 92% (95% CI 78-98%).

Modified EMM parameters

The modified EMM was able to accurately fit the curves, with a goodness of fit parameter R^2 greater than 0.90 for all cases studied here. Some typical examples of the modified EMM fits are shown in Fig. 1 for various benign (top row – FCC, fibroadenoma, and papilloma) and malignant lesions (bottom row - DCIS, IDC, and ILC). The distribution of the primary parameters for all the sub-categories of benign and malignant lesions is shown in Fig. 2. Upon visual inspection, substantial over lap between benign and malignant lesions was evident for the EMM parameters. After fitting all the kinetic curves, the five derived diagnostic parameters were calculated using the Eqs. [2-6].

The average values of all primary and derived parameters were calculated and are summarized in Table 2. From calculated averaged parameters, it can be seen that malignant lesions had significantly faster contrast uptake ('**α'**), steeper initial slope ('**Slope$_{ini}$'**), larger enhancement ratio (**'SER'**) and sharper curvature ('**κ_{peak}'**) than benign lesions. Two tailed unequal variance t-test showed that there was a statistically significant difference between benign and malignant lesions for the parameters of contrast uptake rate '**α'** ($p < 0.03$), initial slope '**Slope$_{ini}$'** ($p < 0.04$), signal enhancement ratio '**SER'** ($p < 0.0007$), and the curvature at the peak '**κ_{peak}**'($p < 0.02$). To evaluate diagnostic performance, ROC curves were generated for all parameters, with calculated 'A_z' values shown in Fig. 3. '***A'*** had the smallest area under ROC curve ('**A_z'**), while **'SER'** had the largest. The ROC curves for the two parameters (Fig. 4) with the largest **'A_z'** values, '**α'** (blue line with solid square) and '**SER',** (red line with solid circle) are statistically equivalent under the bivariate and area test. From these ROC curves we can see that at a sensitivity of ~90% the specificity was ~20-30%, which was within the CI of the specificity achieved with the BI-RADS delayed phase and initial rise descriptors.

It is interesting to study further the kinetic properties of the subtypes of benign and malignant lesions. The calculated average values showed that the primary as well as diagnostic parameters for FCC were very similar to DCIS, which contributed to the majority of the overlap between the benign and malignant lesions. Performing t-test comparisons between these groups (DCIS vs. FCC) yields statistical equivalence ($p > 0.063$ for all parameters). On the other hand, the contrast uptake and washout rates for IDC were much faster than benign lesions. As a result, IDC lesions had the largest '**AUC$_{30}$'**, deepest '**Slope$_{ini}$'**, highest '**SER'** and sharpest '**κ_{peak}'**. In addition, for all primary and derived parameters there was a statistically significant difference (at least $p < 0.02$) between IDC and DCIS lesions. This suggests that the diagnostic accuracy of the modified EMM parameters may be improved if we consider only IDC lesions. To explore this, Fig. 4 also shows ROC curves (lines with open symbols) for '**α'** and '**SER'** when testing benign vs. IDC lesions only. As shown in the figure, these ROC curves demonstrate considerable improvement in the **'A_z'** values compared to their benign vs. all malignant lesions counterparts. At a sensitivity of ~95% the specificity was ~10-30%, which was within the CI achieved with the BI-RADS® classifications.

Finally, ANOVA analysis was used to study the variation of the primary and derived parameters within benign and malignant sub-categories. Three parameters (‘**α’, ‘T_{peak}’**, **‘SER’**) varied significantly by subtype for benign lesions ($p < 0.03$ for all), whereas all but one (‘***A*’, ‘α’, ‘T_{peak}’, ‘AUC_{30}’, ‘$Slope_{ini}$’**, **‘κ_{peak}’**, ‘**SER’**) varied significantly for malignant subtypes ($p < 0.007$ for all).

DISCUSSION

In this study we found that 68% of malignant curves exhibited 'washout', which is similar to prior reports, however 38% of benign curves also showed 'washout', which is higher than many reports (12). This may be because the benign lesions considered in this study were histologically proven benign — in other words, these lesions were suspicious enough to warrant biopsy. Since most obviously benign lesions have 'persistent' type curves and would not be sent to biopsy, this may skew the delayed phase distribution in this study away from the 'persistent' curve type. Szabo et al (10) considered only histologically proven benign lesions, and found that 24% of benign lesions showed 'washout' type curves, a value closer to the one presented here. Because of the large number of benign lesions with 'plateau' and 'washout' type curves in this study, using these descriptors from the BI-RADS® kinetic classification provided high sensitivity and low specificity in diagnosing malignant lesions.

The results demonstrated that the modified EMM fit the 3D DCEMRI data very well, for all cases. All the secondary diagnostic parameters could be easily calculated from the EMM parameters. Thus, we were able to calculate parameters, such as '$\mathbf{AUC_{30}}$' and 'κ_{peak}', which could not be calculated directly from kinetic data comprised of only 6 points. The sensitivity and specificity of the BI-RADS® delayed phase and initial rise classifications were 89-91% and 18-26%, respectively. Using the primary model parameter 'α' and the derived parameter '**SER**', at ~90 % sensitivity the specificity was ~20-30%, which was statistically equivalent to the corresponding BI-RADS results. However, unlike the BI-RADS® classification, the EMM can be used to achieve a continuous spectrum of sensitivity and specificity. For example, at a sensitivity of ~80% the specificity was ~40%.

The diagnostic accuracy of the model parameters may be compromised by the relatively large number of DCIS and ILC lesions in this study, which showed significant overlap with benign lesions. Indeed, most other studies usually focus only on IDC lesions. We found that when considering benign vs. IDC lesions only, the 'plateau' and 'washout' descriptors from the BI-RADS® lexicon had sensitivity and specificity of 97% and 18%, respectively. Similarly, the

'rapid' descriptor from the BI-RADS® lexicon had sensitivity and specificity of 92% and 26%, respectively. The corresponding values for '**α**' and '**SER**' were comparable to the BI-RADS® results. However, at a reasonable sensitivity of ~80%, the specificity of the model parameters improved greatly to ~60%.

The significant overlap of DCIS lesions with benign lesions may be related to similarities in the underlying biology and vasculature(26,27). Because DCIS is the earliest form of malignant breast disease, improving the detection of DCIS is important, and further investigation into the presentation of DCIS would be interesting. The ANOVA results in this study indicate that most of the modified EMM parameters varied significantly across the sub-types of DCIS, ILC and IDC. Uptake and the sharpness and magnitude of washout tended to increase from DCIS to ILC to IDC. DCIS and IDC lesions showed the most difference in all parameters, with DCIS lesions having on average a much longer time to peak enhancement (3.6 minutes) compared with IDC lesions (2 minutes). On the other hand, only three parameters ('**SER'**, '$\mathbf{T_{peak}}$**', 'α'**) showed significant variations among benign lesions; fibroadenomas exhibited a smaller uptake rate and much longer time to peak enhancement than papillomas.

The modified EMM does not make assumptions about the underlying physiology of the lesion. Some assumptions required by two compartment or multi compartment models (14) can lead to fitting errors and subsequent diagnostic errors. On the other hand, this lack of direct correspondence to identifiable physiologic or anatomic features is also the main disadvantage of the modified EMM approach. This problem can be addressed by deriving equations that connect parameters of the modified EMM to physiologic and anatomic parameters associated with various models (i.e. two or more compartment models). The parameters '***A***', '**α**', and '**β**' in the modified EMM can be directly compared with two compartment models described in Eqs. [13-16] of Armitage et al (28). For example to compare the EMM with the Tofts model described in Eq. [13] of Armitage et al, it can be seen that the $\boldsymbol{A} = Dv_eK^{trans}/V_p(K^{trans} - k_{out}v_e)$, $\boldsymbol{\beta} = k_{out}$, and $\boldsymbol{\alpha} + \boldsymbol{\beta} = K^{trans}/v_e$, where D is the dose of administered contrast agent, v_e is the extravascular extracellular space volume fraction, K^{trans} is the transfer constant, V_p is the volume of the plasma,

and k_{out} is rate constant for contrast media elimination. With such relationships, the empirical model can be related to a physiologically motivated model.

There are other limitations to this study:

- Sparse sampling may result in fitting errors. In particular, prior work has suggested that high temporal resolution was required to sample the kinetic curve uptake and transition part of uptake and washout accurately(24)

- Pre-clinical studies suggest that specificity is improved when the tail of the washout curve is sampled for at least 15 minutes; the curves studied here are truncated at about 6 minutes (19)

- Using signal intensity rather than contrast concentration may result in errors due to variability of the native T_1 of the tissue. However, in the present application of the EMM we used signal intensity rather than contrast concentration to follow conventional clinical practice, and to minimize noise amplification.

- The present model does not incorporate an AIF and this omission can introduce variability and systematic error. The model can be modified to accommodate an AIF but this was not done in the data analysis presented here in order to minimize error propagation. Future work will focus on deconvoluting the AIF from the EMM fits to data without amplifying noise.

- To characterize the kinetics of the lesion, only a small ROI was used and this results in lower SNR.

- Although the total number of lesions studied was relatively large, when considering subtypes of benign and malignant lesions (such as fibroadenoma, or ILC) only a few cases were found, raising the issue of statistical validity.

Despite the shortcomings summarized above, these results show that in our patient group, analysis of conventional 3D DCEMRI data with the EMM provides at least the diagnostic accuracy of qualitative kinetic parameters described in the BI-RADS® lexicon, and offers a few key advantages. It can be used to standardize kinetic data between institutions—currently, when radiologists are presented with an outside MRI for evaluation, there is no way to relate the

kinetic findings of the outside case to experience at the home institution. For example, if MR images at the outside institution are acquired every 90 seconds, and at the home institution the dynamic protocol acquires images every 60 seconds, the EMM can be used to present the outside kinetic data with 60 second time resolution. The EMM can be automated and can provide a more objective classification, including rapid and accurate pixel-by-pixel analysis to allow assessment of the spatial distribution of kinetic parameters. It provides continuous variables so that thresholds can be set to achieve desired sensitivity and specificity. It also offers an opportunity to relate semi-quantitative parameters (such as '**SER'**) to more fundamental EMM parameters. More importantly, this model allows for more flexibility in improving sensitivity and specificity in the future by using combinations of variables, corrections for arterial input functions and relating parameters directly to underlying physiological quantities. This model may become valuable as new protocols are being implemented at higher field strength and become more available. With the development parallel imaging techniques, it is now possible to acquire images with relatively high spatial resolution while still acquiring 6 or 7 kinetic data points. Thus, optimizing the diagnostic utility of kinetic data will be more and more important, and these preliminary results have demonstrated that the EMM may be useful for analysis of routine clinical data.

Acknowledgments

We would like to thank the Segal Foundation, the Biological Sciences Division at the University of Chicago, DOD grant W81XWH-06-1-0329 and NIH grants R21 CA104774-01A2 and 2 R01 CA078803-05A2 for financial support.

Table 1. Distributions of BI-RADS® categories for the qualitative assessment of the initial rise and delayed phased of kinetic curves for benign and malignant lesions, as well as the subtypes of benign and malignant lesions considered here. Numbers in parentheses are percentages.

		Initial			***Delayed***		
Type of lesions	**No. cases**	***Rapid***	***Medium***	***Slow***	***Washout***	***Plateau***	***Persistent***
All Benign	**34**	**25 (74%)**	**8 (24%)**	**1 (3%)**	**13 (38%)**	**15 (44%)**	**6 (18%)**
FCC	16	11	4	1	3	11	2
Fibroadenoma	4	2	2	0	2	1	1
Papilloma	7	6	1	0	4	2	1
Others	7	6	1	0	4	1	2
All Malignant	**79**	**70 (87%)**	**7 (9%)**	**2 (3%)**	**51 (65%)**	**21 (27%)**	**7 (9%)**
DCIS	30	26	3	1	15	10	5
IDC	36	33	3	0	28	7	1
ILC	7	6	0	1	4	2	1
Others	6	5	1	0	4	2	0

Table 2. A summary of the primary parameters obtained from fitting kinetic curves by using modified empirical mathematical model and the calculated diagnostic parameters from primary parameters for all malignant and benign lesions. Reported values are mean ± standard deviation for all cases. Numbers in bold indicate that there was a statistic significantly difference between benign and malignant lesions.

Type of lesions	**No. cases**	A	α (min^{-1})	β (min^{-1})	AUC_{30}	$Slope_{ini}$ (min^{-1})	$*T_{peak}$ (min)	κ_{peak}	**SER**
All Benign	**34**	4.2±2.2	**1.6±1.1**	0.045±0.047	0.55±0.35	**6.1±4.6**	3.4±1.8	**-0.30±0.49**	**0.88±0.30**
FCC	16	3.9±1.8	1.3±1.0	0.039±0.046	0.48±0.39	5.3±5.5	4.0±1.6	-0.23±0.56	0.78±0.28
Fibroadenoma	4	6.5±2.6	0.69±0.22	0.050±0.066	0.48±0.25	4.4±2.4	4.2±1.4	-0.22±0.25	0.65±0.19
Papilloma	7	3.6±1.9	2.5±1.1	0.050±0.022	0.62±0.28	7.5±3.6	2.0±1.2	-0.33±0.14	1.08±0.7
Others	7	4.3±2.8	2.0±1.1	0.050±0.063	0.66±0.36	7.4±4.4	3.2±2.0	-0.45±0.64	1.04±0.30
All Malignant	**79**	4.0±2.2	**2.1±1.1**	0.058±0.061	0.71±0.54	**8.7±8.3**	2.8±1.9	**-0.67±1.18**	**1.14±0.48**
DCIS	30	2.8±1.9	1.8±0.9	0.037±0.058	0.40±0.23	4.3±2.6	3.6±2.0	-0.18±0.31	0.96±0.35
IDC	36	4.9±2.0	2.6±1.3	0.072±0.062	1.01±0.62	13.1±10.2	2.0±1.5	-1.12±1.57	1.31±0.55
ILC	7	3.1±2.1	1.5±0.4	0.054±0.062	0.44±0.26	4.6±2.7	3.2±2.0	-0.35±0.40	1.04±0.30
Others	6	5.6±1.4	1.6±0.9	0.087±0.046	0.78±0.38	8.5±4.7	2.3±1.0	-0.82±0.89	1.14±0.57

* For those curves which did not reach a peak within the duration of the experiment, we assumed a time to peak of 5 min.

Figure's Captions:

Figure 1. Examples of MRI signal enhancement vs. time curves (open circles) are shown for a variety of lesions types and fitted with the modified EMM (solid lines). The top row consists of benign lesions, from left to right: fibrocystic change (FCC), fibroadenoma and papilloma. The bottom row consists of malignant lesions, from left to right: ductal carcinoma *in situ* (DCIS), invasive ductal carcinoma (IDC) and invasive lobular carcinoma (ILC).

Figure 2. The distributions of the primary EMM parameters are shown according to lesion type. From top to bottom the primary EMM parameters are the amplitude A, the uptake rate α, and the washout rate β. The open circles display the values of the primary EMM parameter for every case in that subtype of benign lesion, and × marks the average value: fibrocystic change (FCC, n=16), fibroadenoma (n=4), papilloma (n=7), and other benign (n=7). Similarly, the open triangles represent the values of each primary EMM parameter for every case in that subtype of malignant lesion, and × marks the average value: ductal carcinoma *in situ* (DCIS, n=30), invasive ductal carcinoma (IDC, n=36), invasive lobular carcinoma (ILC, n=7), and other malignant (n=6).

Figure 3. The bar graph of $\mathbf{A_z}$ value with standard error is shown for each EMM primary and derived parameter. The $\mathbf{A_z}$ value and the standard error are determined from the fitted binormal ROC curves generated by the ROCKIT software. The standard errors are almost the same for all the cases.

Figure 4. Fitted binormal ROC curves generated by the ROCKIT software are shown for selected parameter α (blue line with solid squares) and **SER** (red line with solid circles). The $\mathbf{A_z}$ values were improved by comparing benign lesions with IDC lesions only, as shown by the ROC curves for α (blue line with open squares) and **SER** (red line with open circles).

Figure 1.

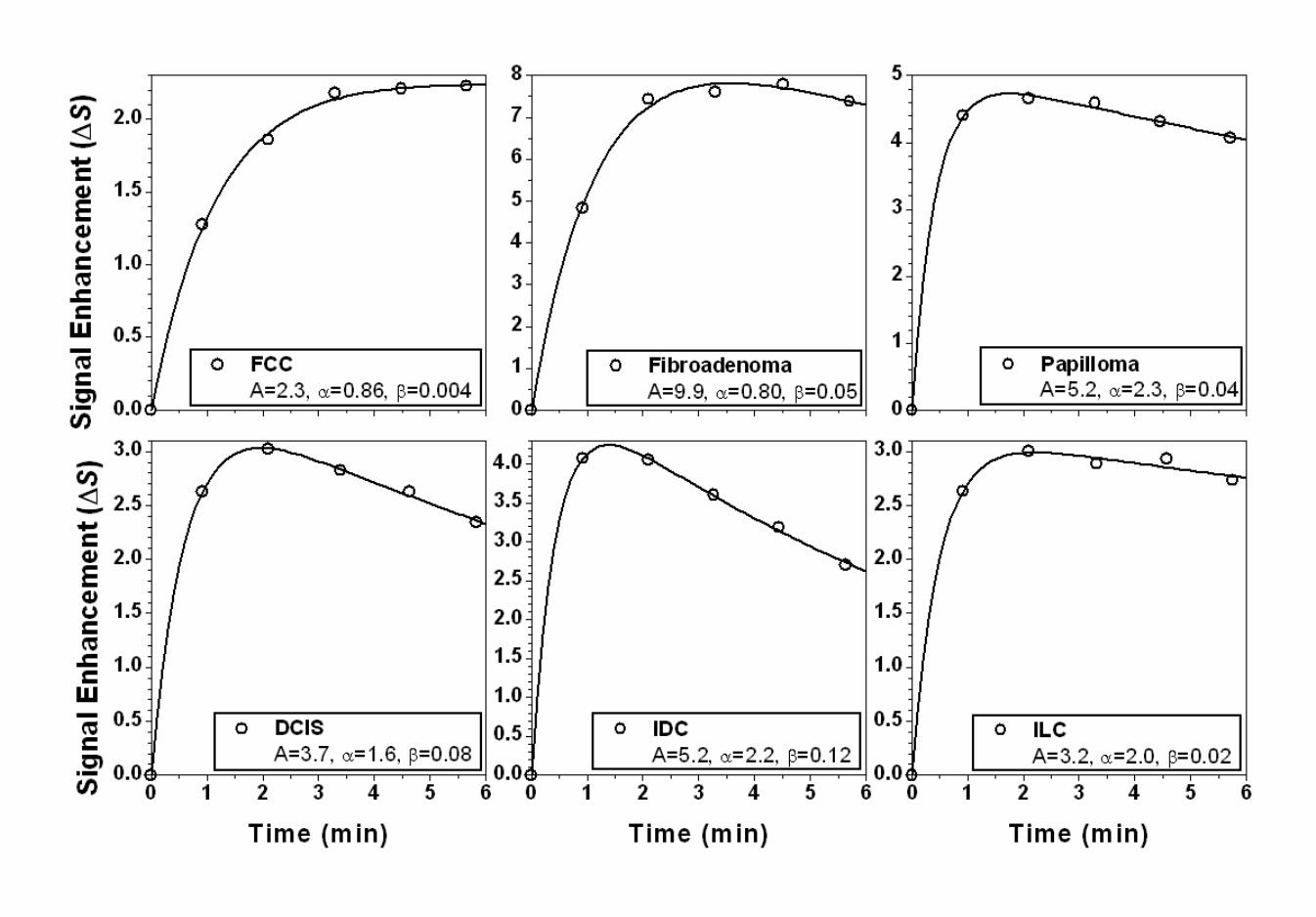
Signal Enhancement (ΔS)
FCC
A=2.3, α=0.86, β=0.004
Fibroadenoma
A=9.9, α=0.80, β=0.05
Papilloma
A=5.2, α=2.3, β=0.04
DCIS
A=3.7, α=1.6, β=0.08
IDC
A=5.2, α=2.2, β=0.12
ILC
A=3.2, α=2.0, β=0.02
Time (min)

Figure 2.

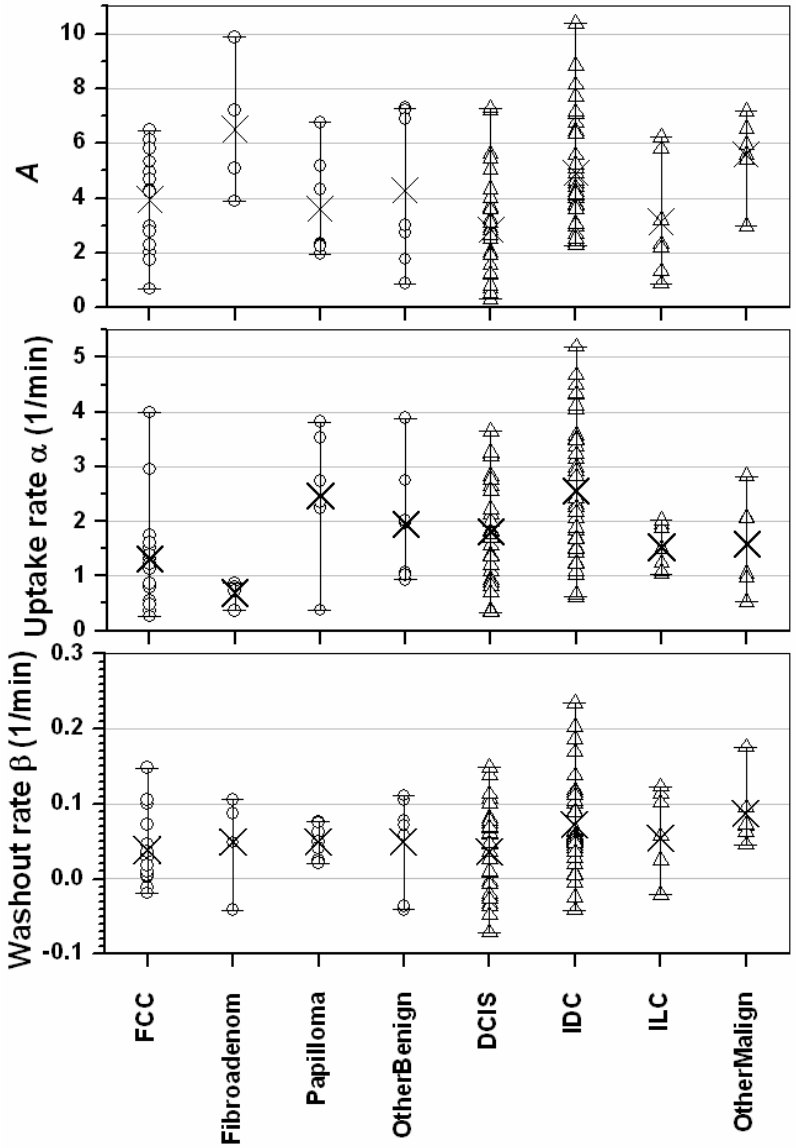
A
Uptake rate α (1/min)
Washout rate β (1/min)
FCC
Fibroadenom
Papilloma
OtherBenign
DCIS
IDC
ILC
OtherMalign

Figure 3.

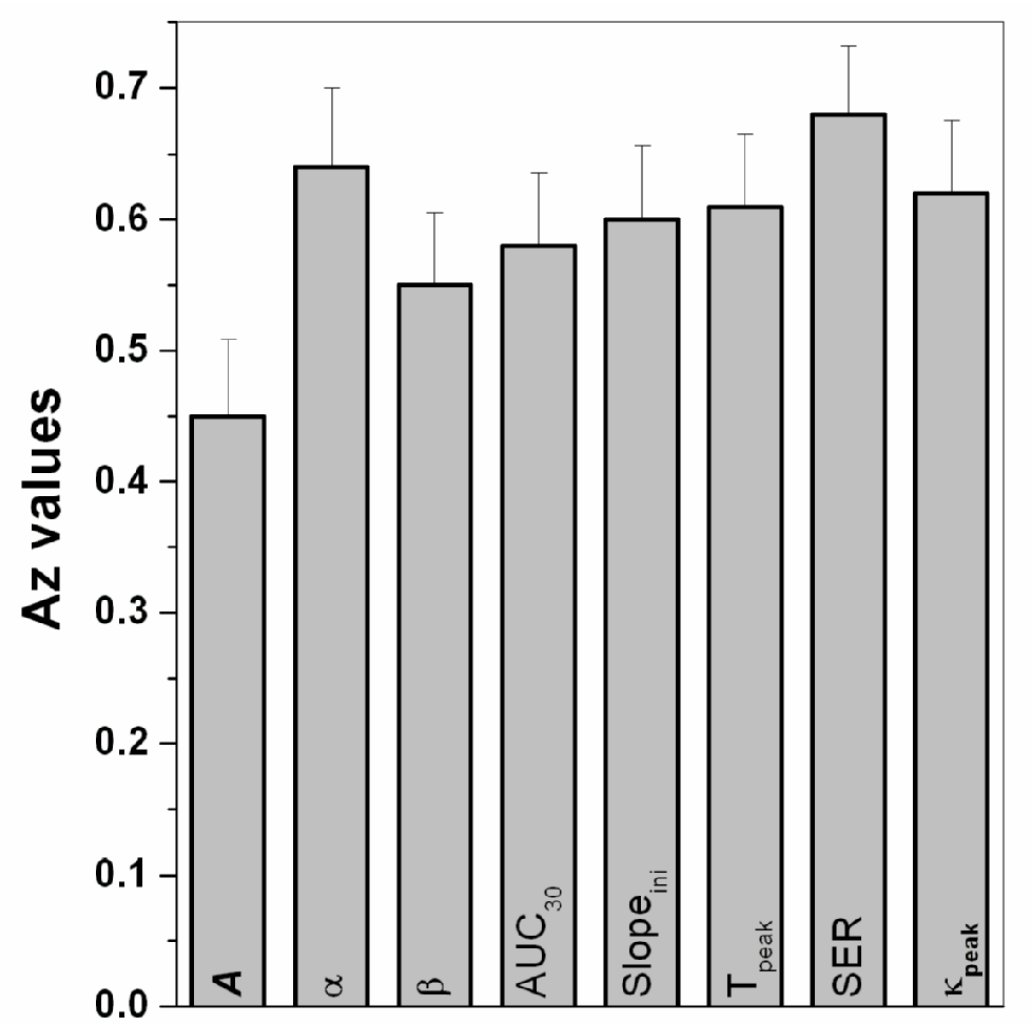
Az values
0.0
0.1
0.2
0.3
0.4
0.5
0.6
0.7
A
α
β
AUC30
Slopeini
Tpeak
SER
kpeak

Figure 4.

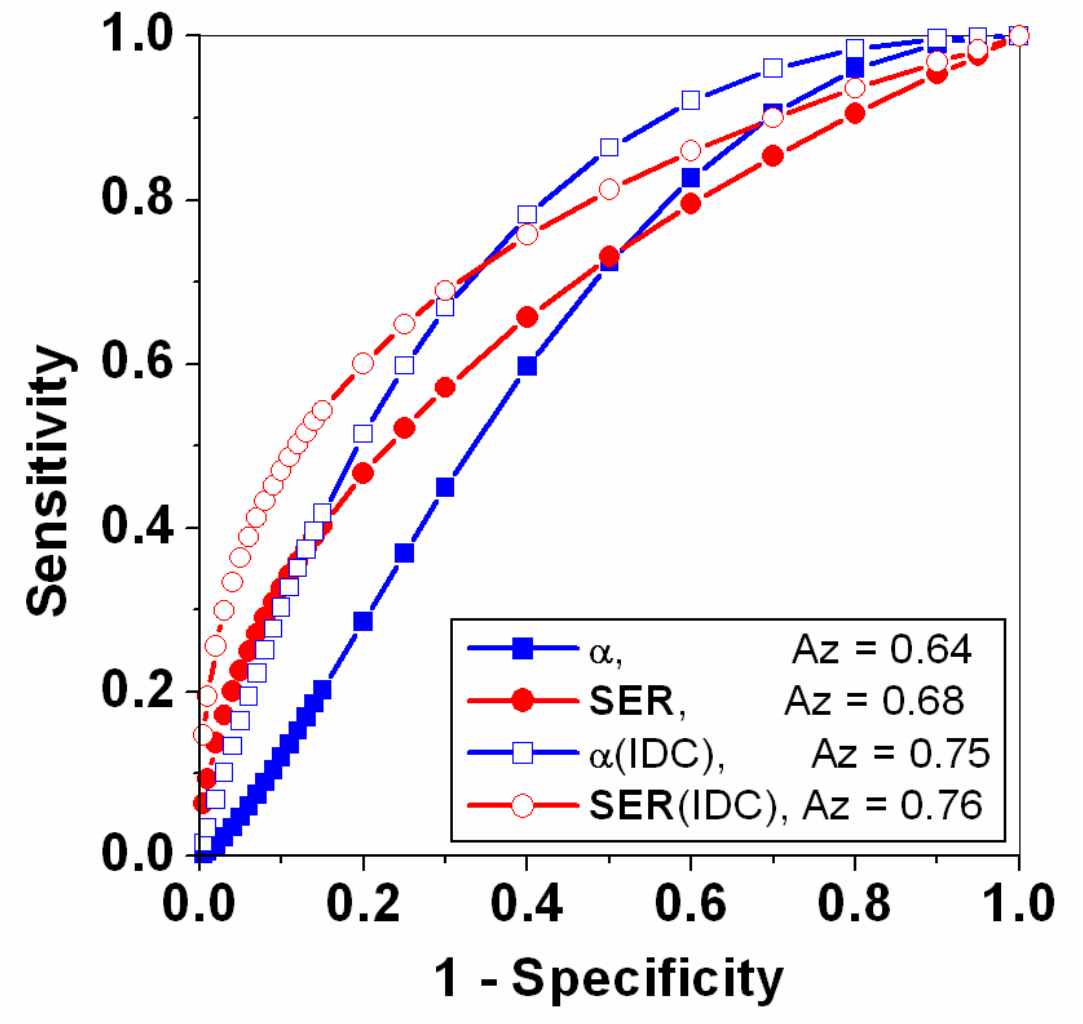
1.0
0.8
0.6
0.4
0.2
0.0
Sensitivity
0.0
0.2
0.4
0.6
0.8
1.0
1 - Specificity
α, Az = 0.64
SER, Az = 0.68
α(IDC), Az = 0.75
SER(IDC), Az = 0.76

References

1. Tabar L, Dean PB. Mammography and breast cancer: the new era. Int J Gynaecol Obstet 2003;82(3):319-326.
2. Abraham DC, Jones RC, Jones SE, Cheek JH, Peters GN, Knox SM, Grant MD, Hampe DW, Savino DA, Harms SE. Evaluation of neoadjuvant chemotherapeutic response of locally advanced breast cancer by magnetic resonance imaging. Cancer 1996;78(1):91-100.
3. Boetes C, Mus RD, Holland R, Barentsz JO, Strijk SP, Wobbes T, Hendriks JH, Ruys SH. Breast tumors: comparative accuracy of MR imaging relative to mammography and US for demonstrating extent. Radiology 1995;197(3):743-747.
4. Warren RM, Pointon L, Thompson D, Hoff R, Gilbert FJ, Padhani A, Easton D, Lakhani SR, Leach MO. Reading protocol for dynamic contrast-enhanced MR images of the breast: sensitivity and specificity analysis. Radiology 2005;236(3):779-788.
5. Heywang-Kobrunner SH, Bick U, Bradley WG, Jr., Bone B, Casselman J, Coulthard A, Fischer U, Muller-Schimpfle M, Oellinger H, Patt R, Teubner J, Friedrich M, Newstead G, Holland R, Schauer A, Sickles EA, Tabar L, Waisman J, Wernecke KD. International investigation of breast MRI: results of a multicentre study (11 sites) concerning diagnostic parameters for contrast-enhanced MRI based on 519 histopathologically correlated lesions. Eur Radiol 2001;11(4):531-546.
6. Orel SG. MR imaging of the breast. Radiol Clin North Am 2000;38(4):899-913.
7. Kuhl CK, Schild HH, Morakkabati N. Dynamic bilateral contrast-enhanced MR imaging of the breast: trade-off between spatial and temporal resolution. Radiology 2005;236(3):789-800.
8. Goto M, Ito H, Akazawa K, Kubota T, Kizu O, Yamada K, Nishimura T. Diagnosis of breast tumors by contrast-enhanced MR imaging: comparison between the diagnostic performance of dynamic enhancement patterns and morphologic features. J Magn Reson Imaging 2007;25(1):104-112.
9. Bazzocchi M, Zuiani C, Panizza P, Del Frate C, Soldano F, Isola M, Sardanelli F, Giuseppetti GM, Simonetti G, Lattanzio V, Del Maschio A. Contrast-enhanced breast MRI in patients with suspicious microcalcifications on mammography: results of a multicenter trial. AJR Am J Roentgenol 2006;186(6):1723-1732.
10. Szabo BK, Aspelin P, Wiberg MK, Bone B. Dynamic MR imaging of the breast. Analysis of kinetic and morphologic diagnostic criteria. Acta Radiol 2003;44(4):379-386.
11. Kuhl CK, Schild HH. Dynamic image interpretation of MRI of the breast. J Magn Reson Imaging 2000;12(6):965-974.
12. Kuhl CK, Mielcareck P, Klaschik S, Leutner C, Wardelmann E, Gieseke J, Schild HH. Dynamic breast MR imaging: are signal intensity time course data useful for differential diagnosis of enhancing lesions? Radiology 1999;211(1):101-110.
13. Cron GO, Kelcz F, Santyr GE. Improvement in breast lesion characterization with dynamic contrast-enhanced MRI using pharmacokinetic modeling and bookend T(1) measurements. Magn Reson Med 2004;51(5):1066-1070.
14. Armitage P, Behrenbruch C, Brady M, Moore N. Extracting and visualizing physiological parameters using dynamic contrast-enhanced magnetic resonance imaging of the breast. Med Image Anal 2005;9(4):315-329.

15. Furman-Haran E, Degani H. Parametric analysis of breast MRI. J Comput Assist Tomogr 2002;26(3):376-386.
16. Furman-Haran E, Schechtman E, Kelcz F, Kirshenbaum K, Degani H. Magnetic resonance imaging reveals functional diversity of the vasculature in benign and malignant breast lesions. Cancer 2005;104(4):708-718.
17. Tofts PS, Berkowitz B, Schnall MD. Quantitative analysis of dynamic Gd-DTPA enhancement in breast tumors using a permeability model. Magn Reson Med 1995;33(4):564-568.
18. Heiberg EV, Perman WH, Herrmann VM, Janney CG. Dynamic sequential 3D gadolinium-enhanced MRI of the whole breast. Magn Reson Imaging 1996;14(4):337-348.
19. Fan X, Medved M, River JN, Zamora M, Corot C, Robert P, Bourrinet P, Lipton M, Culp RM, Karczmar GS. New model for analysis of dynamic contrast-enhanced MRI data distinguishes metastatic from nonmetastatic transplanted rodent prostate tumors. Magn Reson Med 2004;51(3):487-494.
20. Moate PJ, Dougherty L, Schnall MD, Landis RJ, Boston RC. A modified logistic model to describe gadolinium kinetics in breast tumors. Magn Reson Imaging 2004;22(4):467-473.
21. Evelhoch JL. Key factors in the acquisition of contrast kinetic data for oncology. J Magn Reson Imaging 1999;10(3):254-259.
22. Buadu LD, Murakami J, Murayama S, Hashiguchi N, Sakai S, Masuda K, Toyoshima S, Kuroki S, Ohno S. Breast lesions: correlation of contrast medium enhancement patterns on MR images with histopathologic findings and tumor angiogenesis. Radiology 1996;200(3):639-649.
23. Esserman L, Hylton N, George T, Weidner N. Contrast-Enhanced Magnetic Resonance Imaging to Assess Tumor Histopathology and Angiogenesis in Breast Carcinoma. Breast J 1999;5(1):13-21.
24. Fan X MM, Karczmar GS, Yang C, Foxley S, Arkani S, Recant W, Zamora MA, Abe H, Newstead GM. Diagnosis of suspicious breast lesions using an empirical mathematical model for dynamic contrast-enhanced MRI. Magnetic Resonance Imaging 2007 (In press).
25. Metz CE, Herman BA, Shen JH. Maximum likelihood estimation of receiver operating characteristic (ROC) curves from continuously-distributed data. Stat Med 1998;17(9):1033-1053.
26. Arpino G, Laucirica R, Elledge RM. Premalignant and in situ breast disease: biology and clinical implications. Ann Intern Med 2005;143(6):446-457.
27. Kumar AS, Chen DF, Au A, Chen YY, Leung J, Garwood ER, Gibbs J, Hylton N, Esserman LJ. Biologic significance of false-positive magnetic resonance imaging enhancement in the setting of ductal carcinoma in situ. Am J Surg 2006;192(4):520-524.
28. Armitage P, Behrenbruch C, Brady M, Moore N. Extracting and visualizing physiological parameters using dynamic contrast-enhanced magnetic resonance imaging of the breast. Med Image Anal 2005;9(4):315-329.

Qualitative and Quantitative Characteristics of Parenchymal Enhancement on Breast MRI

To be submitted for Publication in the American Journal of Roentgenology
Original Research Article
Word Count:3061

Corresponding Author:

Dr. Gillian Newstead
University of Chicago
Department of Radiology
5841 S. Maryland Ave
MC 2026
Chicago, IL 60637
Telephone: 773-702-2781
Fax: 773-834-9047
Email: gnewstead@radiology.bsd.uchicago.edu

Acknowledgements

We would like to thank the Segal Foundation, the Biological Sciences Division at the University of Chicago, DOD grant W81XWH-06-1-0329 and NIH grants R21 CA104774-01A2 and 2 R01 CA078803-05A2 for financial support.

Introduction

Dynamic contrast enhancement MRI (DCEMRI) of the breast is being used increasingly for several purposes including diagnostic imaging, post-treatment evaluation and for high-risk screening(1-3). DCEMRI provides 3D morphologic and kinetic information of lesions that enhance relative to the surrounding normal parenchyma, and the vast majority of prior reports on DCEMRI focus on the characteristics of benign and malignant lesions(3-6). However, it may also be important to study the characteristics of normal parenchymal enhancement, since strongly enhancing parenchyma has the potential to obscure lesion perception. Furthermore, as more and more asymptomatic women obtain MRI for follow-up and high risk screening purposes (1), characterization of normal breast tissue will become more important.

There have been relatively few prior studies of parenchymal enhancement on breast MRI in asymptomatic women. Premenopausal between 34-50 years show greater parenchymal enhancement than other age ranges (7). It has also been shown to be highest in week 1 and week 4 of the menstrual cycle (8, 9). Women who are on hormone replacement therapy (HRT) also exhibit increased parenchymal enhancement compared to those who are not(10, 11). Women who have had radiation therapy tend to show a quiet breast after 1 year post therapy(12). The number of patients in these studies has been relatively small.

The purpose of this study was to perform a comprehensive evaluation of parenchymal enhancement in a group of 180 asymptomatic women. The pattern of parenchymal enhancement was qualitatively evaluated according to a classification system developed by one of the authors

(GMN). A quantitative evaluation of the kinetics of the enhancement was also performed. These qualitative and quantitative characteristics of parenchymal enhancement were studied by stratifying the population by menopause status, breast density, and risk of developing breast cancer.

Materials and Methods

Patients

At our institution, it is a routine protocol to obtain breast MRI for diagnostic imaging, to evaluate extent of disease, for post-treatment evaluation and for high risk screening. We maintain a clinical database of all breast examinations performed at our institution. An IRB approved retrospective review was performed of this database under full HIPAA compliance and with informed consent waived. This review of 1770 records from April 2002- December 2004, yielded 180 consecutive asymptomatic patients with normal MR findings who were appropriate for this study: with known menopausal status, with complete detailed patient history forms, with digital mammograms available, and with dynamic data able to be processed by homemade software. 87/180 were referred for MRI due to prior imaging results (such as calcifications), 46/180 due to clinical findings (such as ductal discharge), 40 for screening, and 7 for follow-up. The average patient age was 53 years, with a range of 20 to 84 years.

MRI Analysis

Dynamic Protocol: MR imaging was performed on a 1.5T GE Signa scanner (GE Healthcare, Milwaukee, WI) using a dedicated 4 channel breast coil (Invivo, Orlando, FL) with the patient in the prone position. Two protocols had been used study. In the first, one pre and five post-contrast images were acquired in the coronal plane using a T_1-weighted 3D spoiled grass sequence (TR/TE= 7.7 msec/4.2 msec, flip angle 30 degrees, slice thickness of 3 mm and in plane resolution of 1.4 mm) with no fat saturation. The first post-contrast acquisition was started

20 seconds after contrast injection and the remaining images were acquired every 68 seconds. In the second dynamic protocol there were three post-contrast acquisitions. The first two post-contrast acquisitions were obtained as before, followed by acquisition of high resolution sagittal images for 128 seconds, and returning to a final dynamic, 68 second, acquisition. Gadodiamide (Omniscan; Nycomed-Amersham, Princeton, NJ) was injected intravenously at a dose of 0.1 mmol/kg followed by a 20 ml saline flush at the rate of 2.0 ml /sec. The following MR analysis was performed on subtraction images viewed using homemade software.

Parenchymal Enhancement Pattern (PEP): The parenchymal enhancement pattern (PEP) was classified according to a system developed by one radiologist with 14 years of MR experience. This system classifies the PEP on the last post-contrast (~ 6 min) coronal subtraction images as minimal, homogeneous, heterogeneous or nodular. To do this, the parenchyma was first located on non-subtracted pre-contrast images, then examined on the last post contrast image set and classified as: 1) *minimal* appreciable enhancement, 2) *homogeneous* enhancement of the parenchyma, 3) *heterogeneous* enhancement of the parenchyma, and 4) *nodular* foci of parenchymal enhancement. This was a qualitative assessment of bilateral whole breast density. Examples of this classification system are shown in Figure 1. One reader with 3 years of breast MR experience performed a retrospective classification of the PEP according to this method. This analysis was not blinded to patient identification (name and MRN) but was blinded to other patient information and clinical history. It was also blinded to the mammographic classification of breast density (presented below).

Parenchymal Enhancement Kinetics (PEK): In women with homogeneous, heterogeneous or nodular parenchymal enhancement, we were interested in quantifying the enhancement magnitude and kinetics. Using institutional software, the same reader generated kinetic curves by manually tracing a region of interest (ROI) around the most enhancing part of the parenchyma as it appeared on the last post contrast image in the coronal plane. The average ROI size was 7.3 pixels. Quantitative kinetic parameters were derived from the curves. Percent enhancement (E_1, E_2, E_{peak}) and the time to peak enhancement were measured for each curve as performed in Szabo et al(5). Further details on calculation of these enhancement parameters can be found in the Appendix.

Menopausal Status and Age: We determined the menopausal status and age for each patient by retrospectively reviewing detailed patient history forms.

Breast Density Evaluation: Breast density was evaluated using both x-ray mammograms and breast MRI.

Breast Density on X-Ray Mammograms: Digital mammograms were retrospectively reviewed by one radiology resident. The breast density was classified according to the BI-RADS® lexicon as: mammo density 1=almost entirely fat, mammo density 2=scattered fibroglandular tissue, mammo density 3= heterogeneously dense and mammo density 4=extremely dense. This analysis was performed with knowledge of patient identification (name and MRN) but without knowledge of other patient information, clinical history, or the MR findings of PEP or PEK.

Breast Volume on MRI: Five months after performing the MR PEP and PEK analysis, the same reader again retrospectively reviewed the MR images. The breast density was classified in a similar manner as in the x-ray mammographic case: MR density 1=almost entirely fat, MR density 2=scattered fibroglandular tissue, MR density 3= heterogeneously dense and MR density 4=extremely dense. This analysis was performed with knowledge of patient identification (name and MRN) and without knowledge of the x-ray mammographic breast density findings

Classification of Risk: For each patient we determined the lifetime risk of developing breast cancer according to the Gail model (13) based on information gathered from detailed personal history forms. We then segmented the population of 180 women into three groups after reviewing the detailed patient history forms:

Risk group 1. Women who are highly likely to be recommended for screening have > 25% lifetime risk by the Gail model(1).

Risk group 2: There is insufficient evidence that is for or against screening in women with any of the following: *i)* prior diagnosis of ADH, LCIS or ALH, *ii)* heterogeneously or extremely dense breasts, *iii)* personal history of breast cancer, *iv)* 15-25% lifetime risk by Gail model.

Risk group 3: Women with a < 15% lifetime risk according to Gail model are likely not suitable for screening.

Statistical Analysis : We studied the parenchymal enhancement characteristics of the whole population, as well as these subcategories:

1. Menopause: comparing the PEP and PEK between premenopausal vs. postmenopausal women, and also determining how PEK varies with age.

2. Breast density: comparing the PEP and PEK among women with different breast density, separately for density assessed on x-ray mammograms and breast MRI
3. Risk: comparing the PEP and PEK among women in different risk groups.

The PEP distribution (% minimal, % homogeneous, % heterogeneous, % nodular) was determined for the whole population, as well as these subpopulations. For each of the quantitative kinetic parameters (E_1, E_2, E_{peak}) the mean and standard error on the mean of these parameters were calculated for the whole population as well as the subpopulations of presented above. In addition to calculating the mean and standard error on the mean for all categories of interest, we were also interested in determining how many cases exhibited marked enhancement. To measure this, we also measured the number of cases with $E_2 > 200\%$.

To test for significance of the PEP classifications among lesions stratified into the subcategories presented above, the χ^2 – test was used, with a p value of < 0.05 indicating statistical significance. To compare the means of the kinetic parameters in each of these subpopulations, ANOVA analysis was used, with a p value of < 0.05 indicating statistical significance.

Results

The distribution of PEP was: 58% (104/180) minimal, 5% (9/180) homogeneous, 18% (33/180) heterogeneous, and 19% (34/180) nodular. 175/180 of curves reached the peak enhancement at the last post contrast point. Of the 76 cases of non-minimal enhancement (i.e., homogeneous, heterogeneous or nodular PEP), the average E_1=98 ± 6 %, E_2 =147± 7 %, and E_{peak}=210± 9%. Women with heterogeneous PEP had a higher E_2 and E_{peak} than women with nodular PEP (p< 0.043). 22% (17/76) of cases with non-minimal PEP showed E_2 > 200%. In particular, 12% (2/34) of cases with nodular PEP had E_2> 200%.

Menopause and Age

59% (106/180) of the women were postmenopausal with an average age of 60 years, and 41% (74/180) were premenopausal with an average age of 43 years. The distribution of PEP varied significantly between postmenopausal and premenopausal women, showing 28% (21/74) and 78% (83/106) minimal PEP, respectively ($p < 0.001$ by χ^2-test, Figure 2). There was no statistically significant difference in average PEK parameters among premenopausal and postmenopausal women by ANOVA analysis (Table 1). The PEK parameters E_1, E_2, and E_{peak}, decreased with increasing age (Figure 3).

Breast Density

Breast Density on Mammograms: The distribution of breast density was 0.5% (1/180) mammo density 1, 45% (81/180) mammo density 2, 37% (66/180) mammo density 3, 18% (32/180)

mammo density 4. The distributions of PEP for women with mammo density 2, 3 and 4 breast density were statistically significantly different, with 68%, 56% and 34% showing minimal PEP, respectively ($p = 0.04$, by χ^2-test, Table 2). In addition, there was a statistically significant difference in PEK parameters: women with category 2 dense breasts had significantly lower E_2 and E_{peak} than women with category 4 dense breasts ($p < 0.0001$ by ANOVA analysis, Table 2). Furthermore, 15% (4/26) of the 26 cases with non-minimal PEP in women with category 2 dense breasts exhibited an $E_2 > 200\%$, compared with 43% (9/21) of women with category 4 dense breasts.

Breast Volume on MRI: The distribution of breast density on MRI was 21% (38/180) MR density 1, 37% (66/180) MR density 2, 24% (43/180) MR density 3, 18% (33/180) MR density 4. The distributions of PEP for women with MR density 1,2, 3 and 4 breast density were statistically significantly different, with 89%, 61%, 51% and 24% showing minimal PEP, respectively ($p <0.001$, by χ^2-test, Table 3). In addition, there was a statistically significant difference in PEK parameters: women with MR density 2 dense breasts had significantly lower E_2 and E_{peak} than women with MR density 4 dense breasts ($p < 0.04$ by ANOVA analysis, Table 3). Furthermore, 0% (0/4) of the 4 cases with non-minimal PEP in women with MR density 1 dense breasts exhibited an $E_2 > 200\%$, compared with 32% (8/25) of women with MR density 4 dense breasts.

Risk Classifications

6/180 of women were classified as risk group 1, 122/180 were classified as risk group 2 and 52/180 were classified as risk group 3. There was no significant difference in PEP distribution

among these three groups (Table 4). However, there was a difference in the PEK parameters: according to ANOVA analysis the three risk groups differed significantly in E_{peak} (p=0.007), E_1 (p=0.003) and E_2 (p=0.001).

Discussion

Characterizing normal tissue enhancement on MRI will become more important as more women get follow-up and high risk screening MR examinations. In our study, we have documented the qualitative (PEP) and quantitative (PEK) parenchymal enhancement characteristics of 180 asymptomatic women. We have found that 58% (104/180) showed minimal parenchymal enhancement and the remaining 42% (76/180) displayed parenchymal enhancement of some kind: 5% (9/180) homogeneous, 18% (33/180) heterogeneous, and 19% (34/180) nodular. In women who showed non-minimal enhancement (n=76) we found that the average E_1=98%, E_2=147% and E_{peak}=210%.

Parenchymal enhancement may compromise lesion conspicuity. In this study we have found that 9% of the total population (17/180) exhibited greater than 200% enhancement at the second post-contrast time point ~2min. This is comparable to the enhancement characteristics DCIS lesions(14). Furthermore, DCIS lesions show variable kinetics, with both plateau and persistent type curves. We have found that in 97% of cases the parenchymal kinetic curve was persistent, thus kinetics may not always help to distinguish DCIS from enhancing parenchyma (14-16). Because of this variable kinetics pattern, some have suggested that the distinctive non-mass like morphology of DCIS should be of primary diagnostic utility(17). However, parenchymal enhancement is also non-mass like, and in particular nodular parenchymal enhancement in the coronal plane may mimic DCIS—here, we have found that 12% (4/34) of cases of nodular PEP enhance more than 200% at ~2 min. In a region of enhancing parenchyma it may be difficult to perceive a lesion. Thus, imaging earlier decreases the effect of enhancing parenchyma on lesion

conspicuity. This points to the importance of using sufficient temporal resolution to be able to detect enhancing lesions, particularly DCIS, from enhancing parenchyma.

Our findings regarding the effect of menopause on parenchymal enhancement are concordant with prior studies(7). We have found that the pattern of parenchymal enhancement differs for pre and postmenopausal women, with the latter group having 78% (83/106) minimal PEP, compared with 28% (21/74) for the premenopausal group. Interestingly, the magnitude of the enhancement, as measured by E_1, E_2 and E_{peak} did not vary significantly among the two groups. This implies that although postmenopausal women are more likely to exhibit minimal parenchymal enhancement, when there is enhancement, the kinetics are similar to the premenopausal group.

By considering both MR and x-ray mammographic measures of breast density, we have found that more less breasts are more likely to demonstrate minimal PEP, and exhibit a smaller magnitude of enhancement. In some sense this isn't very surprising—we would expect that the denser the breast tissue, the more capacity there is for some kind of parenchymal enhancement. However, it may be the converse that is more interesting: 34% of women with extremely dense breasts on x-ray mammography, and 24% of women with extremely dense breasts on MRI, show minimal parenchymal enhancement (Figure 4).

Variations in parenchymal enhancement reported in the literature have been attributed to variations in estrogen levels(9). In the normal breast, estrogen acts to cause epithelial cells to proliferate. Postmenopausal women no longer produce estrogen in the ovaries, however have

been shown to locally produce estrogen in the bone, brain and adipose breast tissue(18). Hormone therapies, such as Tamoxifen and aromatase inhibitors work to reduce the levels and action of estrogen, recognizing that estrogen levels may be related to breast cancer risk (19). Thus, if parenchymal enhancement is related to estrogen levels, then perhaps it is also related to breast cancer risk. Breast density has also been linked to breast cancer risk and we have demonstrated that certain patterns of PEP vary among breasts of different density(20). Perhaps parenchymal enhancement may eventually provide a refined measure of breast cancer risk.

There are several limitations to this study. This was a retrospective review performed by two single readers of the MRI and mammograms. Although the MR and x-ray mammographic findings were obtained from different readers, and the analysis was performed blinded to clinical history the factors considered in this study, this still raises the question of reproducibility and bias. In addition, all the patient history information was obtained retrospectively from prior patient forms and statements. Importantly, in this retrospective review, we were not able to control for menstrual cycle status. The kinetic parameters may be compromised by the two dynamic protocols were used in this study. We aimed to minimize the effect that this may have on the kinetics by considering parameters that depend only on the first and last point which are at similar times for both protocols. In addition, in cases of the small foci of enhancement in nodular PEP, or for women with only scattered fibroglandular tissue, perhaps the ROI could not be drawn small enough, reducing the apparent signal intensity increase.

Finally, in this study we have presented a new classification system of parenchymal enhancement, which may need some adjustments. For example, perhaps the PEP should be

classified on the first post contrast image. Here, we have selected the last post contrast image set because the parenchyma can be more accurately perceived at later times; we can infer the enhancement characteristics at the first and second post contrast points via the kinetic parameters E_1 and E_2. This work provides preliminary assessment of parenchymal enhancement patterns and kinetics and may form the basis for a larger study with increased readers and improved analysis, including CAD assessments to quantify breast density and enhancement.

To summarize, we have found that 42% of asymptomatic women presenting for MRI exhibit parenchymal enhancement. 9% of the cases showed greater than 200% enhancement at ~2 min—such enhancement has the potential to obscure lesions, particularly DCIS. We have found that while dense breasts are more likely to exhibit homogeneous, heterogeneous or nodular patterns of parenchymal enhancement, and less dense breasts are more likely to have minimal enhancement, the association isn't very strong—over one third of women with extremely dense breasts show no appreciable parenchymal enhancement. As expected, we have found that the patterns of parenchymal enhancement depend strongly on menopausal status. However, 25% of postmenopausal women do exhibit some enhancement, and the quantitative kinetics of this enhancement is similar to the premenopausal counterparts. We have also suggested that because of its probable link with estrogen levels, parenchymal enhancement may also be related to breast cancer risk. These preliminary results point to future work on the follow-up of many of these women with strong parenchymal enhancement.

Appendix

The *percent enhancement* measures the uptake of contrast in the lesion relative to the pre-contrast signal level,

$$E_1 = 100 \times \frac{S_1 - S_0}{S_0}$$

$$E_1 = 100 \times \frac{S_1 - S_0}{S_0}$$

$$E_{peak} = 100 \times \frac{S_{peak} - S_0}{S_0},$$

where E_1 is the initial percent enhancement, E_2 is the percent enhancement at the second post contrast point, E_{peak} is the peak percent enhancement, S_1 is the signal in the ROI at the first post contrast point, S_2 is the signal in the ROI at the second post contrast point, S_{peak} is the peak signal intensity and S_0 is the pre-contrast signal intensity in the ROI.

The *time to peak enhancement* (T_{peak}) is the time in seconds between the injection of contrast and the peak of the signal intensity vs. time curve.

Table 1: Parenchymal enhancement characteristics for premenopausal and postmenopausal women.

	Premenopause	**Postmenopause**
Total	74	106
Minimal PEP	21	83
Homogeneous PEP	5	2
Heterogeneous PEP	27	8
Nodular PEP	21	13
Average E_{peak} (%)	223.0588	179.2314
Average E_1(%)	103.7831	83.85174
Average E_2(%)	156.7533	125.5073
# E_2 >200%	13	4

Table 2: Parenchymal enhancement characteristics for women with breast density 1-4, as classified on x-ray mammograms.

	Mam Density 1and 2	**Mam Density 3**	**Mam Density 4**
Total	82	66	32
Minimal PEP	56	37	11
Homogeneous PEP	2	4	1
Heterogeneous PEP	14	11	10
Nodular PEP	10	14	10
Average E_{peak} (%)	163.665277	211.9511	263.931333
Average E_1(%)	74.2826573	100.738012	122.682935
Average E_2(%)	109.295462	144.783524	197.81859
# Premen	21	30	23
# Postmen	61	36	9
# E_2>200%	4	4	9

Table 3: Parenchymal enhancement characteristics for women with breast density 1-4, as classified on breast MRI.

	MR Density 1	**MR Density 2**	**MR Density 3**	**MR Density 4**
Total	38	66	43	33
Minimal PEP	34	40	22	8
Homogeneous PEP	2	1	3	1
Heterogeneous PEP	1	15	8	11
Nodular PEP	1	10	10	13
Average E_{peak} (%)	69.807375	185.115142	236.240543	235.6465
Average E_1(%)	39.75305	80.7405381	119.638612	106.336642
Average E_2(%)	42.27465	124.119208	164.675152	173.608736
# Premen	7	20	21	26
# Postmen	31	46	22	7
# E_2 >200%	0	4	5	8

Table 4: Parenchymal enhancement characteristics for women in risk group 1-3.

	Risk group 1	**Risk group 2**	**Risk group 3**
Total	6	122	52
Minimal PEP	4	68	32
Homogeneous PEP	0	7	0
Heterogeneous PEP	1	23	11
Nodular PEP	1	24	9
Average E_{peak} (%)	467.901	208.028624	188.75447
Average E_1(%)	268.9735	95.8197089	85.84409
Average E_2(%)	391.8935	146.013326	126.3044
# Premen	1	56	17
# Postmen	5	66	35
# E_2 >200%	2	11	4

Figure Captions

Figure 1: Examples of the parenchymal enhancement pattern (PEP) classification system.

Figure 2: Distribution of PEP for premenopausal (n=74) and postmenopausal (n=106) women.

Figure 3: Variations of kinetic parameters E_1, E_2, E_{peak} by age.

Figure 4: Example of dense breast with minimal parenchymal enhancement.

Figure 1: Examples of the parenchymal enhancement pattern (PEP) classification system.

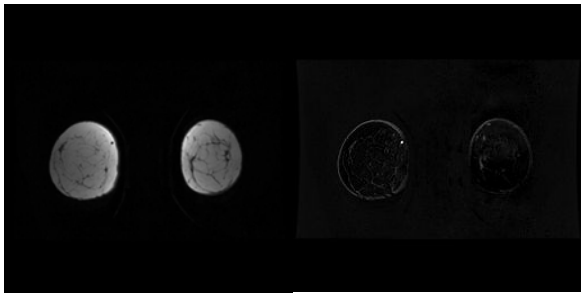

Minimal

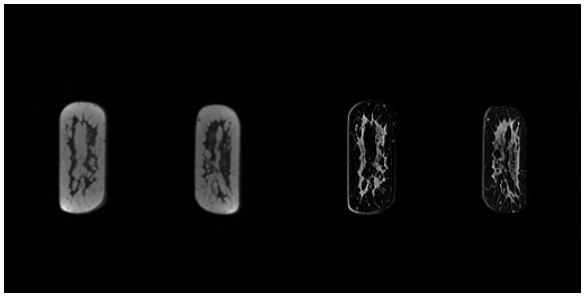

Homogeneous

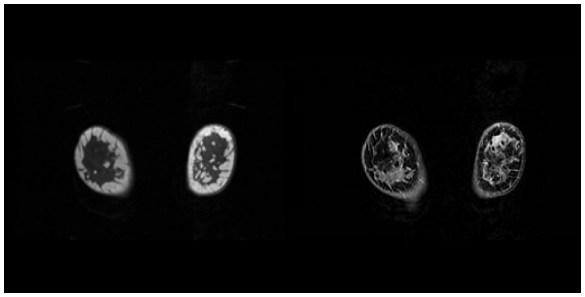

Heterogeneous

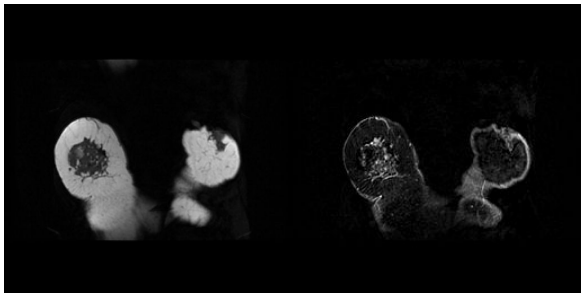

Nodular

Figure 2: Distribution of PEP for premenopausal (n=74) and postmenopausal (n=106) women.

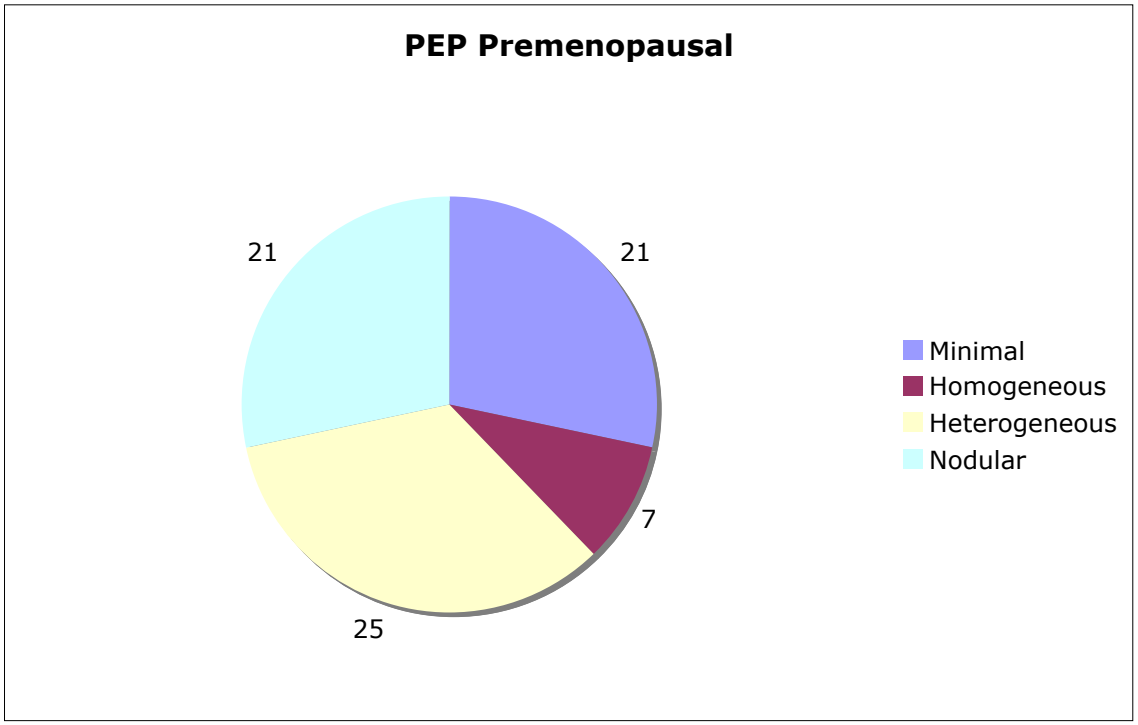

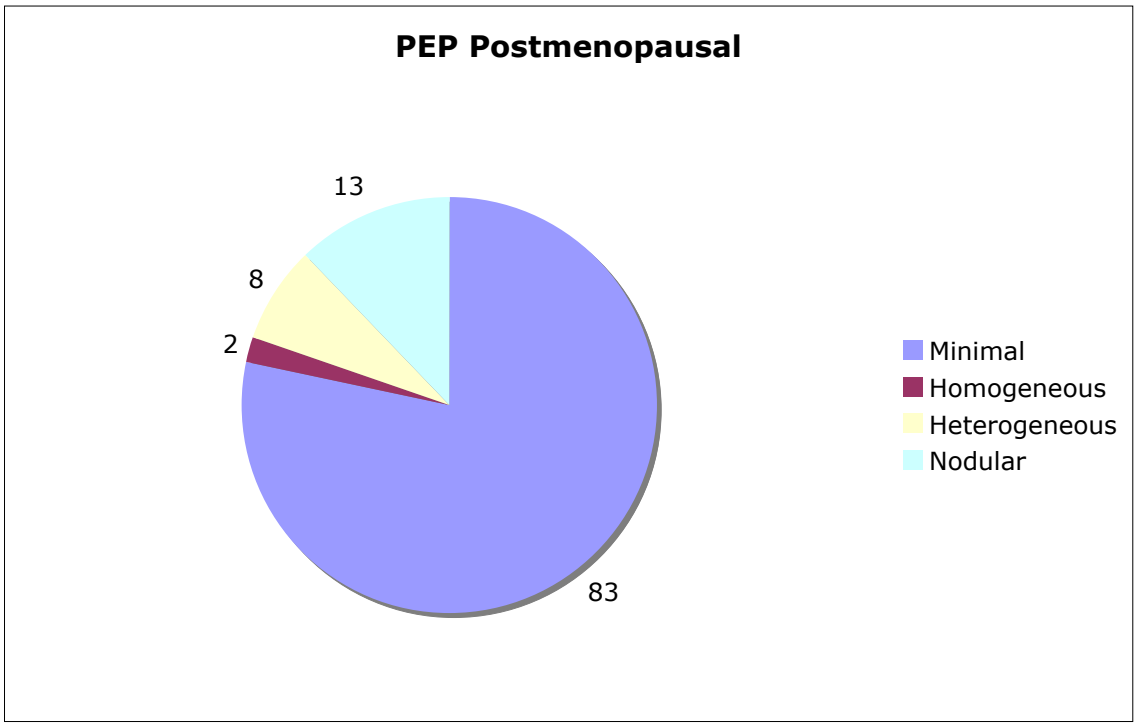

Figure 3: Variations of kinetic parameters E_1, E_2, E_{peak} by age.

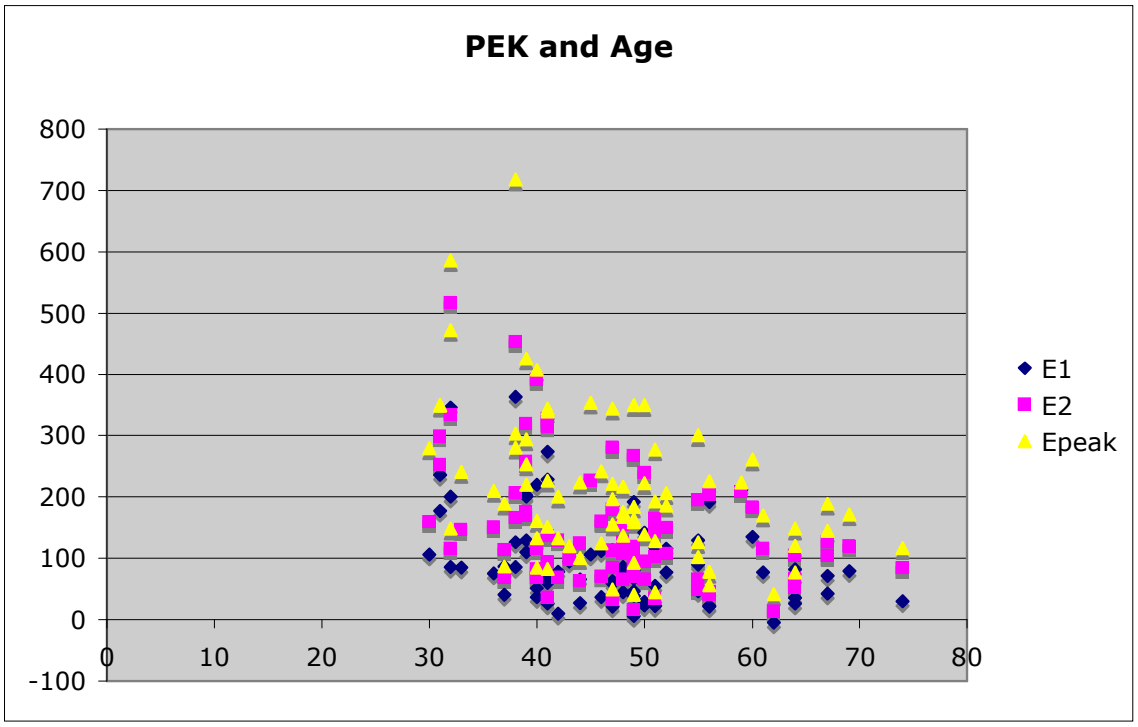

Figure 4: Example of dense breast with minimal parenchymal enhancement.

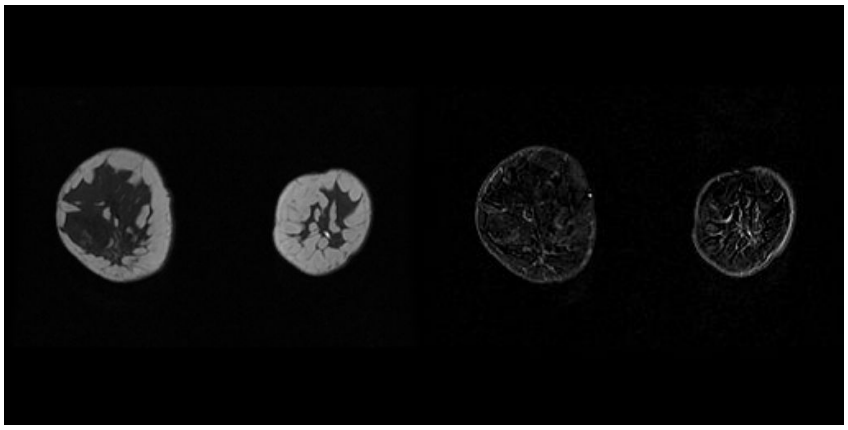

References

1. Lehman CD. Role of MRI in screening women at high risk for breast cancer. J Magn Reson Imaging 2006; 24:964-970.
2. Hylton N. MR imaging for assessment of breast cancer response to neoadjuvant chemotherapy. Magn Reson Imaging Clin N Am 2006; 14:383-389, vii.
3. Kuhl CK, Schild HH. Dynamic image interpretation of MRI of the breast. J Magn Reson Imaging 2000; 12:965-974.
4. Kuhl CK, Mielcareck P, Klaschik S, et al. Dynamic breast MR imaging: are signal intensity time course data useful for differential diagnosis of enhancing lesions? Radiology 1999; 211:101-110.
5. Szabo BK, Aspelin P, Wiberg MK, Bone B. Dynamic MR imaging of the breast. Analysis of kinetic and morphologic diagnostic criteria. Acta Radiol 2003; 44:379-386.
6. Oshida K, Nagashima T, Ueda T, et al. Pharmacokinetic analysis of ductal carcinoma in situ of the breast using dynamic MR mammography. Eur Radiol 2005; 15:1353-1360.
7. Muller-Schimpfle M, Ohmenhauser K, Claussen CD. [Effect of age and menstrual cycle on mammography and MR mammography]. Radiologe 1997; 37:718-725.
8. Delille JP, Slanetz PJ, Yeh ED, Kopans DB, Garrido L. Physiologic changes in breast magnetic resonance imaging during the menstrual cycle: perfusion imaging, signal enhancement, and influence of the T1 relaxation time of breast tissue. Breast J 2005; 11:236-241.
9. Kuhl CK, Bieling HB, Gieseke J, et al. Healthy premenopausal breast parenchyma in dynamic contrast-enhanced MR imaging of the breast: normal contrast medium enhancement and cyclical-phase dependency. Radiology 1997; 203:137-144.
10. Delille JP, Slanetz PJ, Yeh ED, Kopans DB, Halpern EF, Garrido L. Hormone replacement therapy in postmenopausal women: breast tissue perfusion determined with MR imaging--initial observations. Radiology 2005; 235:36-41.
11. Pfleiderer SO, Sachse S, Sauner D, et al. Changes in magnetic resonance mammography due to hormone replacement therapy. Breast Cancer Res 2004; 6:R232-238.
12. Padhani AR, Yarnold J, Regan J, Husband JE. Dynamic MRI of breast hardness following radiation treatment. J Magn Reson Imaging 2003; 17:427-434.
13. Gail MH, Brinton LA, Byar DP, et al. Projecting individualized probabilities of developing breast cancer for white females who are being examined annually. J Natl Cancer Inst 1989; 81:1879-1886.
14. Arkani. MR Imaging of Pure Ductal Carcinoma in situ.
15. Mariano MN, van den Bosch MA, Daniel BL, et al. Contrast-enhanced MRI of ductal carcinoma in situ: characteristics of a new intensity-modulated parametric mapping technique correlated with histopathologic findings. J Magn Reson Imaging 2005; 22:520-526.
16. Esserman LJ, Kumar AS, Herrera AF, et al. Magnetic resonance imaging captures the biology of ductal carcinoma in situ. J Clin Oncol 2006; 24:4603-4610.
17. Harms SE. The use of breast magnetic resonance imaging in ductal carcinoma in situ. Breast J 2005; 11:379-381.
18. Simpson ER. Biology of aromatase in the mammary gland. J Mammary Gland Biol Neoplasia 2000; 5:251-258.

19. Altundag K, Ibrahim NK. Aromatase inhibitors in breast cancer: an overview. Oncologist 2006; 11:553-562.
20. Byng JW, Yaffe MJ, Jong RA, et al. Analysis of mammographic density and breast cancer risk from digitized mammograms. Radiographics 1998; 18:1587-1598.

ABSTRACTS

Molecular Markers and DCEMRI of Breast Cancer: Relationship with Kinetics in Invasive Ductal Carcinoma

S. Arkani[1], H. Abe[1], A. Shimauchi[1], G. Karczma[1], and G. Newstead[1]
[1]Radiology, University of Chicago, Chicago, IL, United States

Introduction: Molecular markers such as estrogen receptor (ER), progesterone receptor (ER), and human epidermal growth factor receptor 2 (HER2/neu) are very important for predicting outcome and guiding treatment choices for breast cancer patients. Her2/neu positive and ER negative lesions tend to have poorer prognosis, and targeted therapies are available for Her2/Neu and ER positive lesions. Since kinetics of contrast media uptake and washout measured by dynamic contrast enhanced MRI are related to the underlying physiology and biology of lesions, it is possible that kinetic parameters could be used as surrogates for molecular markers. This would have the advantage that receptor status could be evaluated non-invasively and with high spatial resolution, which would be important in choosing subsequent therapy and guiding biopsy. Some prior reports have shown greater enhancement and washout for ER negative lesions, but have not studied PR or HER2/Neu status [1,2]. The purpose of this study was to perform a systematic evaluation of the kinetic characteristics of 145 invasive ductal carcinoma (IDC) lesions classified by ER, PR and Her2/Neu status.

Methods: 138 patients with 145 histologically proven IDC lesions with known ER, PR and Her2/Neu status were selected for IRB approved review. These lesions were classified as: ER positive (n=101), ER negative (n=44), PR positive (n=76), PR negative (n=69), Her2/Neu positive (n=25) and Her2/Neu negative (n=120). One pre and five post-contrast images were acquired in the coronal plane using 3D T_1-weighted SPGR (TR/TE = 7.7/4.2 msec, flip angle = 30˚, slice thickness = 3 mm, in plane resolution = 1.4 mm, 68 sec acquisition). To generate the kinetic curve, an experienced radiologist traced a small region of interest (ROI) around what was perceived to be the most enhancing part of the lesion on the first post-contrast image. The kinetic curve represents the signal intensity in the ROI over time. Subsequent analysis of kinetic curve shape was made according to the BI-RADS lexicon: initial rise (rapid, medium, slow) and delayed phase (persistent, plateau, washout). In addition, several quantitative parameters were derived from the kinetic curves: initial enhancement percentage $E_1=100x(S_1-S_0)/S_0$, the time to peak enhancement T_{peak}, and the signal enhancement ratio $SER_1 = (S_1-S_0)/(S_{last}-S_0)$, where S_0 is the pre-contrast signal intensity in the ROI, S_1 is the signal intensity at the first post contrast injection time point and S_{last} is the signal intensity at the last post contrast point[3]. A $SER_1 > 1.1$ indicates washout relative to the first post contrast point, while $9.9 < SER_1 < 1.1$ represents a plateau curve.

Results: Overall, 92% of lesions showed rapid initial enhancement, and 74% exhibited washout curves. The classification of the initial intensity increase and delayed phase according to BI-RADS lexicon did not differ significantly based on ER, PR and Her2/Neu status. The average values for the kinetic parameters were: E_1=307%, SER_1=1.13, T_{peak}=2.37 minutes. As shown in **Table 1**, ER negative lesions had a larger E_1 and SER_1, and a shorter T_{peak} compared with ER positive lesions, with p values < 0.03 for all parameters. Based on the SER_1 values, ER positive lesions exhibited plateau curves on average, while ER negative lesions showed a strong washout. PR negative lesions exhibited a stronger washout compared with PR positive lesions, with p

value < 0.02, but the other kinetic parameters did not show statistically significant differences. Her2/Neu negative and positive lesions were statistically equivalent.

Discussion: The kinetic characteristics of ER/PR negative lesions and ER/PR positive lesions showed some statistically significant differences (p <0.03), with ER negative lesions exhibiting the highest E_1, SER_1 and the shortest T_{peak} compared with all other categories. Previous reports have demonstrated that higher SER_1 values correlated with higher vascularity[3]. This implies that ER and PR negative lesions possess higher vascularity compared to their positive counterparts. These results also suggest that PR and in particular ER status may be related to tumor angiogenesis in a way that Her2/Neu status is not. If these preliminary results can be validated in a larger trial with more detailed kinetic analysis, this would suggest that reliable surrogates for these molecular markers can be measured non-invasively, in real-time and with high spatial resolution by MRI. DCEMRI could be used to guide biopsies and assess the spatial distribution of hormone receptors—in larger lesions it is difficult and time consuming for the pathologist to asses the receptor status in the whole lesion. Although preliminary, this study may point to a role for DCEMRI in evaluating hormone receptors and selecting appropriate hormone based therapy.

Acknowledgements: We would like to thank the NIH grant R21 CA104774-
01A2 and DOD BCRP BC050329 for support

References: [1]Szabo et al. Eur Radiol. 2003 Nov; 13(11)2425-35.
[2]Teifke et al. Radiology. 2006 May; 239(2): 351-60.
[3] Esserman et al. Breast J. 1999 Jan; 5(1): 13-21.

	ER –ve (n=44)	**ER +ve (n=101)**	**PR –ve (n=69)**	**PR +ve (n=76)**
E_1 **(%)**	351±19	288±16	328±18	287±18
SER_1	1.36±0.12	1.03±0.04	1.25±0.08	1.03±0.04
T_{peak} **(min)**	1.83±0.17	2.61±0.16	2.13±0.17	2.59±0.18

Table1: Kinetic parameters for ER/PR positive and negative lesions (mean ± standard error on mean).

Improving the Diagnostic Accuracy of 3D Breast DCEMRI Data Using an Empirical Mathematical Model

S. Arkani[1], X. Fan[1], H. Abe[1], G. Karczmar[1], R. Schmidt[1], and G. Newstead[1]

[1]Radiology, University of Chicago, Chicago, IL, United States

Introduction: The majority of mathematical models applied to breast DCEMRI require high temporal resolution and protocols that are not clinically feasible[1]. The purpose of this study is to apply an empirical mathematical model (EMM) to kinetic data from breast DCEMRI acquired under a clinical protocol with sparse time resolution, and to determine if the sensitivity and specificity can be improved compared with qualitative BI-RADS descriptors of kinetics.

Methods: 34 benign and 79 malignant lesions were selected for review under an IRB approved protocol. One pre and five post-contrast images were acquired in the coronal plane using 3D T_1-weighted SPGR (TR/TE = 7.7/4.2 msec, flip angle = 30˚, slice thickness = 3 mm, and in plane resolution = 1.4 mm, 68 sec acquisition). The radiologist traced a small region of interest (ROI) around what was perceived to be the most enhancing part of the lesion on the first post-contrast image. The kinetic curve represents the signal intensity in the ROI vs. time. This curve was assessed by the radiologist according to the BI-RADS lexicon for initial rise (rapid, medium, slow) and delayed phase (persistent, plateau, washout). The kinetic curve was also analyzed quantitatively using the EMM: $\Delta S(t) = A \cdot \left(1 - e^{-\alpha t}\right) \cdot e^{-\beta t}$, where A is the upper limit of signal intensity, α is the rate of signal increase (min^{-1}), β is the rate of signal decrease during washout (min^{-1}). Several secondary parameters were also derived from this equation including the initial slope ($\mathbf{Slope_{ini}}$), curvature at the peak ($\boldsymbol{\kappa_{peak}}$) and the signal enhancement ratio ($\mathbf{SER_{60}}$)[2]. ROC analysis was used to compare the sensitivity and specificity of the model parameters with the BI-RADS descriptors. In addition, the average parameter values were studied for subtypes of malignant lesions: ductal carcinoma in situ (DCIS, n=30), invasive ductal carcinoma (IDC, n=36) and invasive lobular carcinoma (ILC, n=7).

Results: The classification of the initial intensity increase according to BI-RADS did not differ significantly between malignant and benign lesions, but the delayed phase was significantly different, with 65% of malignant lesions and 38% of benign lesions showing washout curves ($p < 0.05$). The BI-RADS delayed phase descriptors had sensitivity and specificity of 91% and 18%, respectively. The EMM was able to accurately fit these curves. There was a statistically significant difference between benign and malignant lesions for the parameters: $\boldsymbol{\alpha}$ ($p < 0.03$), $\mathbf{Slope_{ini}}$ ($p < 0.04$), $\boldsymbol{\kappa_{peak}}$ ($p < 0.02$) and $\mathbf{SER_{60}}$ ($p < 0.0007$) (**Table 1**). The ROC curves for $\boldsymbol{\alpha}$ and $\mathbf{SER_{60}}$ in **Fig. 1** demonstrates improvement in the diagnostic performance compared with the BI-RADS categories—at a sensitivity of 90%, the specificity was 20-30%. The kinetic parameters of DCIS lesions overlapped considerably with many benign lesions, suggesting that diagnostic performance could be improved if only IDC lesions were considered, as is most commonly done elsewhere. To explore this, **Fig. 1** also shows ROC curves for $\boldsymbol{\alpha}$ and $\mathbf{SER_{60}}$ discriminating benign vs. IDC lesions only, which have larger A_z values and demonstrate improved diagnostic accuracy compared to the benign vs. all malignant counterparts.

Discussion: Malignant lesions had a larger uptake rate, larger initial slope, sharper curvature at the peak and stronger washout compared with benign lesions ($p < 0.04$). The specificity reported here is lower than some other reports[3]. This may be because the benign cases studied here required biopsy, and thus were the more suspicious
benign lesions with features that may overlap more with malignant lesions—in particular DCIS, which comprised a large proportion of the malignant lesions studied here. Increased time

resolution would take better advantage of the EMM and would likely improve the diagnostic accuracy. These results show that analysis of DCEMRI data with the EMM provides at least the diagnostic accuracy of the BI-RADS classifiers, and offers a few key advantages. It can be automated and can provide a more objective classification. It provides continuous variables so that thresholds can be set to achieve desired sensitivity and specificity—for example, at a sensitivity of ~65% the specificity was ~60 %, which is good diagnostic accuracy in a population with suspicious benign lesions. It also offers an opportunity to relate semi-quantitative parameters (such as $\mathbf{SER_{60}}$) to more fundamental EMM parameters, allowing comparisons to be made across institutions with different protocols. More importantly, this model allows for more flexibility in improving sensitivity and specificity in the future by using combinations of variables, corrections for arterial input functions and relating parameters directly to underlying physiological quantities. This suggests that the EMM may be useful for analysis of routine clinical data.

Acknowledgements: We would like to thank the NIH grant R21 CA104774-01A2 for support.

[1]Armitage et al. Med Image Anal. 2005 Aug; 9(4): 315-29.
[2]Esserman et al. Breast J. 1999 Jan; 5(1): 13-21.
[3]Kuhl et al. Radiology. 1999 Apr; 211(1):101-10.

Figure 1: ROC curves for α and $\mathbf{SER_{60}}$.

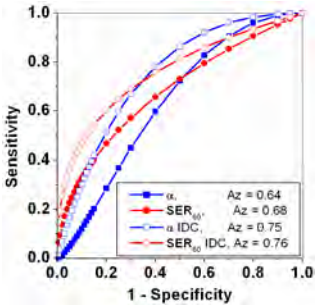

	Benign (n=34)	**Malignant (n=79)**
$\boldsymbol{\alpha}$ **(min^{-1})**	1.6±1.1	2.1±1.1
Slope$_{ini}$ (min^{-1})	6.1±4.6	8.7±8.3
κ_{peak}	-0.30±0.49	-0.67±1.18
$\mathbf{SER_{60}}$	0.88±0.30	1.14±0.48

Table 1: Primary & derived EMM parameters.

MRI of Ductal Carcinoma *in situ* and Other Early Mammary Cancers in Transgenic Mice

S. Arkani[1], S. Conzen[2], T. Krausz[3], G. Newstead[1], and G. Karczmar[1]

[1]Radiology, University of Chicago, Chicago, IL, United States, [2]Hematology/Oncology, University of Chicago, Chicago, IL, United States, [3]Pathology, University of Chicago, Chicago, IL, United States

Introduction: The majority of MR studies of mammary cancer in mice focus on large, palpable tumors that are not orthotopic[1,2]. This poses significant problems for drug development and for development of improved imaging methods that target early cancer. Here, we report a novel approach to imaging rodent mammary cancer. High resolution MR was used to image early pre-invasive murine ductal carcinoma in situ (DCIS) and minimally invasive stages of mammary cancer in a transgenic model of spontaneous breast cancer, and the images were correlated with histological sections.

Methods: A pair of inguinal mammary glands was imaged in ten Sv40 large T antigen transgenic female mice. The mice were imaged and immediately sacrificed at various ages between 10-18 weeks of age. The mammary glands were then excised, fixed overnight in formalin and submitted for paraffin embedding, sectioning and H&E staining. The tissue slices were evaluated by an experienced pathologist (TK). MR imaging was performed on a 4.7 T Bruker scanner using a home built surface coil that produced high flux density in the mammary gland. FLASH GE images were obtained (TR/TE: 675/7 ms, axial orientation, slice thickness 0.5 mm, in plane resolution 117 microns, FOV=3.0x3.0cm) with and without fat suppression. High spectral and spatial resolution images were also acquired with slice thickness of 0.5 mm, in-plane resolution of 117 microns and spectral resolution of ~ 6 Hz. Dynamic contrast enhanced images were also obtained (TR/TE: 30/3.5 ms, slice thickness 1.0 mm, in plane resolution 117 microns). To facilitate comparisons with histology, a polyethylene mesh with 2.5 mm spacing was embedded in partially deuterated agar and wrapped around the mouse. The agar reduced susceptibility artifacts and also produced a pattern on MRI that was used for registration of tissue slices and images. To perform the correlation of histology with MRI, one representative H&E section was selected per mouse. On each section, the lymph node, tumors and ducts distended with DCIS were counted, and their grid locations noted. The corresponding grid positions in the MR images were examined to see if correlative structures were discernable.

Results: Fig. 1 shows FLASH GE images with fat saturation and the corresponding pathology for two different mice. The correlations indicated in the figure were made via the grid and corresponding structures are noted in the figure. In all ten cases, the mammary gland and the lymph node were accurately identified, and the position of the lymph node on histological sections correlated with MRI to within 2 mm. 'Gold standard' evaluation of the pathologist demonstrated that MRI detected 1/1 large (~5mm) tumor, 8/9 small non-palpable tumors ~0.5-1.5 mm in size, and 11/13 ducts distended with DCIS ~ 300-500 microns in diameter. These findings were clearly distinguishable from normal gland.

Discussion: To our knowledge, this is the first report of MR imaging of early, spontaneous mouse mammary cancer. The detection of very early cancers, including DCIS, in a mouse model

opens new possibilities for research and for clinical applications. Because of its similarity to human breast cancer, MRI of early orthotopic murine mammary cancer will be an important tool for **a)** development of therapies that target early cancers **b)** developing improved MR imaging methods for detection of early cancers and pre-cancerous conditions **c)** discovering new MRI markers for cancer risk.

Figure 1: FLASH GE *in vivo* images with fat saturation for 12 week (left) and 16 week (right) old mice. Please note: the H&E sections are coronal slices, while the MRI are axial and a grid is used to correlate the two. Nevertheless, below close correspondence can be seen between the DCIS, small tumors, and lymph nodes on histology and MRI.

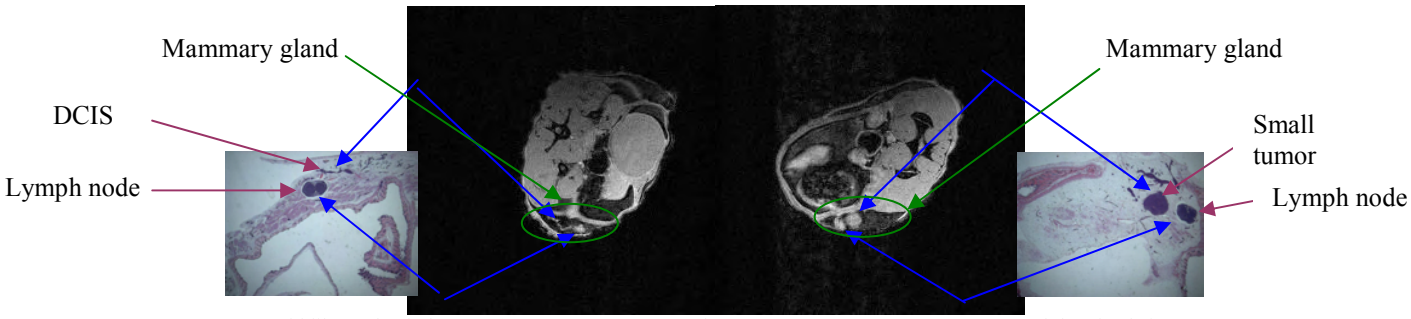

Acknowledgements: We would like to thank the NIH (R01 EB003108-02) and UCCRC (P30 CA14599-31) grants and the Florsheim Foundation for support.

References: [1] Cohen et al. Int J Cancer. 2006 Apr 1:118(7); 1609-17.
[2] Rodrigues et al. MAGMA. 2004 Dec; 17(3-6):260-70.

MR Imaging of Pure Ductal Carcinoma in Situ: Kinetics, Morphology and Correlation with Mammographic Presentation and Nuclear Grade

Purpose: To perform a systematic evaluation of the kinetic and morphologic characteristics of 82 pure DCIS lesions on DCEMRI and to classify these characteristics by nuclear grade and mammographic presentation.

Materials and Methods: 80 patients with 82 histologically proven pure DCIS lesions were selected for IRB approved review. Histologic classification: 14 low, 25 intermediate and 37 high grade pure DCIS lesions with 6 unclassified. The mammographic findings of 63 lesions were assessed and classified as: pleomorphic or linear calcifications (n=32), fine or punctate calcifications (n=14), mass presentation (n=8) and occult (n=9). Dynamic MR protocol: 1 pre and 5 post-contrast images acquired in the coronal plane using a 3D SPGR sequence with 68 s timing. Kinetic curves were generated by two experienced radiologists by using homemade software to manually tracing a region of interest (ROI) around the most enhancing part of the lesion on subtraction images and plotting the signal intensity vs. time. Subsequent analysis of lesion morphology and kinetic curve shape was made according to the BiRads lexicon. In addition, several quantitative parameters were derived from the kinetic curves: initial and peak enhancement percentage (E1 and Epeak) and washout ratio (W).

Results: The morphology of pure DCIS lesions was predominantly non-mass, clumped or heterogeneous enhancement in a segmental or linear distribution. This morphology persisted by nuclear grade and mammographic presentation. 45% and 27% of lesions showed qualitative washout and plateau curves, respectively. The average kinetic parameters were: E1=201 %, Epeak=256%, W=1.08. Thus, quantitatively pure DCIS lesions enhanced moderately and plateau. There was no statistically significant difference in the enhancement kinetics across lesion nuclear grade. Lesions with mass like appearance on mammography and those with pleomorphic or linear calcifications had more suspicious kinetics with a strong washout.

Conclusion: Pure DCIS lesions display a variety of contrast media uptake a washout characteristics. This variability may be correlated to mammographic appearance, rather than nuclear grade. Recognition of the unique morphology and kinetics of pure DCIS may aid in improving the detection of early breast cancer.

Dynamic MR Imaging of Invasive Ductal Carcinoma: Studying Kinetics by Estrogen Receptor, Progesterone Receptor and Her2/Neu Amplification Status.

Object or Purpose: To perform a systematic evaluation of the kinetic characteristics of 145 invasive ductal carcinoma (IDC) lesions classified by estrogen receptor (ER), progesterone receptor (PR) and Her2/Neu gene amplification status.

Materials and Methods: 138 patients with 145 histologically proven IDC lesions with known ER, PR and Her2/Neu status were selected for IRB approved review. These lesions were classified as: ER positive (n=101), ER negative (n=44), PR positive (n=76), PR negative (n=69), Her2/Neu positive (n=25) and Her2/Neu negative (n=120). Dynamic MR protocol: 1 pre and 5 post-contrast images acquired in the coronal plane using a 3D SPGR sequence with 68 s timing. Kinetic curves were generated by two experienced radiologists by using homemade software to manually trace a region of interest (ROI) around the most enhancing part of the lesion on subtraction images and plot the signal intensity vs. time (or kinetic) curve. Subsequent analysis of kinetic curve shape was made according to the BiRads lexicon: initial rise (rapid, medium, slow) and delayed phase (persistent, plateau, washout). In addition, several quantitative parameters were derived from the kinetic curves: initial enhancement percentage (E_1), a measure of washout relative to the first post contrast point (W_1), and the time to peak enhancement (T_peak).

Results: Overall, 92% of lesions showed rapid initial enhancement, and 74% exhibited washout curves. The average values for the kinetic parameters were: E_1=306%, W_1=1.12, T_peak=126 seconds. ER negative lesions had a stronger initial enhancement, stronger washout and a shorter time to peak enhancement (E_1=351%, W_1=1.36, T_peak=94 seconds) compared with ER positive lesions (E_1=286%, W_1=1.02, T_peak=142 seconds), with p values < 0.03 for all parameters. PR negative lesions exhibited a stronger washout (W_1=1.25) compared with PR positive lesions (W_1=1.01), with p value < 0.01, but were otherwise statistically equivalent. Her2/Neu negative and positive lesions were statistically equivalent.

Significance of the Conclusions: The kinetic characteristics of ER and PR positive and negative lesions showed some statistically significant differences ($p < 0.03$), with ER negative lesions showing the strongest initial enhancement, shortest time to peak enhancement and strongest washout. This suggests that PR and in particular ER status may be related to vasculature in a way that Her2/Neu status is not. These findings may provide new ways of understanding kinetic data presented in dynamic MR images.

Parenchymal Enhancement on Breast MRI May be a Marker for Cancer Risk: Correlation of Parenchymal Enhancement with Breast Density

S Arkani MSc., V Chen MD., C Cranford MD., L Zak, H Abe MD., PhD., G Karczmar PhD., R Schmidt MD., O Olopade MD., G Newstead MD.

Purpose

To classify the parenchymal enhancement pattern at MR imaging and to correlate with mammographic breast density in a cohort of high risk women.

Methods

The study population consisted of 181 women with either a genetic predisposition, a personal history or a 5 year relative risk of breast cancer of greater than 1.7 as calculated by the Gail model. All patients were imaged with a 3D bilateral dynamic MR sequence, without consideration of menstrual status. No patient had any abnormal finding. Breast density was classified independently by three readers on digital x-ray mammograms according to the BI-RADS categories: 1=almost entirely fat, 2= scattered fibroglandular tissue, 3=heterogeneously dense, 4=extremely dense. The MR parenchymal pattern of enhancement for each case was classified separately by three readers as minimal, homogeneous, heterogeneous or nodular. This classification was performed by visual analysis of the enhancement pattern on 6 minute post-contrast subtracted coronal images. Parenchymal signal intensity vs. time curves were generated by manually tracing a region of interest around the total parenchyma visible in a selected pre-contrast coronal slice. The peak magnitude of parenchymal enhancement relative to the pre-contrast signal intensity E_peak[%] was measured.

Results

Distribution of patients by BI-RADS mammographic density: 1% (n=1) category 1; 49% (n=88) category 2; 35% (n=63) category 3; 16% (n=29) category 4. MRI parenchymal enhancement pattern distribution: 41% (n=75) minimal; 9% (n=17) homogeneous; 31% (n=56) heterogeneous; 18% (n=33) nodular. The observable peak enhancement occurred at the last post contrast minute (6 minute) in 94% of the total population. The average E_peak was 45 +- 4% overall. 53% of breasts with scattered fibroglandular tissue show minimal parenchymal enhancement while 34% show heterogeneous or nodular patterns. Conversely, only 30 % of heterogeneously or extremely dense breasts show minimal enhancement while 64 % show heterogeneous or nodular enhancement. The average E_peak was 51% for heterogeneously and extremely dense breasts and 36% for breasts with scattered fibroglandular tissue.

Conclusions

A statistically significant correlation between mammographic density and magnitude (E_peak) and pattern (heterogeneous and nodular) of parenchymal enhancement was found ($p < 0.01$). Although further study is needed, this observation might lead to an improved reproducible quantification method of assessing breast cancer risk based on breast enhancement patterns.

CV

Personal Information

Sanaz (Sunny) Arkani-Hamed
Department of Medical Physics, University of Chicago
5841 S.Maryland Ave, Chicago, IL 60615
(773) 834-3170
sarkani@uchicago.edu

Education

PhD Candidate **University of Chicago, USA**
Medical Physics, September 2004 -

MSc **University of Chicago, USA**
Physics, May 2003.

BSc **University of Toronto, Canada**
Mathematics and Physics, May 2001.

Research Experience

Research Associate **Department of Radiology, University of Chicago**
January 2004-August 2004. Supervisor: Dr. Gillian Newstead
Breast DCEMRI.

Research Assistant **Department of Physics, University of Chicago**
January 2002-August 2002. Supervisor: Prof. Sean Carroll.
Cosmology.

Student Research **Department of Mathematics, University of Toronto**
May 2001- September 2001. Supervisor: Prof. Lisa Jeffrey.
Topology of Gauge Fields.

Student Research **Department of Physics, University of Toronto**
May 2000- May 2001. Supervisor: Prof. Ted Shepherd.
Atmospheric Physics.

Student Research **Department of Physics, University of Toronto**
May 1999-September 1999. Supervisor: Prof. Dwayne Miller.
Biophysics.

Awards

RSNA Trainee Research Award, November 2006
Deans Fellowship Biological Sciences Division University of Chicago
One of two fellowships for graduate students in Medical Physics
National Sciences and Engineering Research Council Scholarship (NSERC) Post Gradute Scholarship
Ontario Graduate Scholarship
NSERC Undergaduate Student Research Award USRA
summer research: Physics: 1999, 2000 and Mathematics: 2001
3T0 M&P Associates Scholarship
award for academic achievement in Mathematics and Physics Specialist Program, U of Toronto
1998, 1999
University of Toronto Scholar
1997
Trinity College Chancellor Scholarship
for academic achievement 1998, 1999, 2000, 2001
Prince of Wales Award

Teaching Experience

Teaching Assistant:
Physical Sciences for Non-Scientists I and II, University of Chicago
Physics for Life Sciences, University of Chicago
Calculus, University of Toronto